DOCTORAATSPROEFSCHRIFT

2007 | School voor Levenswetenschappen

A primary culture of proximal tubule cells of the mouse kidney on collagen-coated membranes: characterization, electrophysiological properties and response to stress factors

Proefschrift voorgelegd tot het behalen van de graad van
Doctor in de Biomedische Wetenschappen, te verdedigen door:

Sara TERRYN

Promotor: prof. dr. Emmy Van Kerkhove
Copromotor: prof. dr. Paul Steels

Universiteit Maastricht

universiteit hasselt
CENTRUM
VOOR MILIEUKUNDE

List of Abbreviations

A6	Cell line derived from the kidney of *Xenopus laevis*
AA	Arachidonic acid
AC	Adenylyl cyclase
AEC	Aminoethylcarbazole
α-MG	Alpha-methyl-D-glucopyranoside
ANOVA	Analysis of variance
AQP	Aquaporin
AP	Alkaline phosphatase
AP-2β	Activator protein 2β
α-SMA	Alpha-smooth muscle actin
ATI	Angiotensin receptor type I
ATII	Angiotensin II
ATP	Adenosine trisphosphate
BAPTA	(1,2-bis(o-aminophenoxy)ethane-N,N,N',N'-tetraacetic acid)
BK	Bradykinin
BMP-7	Bone morphogenic protein type 7
BSA	Bovine serum albumin
C	Capacitor/capacitance
cAMP	Cyclic adenosine monophosphate
CD	Collecting duct
CFTR	Cystic Fibrosis Transmembrane Conductance Regulator
C_T	Transepithelial capacitance
DAG	Diacylglycerol
DAT	Dense apical tubules
DBP	VitaminD_3-binding protein
DEA	Diethanolamine
DMEM	Dulbecco's modified Eagle's medium
DMSO	Dimethyl sulfoxide
DS	Dissection solution
ECL	Enhanced chemiluminscence
ECM	Extracellular matrix
EDTA	Ethylene diamine tetraacetic acid
EGTA	Ethylene glycol tetraacetic acid
5,6-EET	5,6-epoxy-eicosatrienoic acid
EMT	Epithelial-to-mesenchymal transdifferentiation
ERK	Extracellular-signal regulated kinases
FCS	Fetal calf serum
FITC	Fluorescein-isothiocyanate
FN	Fibronectin
GLUT	Facilitated glucose transporter
GSH	Glutathione
γ-GT	Gamma-glutamyl transferase
G_T	Transepithelial conductance
HBSS	Hank's buffered saline solution
HC	Hydrocortisone
HEPES	4-(2-hydroxyethyl)-1-piperazine-sulphonic acid
HIF	Hypoxia inducible transcription factor
HNF-1	Hepatocyte nuclear factor 1

I	Current
IF	Intermediate filament
IP_3	Inositoltrisposphate
I_{SC}	Short-circuit current
ITS	Insulin-transferrin-selenium
J_{Na}	Transport rate of sodium per square area
K_d	Dissociation constant
K_m	Michaelis-Menten constant
LAP	Leucine aminopeptidase
LDL	Low-density lipoprotein
LIS	Lateral intercellular space
LLCPK	Cell line derived from proximal tubule cells from porcine kidney
LM	Light microscopy
LMW	Low molecular weight
LTBP	Latent TGF-β1-binding protein
MDCK	Madin-Darbey canine kidney cells
MEM	Modified Eagle's medium
MET	Mesenchymal-to-epithelial transdifferentiation
NaPi	Sodium-dependent phosphate cotransporter
NCC	Na^+/Cl^--cotransporter
NHE_3	Na^+/H^+-exchanger type 3
NMDG	N-methyl-D-glucamine
NRK52E	Cell line derived from proximal tubule cells from rat kidney
P450	P450 epoxygenase
PAS	Periodic acid-Shiff
PBS	Phosphate-buffered saline
PLA_2	Phospholipase A2
PLC	Phospholipase C
PT(C)	Proximal tubule (cell)
PTFE	Polytetrafluoroethylene
PTH	Parathyroid hormone
RBP	Retinol-binding protein
R_S	Series resistance
R_T	Transepithelial resistance
SDS	Sodium dodecyl sulfate
SDS-PAGE	Sodium dodecyl sulfate polyacrylamide gel electrophoresis
SEM	Standard error of the mean
SGLT	Sodium-dependent glucose cotransporter
SLC	Sodium-coupled transporter family
snGFR	Single nephron glomerular filtration rate
TAL	Thick ascending limb of Henle's loop
TEM	Transmission electron microscopy
TGF-β1	Transforming growth factor-β type 1
TKPTS	Cell line derived from proximal tubule cells from mouse kidney
TRIS	Tris-(hydroxymethyl)-aminomethane
V	Voltage
V_{max}	Maximal transport velocity
V_T	Transepithelial potential
ZO-1	Zonula occludens protein-1
Z	Impedance

DOCTORAATSPROEFSCHRIFT

2007 | School voor Levenswetenschappen

A primary culture of proximal tubule cells of the mouse kidney on collagen-coated membranes: characterization, electrophysiological properties and response to stress factors

Proefschrift voorgelegd tot het behalen van de graad van
Doctor in de Biomedische Wetenschappen, te verdedigen door:

Sara Terryn

Promotor: prof. dr. Emmy Van Kerkhove
Copromotor: prof. dr. Paul Steels

Universiteit Maastricht

universiteit hasselt
CENTRUM
VOOR MILIEUKUNDE

D/2007/2451/47

Members of the jury

Prof. dr. M. Ameloot, Universiteit Hasselt, Diepenbeek, BELGIUM, chairman
Prof. dr. E. Van Kerkhove, Universiteit Hasselt, Diepenbeek, BELGIUM, promotor
Prof. dr. P. Steels, Universiteit Hasselt, Diepenbeek, BELGIUM, co-promotor
Prof. dr. I. Lambrichts, Universiteit Hasselt, Diepenbeek, BELGIUM
Prof. dr. W. Van Driessche, Universiteit Hasselt, Diepenbeek, BELGIUM
Prof. dr. L. Verresen, Universiteit Hasselt, Diepenbeek, BELGIUM
Prof. dr. R. Beauwens, Université Libre de Bruxelles, Brussel, BELGIUM
Prof. dr. O. Devuyst, Université Catholique de Louvain, Brussel, BELGIUM
Prof. dr. P. de Leeuw, Universiteit Maastricht, Maastricht, THE NETHERLANDS
Prof. dr. F. Thévenod, Universität Witten/Herdecke, Witten, GERMANY

List of Abbreviations

A6	Cell line derived from the kidney of *Xenopus laevis*
AA	Arachidonic acid
AC	Adenylyl cyclase
AEC	Aminoethylcarbazole
α-MG	Alpha-methyl-D-glucopyranoside
ANOVA	Analysis of variance
AQP	Aquaporin
AP	Alkaline phosphatase
AP-2β	Activator protein 2β
α-SMA	Alpha-smooth muscle actin
ATI	Angiotensin receptor type I
ATII	Angiotensin II
ATP	Adenosine trisphosphate
BAPTA	(1,2-bis(o-aminophenoxy)ethane-N,N,N',N'-tetraacetic acid)
BK	Bradykinin
BMP-7	Bone morphogenic protein type 7
BSA	Bovine serum albumin
C	Capacitor/capacitance
cAMP	Cyclic adenosine monophosphate
CD	Collecting duct
CFTR	Cystic Fibrosis Transmembrane Conductance Regulator
C_T	Transepithelial capacitance
DAG	Diacylglycerol
DAT	Dense apical tubules
DBP	VitaminD_3-binding protein
DEA	Diethanolamine
DMEM	Dulbecco's modified Eagle's medium
DMSO	Dimethyl sulfoxide
DS	Dissection solution
ECL	Enhanced chemiluminscence
ECM	Extracellular matrix
EDTA	Ethylene diamine tetraacetic acid
EGTA	Ethylene glycol tetraacetic acid
5,6-EET	5,6-epoxy-eicosatrienoic acid
EMT	Epithelial-to-mesenchymal transdifferentiation
ERK	Extracellular-signal regulated kinases
FCS	Fetal calf serum
FITC	Fluorescein-isothiocyanate
FN	Fibronectin
GLUT	Facilitated glucose transporter
GSH	Glutathione
γ-GT	Gamma-glutamyl transferase
G_T	Transepithelial conductance
HBSS	Hank's buffered saline solution
HC	Hydrocortisone
HEPES	4-(2-hydroxyethyl)-1-piperazine-sulphonic acid
HIF	Hypoxia inducible transcription factor
HNF-1	Hepatocyte nuclear factor 1

I	Current
IF	Intermediate filament
IP_3	Inositoltrisposphate
I_{SC}	Short-circuit current
ITS	Insulin-transferrin-selenium
J_{Na}	Transport rate of sodium per square area
K_d	Dissociation constant
K_m	Michaelis-Menten constant
LAP	Leucine aminopeptidase
LDL	Low-density lipoprotein
LIS	Lateral intercellular space
LLCPK	Cell line derived from proximal tubule cells from porcine kidney
LM	Light microscopy
LMW	Low molecular weight
LTBP	Latent TGF-β1-binding protein
MDCK	Madin-Darbey canine kidney cells
MEM	Modified Eagle's medium
MET	Mesenchymal-to-epithelial transdifferentiation
NaPi	Sodium-dependent phosphate cotransporter
NCC	Na^+/Cl^--cotransporter
NHE_3	Na^+/H^+-exchanger type 3
NMDG	N-methyl-D-glucamine
NRK52E	Cell line derived from proximal tubule cells from rat kidney
P450	P450 epoxygenase
PAS	Periodic acid-Shiff
PBS	Phosphate-buffered saline
PLA_2	Phospholipase A2
PLC	Phospholipase C
PT(C)	Proximal tubule (cell)
PTFE	Polytetrafluoroethylene
PTH	Parathyroid hormone
RBP	Retinol-binding protein
R_S	Series resistance
R_T	Transepithelial resistance
SDS	Sodium dodecyl sulfate
SDS-PAGE	Sodium dodecyl sulfate polyacrylamide gel electrophoresis
SEM	Standard error of the mean
SGLT	Sodium-dependent glucose cotransporter
SLC	Sodium-coupled transporter family
snGFR	Single nephron glomerular filtration rate
TAL	Thick ascending limb of Henle's loop
TEM	Transmission electron microscopy
TGF-β1	Transforming growth factor-β type 1
TKPTS	Cell line derived from proximal tubule cells from mouse kidney
TRIS	Tris-(hydroxymethyl)-aminomethane
V	Voltage
V_{max}	Maximal transport velocity
V_T	Transepithelial potential
ZO-1	Zonula occludens protein-1
Z	Impedance

List of Figures

List of Tables

Chapter 1

Introduction

1.1 Introduction

Over the years, a large number of *in vitro* models ranging from renal cell lines to isolated perfused tubules have been established. However, epithelial cell lines had to undergo a number of genetic changes in order to survive indefinitely *in vitro*. On the other hand, the isolated perfused tubule is a complex system to study. As a consequence, primary epithelial cell culture systems are needed to check the physiological significance of studies done with established cell lines and in some cases they might be the only way to study specific tubular cell function characteristics in particular (patho)physiological and pharmacological conditions. Furthermore, the increasing use of transgenic and knock-out mouse models should be supported by an *in vitro* model to study the cellular phenotype. Major inherent technical advantages of cultured cells for the study of epithelial transport include their ability to be studied in a controlled environment without systemic neurons and hormonal influences, and their easy accessibility for electrophysiological and imaging techniques. However, primary cell culture also has its limitations such as incomplete differentiation of cells or a limited lifespan, among others.

The objective of this thesis was to establish a primary cell culture of mouse proximal tubule cells. The primary cells were extensively characterized for their proximal tubule origin. To correlate our findings in primary cell cultures with data in the literature, a detailed description of proximal tubule cell morphology and (electro-) physiology is given in section 1.2, 1.3 and 1.4. Finally, we used our cell cultures as a model for the study of renal tubulointerstitial fibrosis. The mechanisms involved in tubulointerstitial fibrosis are described in section 1.5. At the end of this chapter, the different aims of this thesis are summarized.

1.2 The proximal tubule: relationship between function and structure

The kidneys are paired, bean shaped organs located retroperitoneally in the posterior part of the abdomen on each side of the vertebral column; the upper pole of each kidney lies opposite the 12^{th} thoracic vertebra. The nephron is the functional unit of the kidney and about one million are present in each kidney in man (fig. 1.1).

The proximal tubule is the first nephron segment that receives the plasma filtrate from the glomerulus. Structurally, the proximal tubule can be divided into

2 parts, the pars convoluta, a tortuous tubule which continues into the pars recta or the straight proximal tubule. These two parts can be ultrastructurally subdivided into 3 segments: the S1 segment that comprises the beginning and middle portion of the convoluted tubule; the S2 segment which comprises the final portion of the convoluted tubule and the first portion of the pars recta; and the S3 segment which comprises the remainder of the straight part (Kriz & Bankir, 1988). The morphology of the proximal tubule explains its function, being the bulk reabsorption of about two-thirds of filtered Na^+ and H_2O together with an almost complete reabsorption of filtered solutes, like glucose, amino acids and phosphate. The proximal tubule cell is a highly polarized cuboid cell. Both the apical and basolateral membrane are extensively amplified. At the apical membrane, numerous microvilli are organized in a well-developed brush border, while at the basolateral membrane, numerous infoldings form an extensive extracellular compartment bounded by the tight junction at the apical side and the basement membrane at the blood side. The enlargement of the membranes reflects the high transport capacity of the proximal tubule cell. Furthermore, the position of the microvilli seems to be closely related to the tubular flow. If flow increases, the distance between the microvilli enlarges, while at low flow rates the microvilli are closer to each other. The increased distance between microvilli might lead to increased fluid and solute reabsorption (Maunsbach et al., 1987). Recently, it was shown in isolated mouse proximal tubules that changes in luminal flow induce variations in microvillous torque, which regulates luminal cell membrane transport activity of both NHE_3 and H^+-ATPase. This bending effect of microvilli on intramembranous transport proteins requires an intact actin cytoskeleton (Du et al., 2004; Du et al., 2006; Weinstein et al., 2007). Also, the size of the basolateral surface area is closely related to the Na^+/K^+-ATPase activity.

To ensure the tubular reabsorption of large amounts of solutes (salts and organic compounds), a considerable amount of ATP is consumed. ATP supply is provided by the large number of elongated mitochondria oriented radially along the vertical folds of the basolateral membrane. The ATP is necessary to drive the Na^+/K^+-ATPase that creates the large inward electrochemical gradient for Na^+ which is essential for the reabsorption of most solutes. The elaborated membrane enlargement and high number of mitochondria in the proximal tubule

cell have been long recognized as a common architecture for epithelial cells capable of high rates of fluid transport (Maunsbach & Boulpaep, 1984; Welling et al., 1987; Welling & Welling, 1988; Maunsbach & Christensen, 1992; Zhai et al., 2003).

Another determinant for fluid transport in epithelia is the tight junction. In the proximal tubule, the tight junctions form a ridge around the apical pole of the cell thereby sealing of the lumen from the lateral intercellular space (LIS). Protein strands interact with proteins from an adjacent cell to form a junctional complex. The number of strands and interruptions determine the tightness of the junction. Usually, in proximal tubule cells, the tight junction is formed by one or two strands and up to 10% of the strands are discontinuous explaining the leakiness of the proximal tubule (Cereijido et al., 1998; Mitic & Anderson, 1998; Schneeberger & Lynch, 2004; Van Itallie & Anderson, 2006).

The proximal tubule possesses a large endocytic apparatus, necessary for the reabsorption of filtered low-molecular weight proteins (LMW-proteins). This is reflected structurally in the presence of numerous large endosomes and dense apical tubules along with a high number of lysosomes, lipid droplets and lipid-like inclusions filled with lysosomal enzymes mainly located in the apical and central part of the cell (Zhai et al., 2003).

Another feature of proximal tubule cells is the presence of an apical primary cilium, which is shown to be involved in flow-sensing and seems to be a key factor in the development of polycystic kidney disease (Praetorius & Spring, 2005).

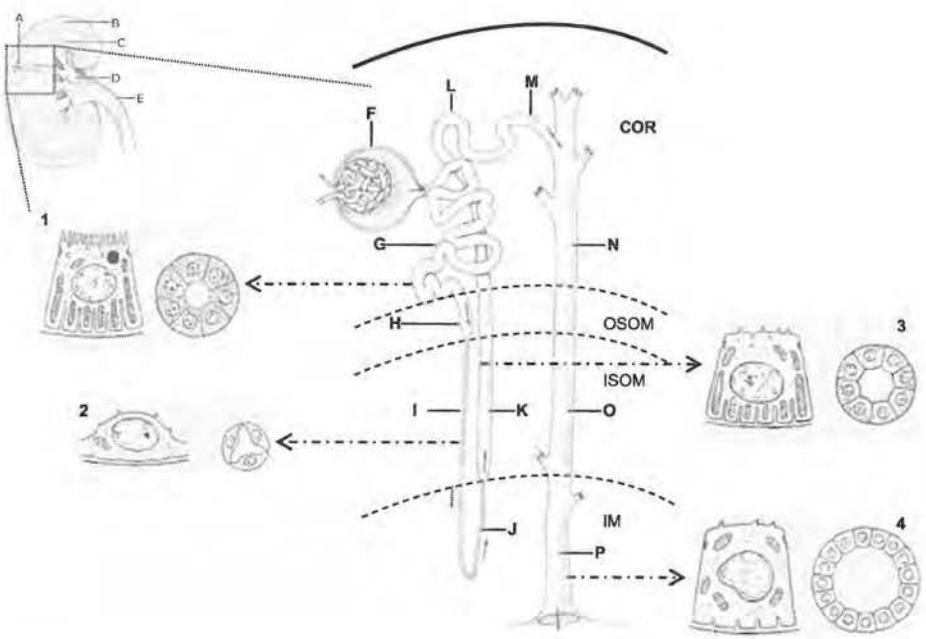

Figure 1.1: Drawing of a kidney and a nephron

The nephron (A) is the functional unit of the kidney and consists of a glomerulus (F) and a tubule structure. The tubule structure consists of; in order of the flow direction (indicated with an arrow): convoluted proximal tubule (G), straight proximal tubule (H), thin descending (I) and ascending limb of the loop of Henle (J), thick ascending limb of Henle's loop (K), distal convoluted tubule (L), connecting tubule (M), cortical collecting duct (N), outer medullary collecting duct (O) and inner medullary collecting duct (P). The proximal tubule (inset 1) is located in the cortical part (B) of the kidney. COR: cortex, OSOM: outer stripe of the outer medulla, ISOM: inner stripe of the outer medulla, IM: inner medulla, inset 1: proximal tubule, inset 2: thin limb of Henle's loop, inset 3: thick ascending limb of Henle's loop, inset 4: collecting duct. In the figure of the kidney (upper left): A: nephron, B: cortex, C: medulla, D: renal papilla, E: ureter (Adapted from Visual Histology, Online Atlas by Moran DT and Rowley JC).

1.3 Enzyme and transport markers of the proximal tubule

Besides typical morphological properties, the proximal tubule possesses a number of functional properties that distinguish it from other nephron segments or can be used to characterize cells in culture.

1.3.1 Enzyme markers

A typical feature is the presence of brush border enzymes, like alkaline phosphatase (AP) and γ-glutamyl transferase (γ-GT). Alkaline phosphatase seems to be involved in the reabsorption of phosphate although its function remains rather unclear in the proximal tubule (Nouwen & De Broe, 1994). In contrast, the function of γ-GT has been studied in more detail (Welbourne & Matthews, 1999; Paolicchi et al., 2003). γ-Glutamyl transferase catalyzes the cystein-containing tripeptide, glutathione (GSH), to the thiol dipeptide, cysteinyl-cystine, and glutamate which can be taken up by the proximal tubule cell via a sodium-dependent transporter, the EAAC1 transporter (Shayakul et al., 1997).

1.3.2 Endocytic uptake of LMW-proteins

Low-molecular weight (LMW) proteins, such as vitaminD_3-binding protein (DBP), transferrin, retinol-binding protein (RBP), β_2- and α_1-microglobulin, among many others, as well as a small amount of albumin (usually between 180mg and 9g per day, Pollock & Poronnik, 2007) are filtered by the glomerulus and need to be reabsorbed to prevent their loss in the urine. In the proximal tubule, receptor-mediated endocytosis has been described as one of the most important uptake mechanisms for the reabsorption of these proteins (fig. 1.2) (Schwegler et al., 1991; Marshansky et al., 1997; Gekle et al., 2004). The filtered LMW proteins bind to the multiligand tandem membrane receptors, megalin and cubilin. Both receptors belong to the low-density lipoprotein (LDL) receptor family. In contrast to megalin, cubilin has little sequence homology with other known endocytic receptors. Since cubilin lacks a transmembrane domain, it is believed to interact with megalin before internalization. As a receptor complex, megalin has been suggested to facilitate the endocytosis and trafficking of cubilin. Proper expression of cubilin is dependent upon amnionless, a 45kDa transmembrane protein. Amnionless interacts with cubilin through EGF-type repeats of cubilin,

forming the cubam-complex (He et al., 2005; Birn, 2006; Birn & Christensen, 2006). Furthermore, structural or functional defects in either one of them results in LMW-proteinuria suggesting that both receptors are essential for the proper reabsorption of proteins (Zhai et al., 2000; Christensen & Birn, 2001; Norden et al., 2002). Once proteins are bound to the receptor, an internalization process is initiated. Adaptor molecules mediate the formation of a cytoplasmic clathrin coat. The ADP ribosylation factor (Arf) 6, among others, has been implicated in coat formation in the endocytic pathway (D'Souza-Schorey & Chavrier, 2006). Although Arf1 has been identified to play a role in the exocytic pathway, localization of Arf1 in the early endosomal pathway has also been described (Gu & Gruenberg, 2000; El Annan et al., 2004). Ligand-receptor complexes are pooled in clathrin-coated pits at the base of the microvilli. Yet unknown signals initiate the invagination of the coated pit. Finally, the vesicle buds off the membrane and protein-receptors complexes are internalized.

An important process along the endocytotic pathway is the proper endosomal acidification which influences ligand-receptor dissociation, vesicle trafficking, endosomal fusion and recycling to the plasma membrane (Christensen et al., 2003; Gekle et al., 2004). Endosomal acidification is established by active transport of protons in the vesicle by the vacuolar proton-pump, V-type H^+-ATPase or shortly V-ATPase (Wagner et al., 2004) and the Na^+/H^+-exchanger (discussed later). A large positive potential is generated by the V-ATPase and, unless this potential is dissipated, the proton pump will stop. Therefore, an electrical shunt is necessary to ensure efficient acidification. The chloride/H^+ exchanger, ClC-5, and the CFTR-channel have both been implicated in the endosomal acidification (Scheel et al., 2005; Jentsch, 2007; Jouret et al., 2007). Both transport systems bring chloride (Cl^-) in and neutralize the positive charges, so active proton pumping can be maintained. Coupling the V-ATPase to a chloride conductance ensures an acidification up to pH ~5 in the lysosomes (Devuyst et al., 2005; Wang et al., 2005; Hryciw et al., 2006). However, not all receptor-mediated endocytosis in the proximal tubule is dependent on ClC-5/CFTR; a significant fraction is also dependent upon Na^+/H^+-exchanger (Gekle et al., 1999; Gekle et al., 2004). The role of the Na^+/H^+-exchanger is limited to the early endosome since the transport will stop once Na^+ is pumped out of the

vesicle. Thus, key markers of the receptor-mediated endocytosis of proteins are the V-ATPase, megalin/cubilin, ClC-5 and the Na^+/H^+-exchanger, NHE_3.

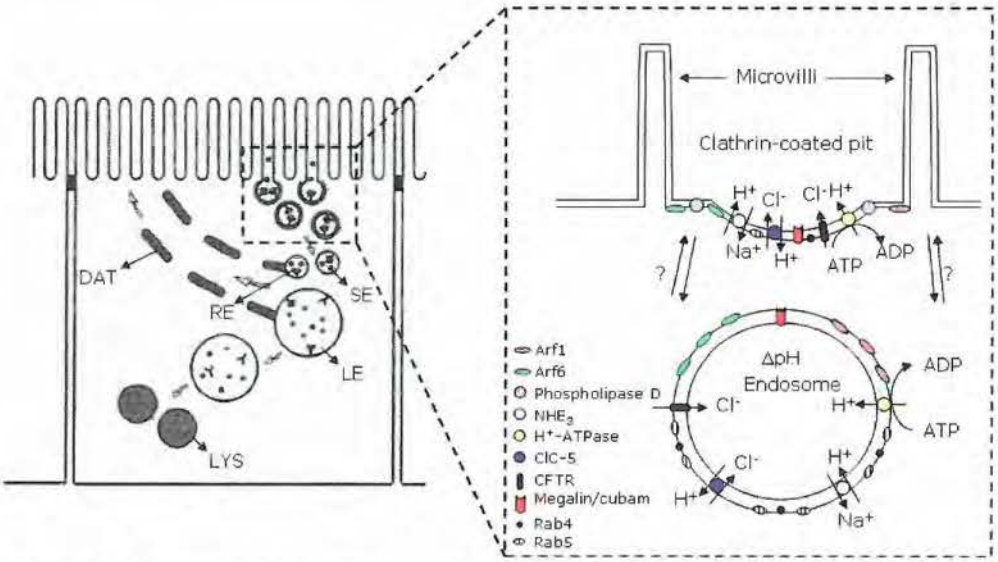

Figure 1.2: The endosomal pathway, endosomal vesicle formation and components of the endosome

Left: After binding of the ligand to megalin/cubam transporters, adapter proteins and bound receptors are pooled in the clathrin-coated pit at the base of the microvilli. The membrane invaginates and ultimately buds off to form the early endosome (inset) which further propagates to the sorting endosome (SE) where receptors and ligands are sorted. The receptors recycle back to the plasma membrane through the recycling endosome (RE) and the dense apical tubules (DAT). Ligands travel to the late endosome (LE) that fuses with the lysosome (LYS) where protein degradation takes place. *Right:* Clathrin-coated vesicles are formed at the base of the microvilli. Endosomal acidification is established by the Na^+/H^+ exchanger (NHE3), V-type H^+-ATPase, CFTR and ClC-5. Numerous chaperones and other molecules, such as ADP ribosylation factor (Arf), Rab GTPases (Rab4 &5) and phospholipases are involved in the formation, trafficking and fusion of the endosomes along the pathway. (Adapted from Christensen & Birn, 2001)

1.3.3 Sodium-dependent transport of solutes

Most reabsorbed solutes are transported against a concentration gradient from the tubular lumen into the proximal tubule cell. They are taken up at the apical membrane by cotransport systems that use the electrochemical gradient of Na^+ generated by the Na^+/K^+-ATPase. They move by facilitated but passive mechanisms from the cell to the interstitial space (fig. 1.3). Organic solutes that do not possess reabsorptive mechanisms are generally secreted. The secretion process also derives energy from the Na^+ electrochemical potential gradient (usually tertiary active transport processes). Furthermore, a low specificity ensures the secretion of a wide variety of solutes, including the by-products of metabolism and foreign substances. These transport processes are omitted from the figure since they are not dealt with in this thesis.

Almost all filtered glucose, phosphate and amino acids are reabsorbed in the proximal tubule. The reabsorption of glucose is characterized by a secondary active uptake driven by the inwardly-directed Na^+ electrochemical potential gradient at the apical membrane followed by a passive, facilitated transport through the GLUT-transporter at the basolateral membrane (Wood & Trayhurn, 2003). The protein responsible for the sodium-dependent uptake is the sodium-dependent glucose cotransporter, SGLT (Wright, 2001). Two types of SGLT have been described in the proximal tubule. The high-affinity, low-capacity transporter or SGLT type 1 in the straight tubule and the low-affinity, high-capacity SGLT2 in the convoluted tubule. A third type, SGLT3, has been identified, which shows transport characteristics that resemble the SGLT2, although there is still some controversy about the location and transport kinetics of this transporter (Table 1.1).

The localization of the 2 types of transporters in the proximal tubule reflects their function. In the S1/S2 segment, a large amount of glucose needs to be reabsorbed, thus the SGLT2, with low-affinity, high-capacity kinetics, is present. In the S3-segment, the remainder of glucose needs to be absorbed and this requires a high-affinity, low-capacity system so virtually no glucose is excreted in the urine. The Na^+-dependent system in the brush border transports the D-isomers of glucose, galactose and α- or β-methyl-D-glucoside, but 2-deoxy-D-glucose is only poorly transported.

SGLT can be inhibited by phloridzin at low concentrations, whereas the basolateral glucose transporter is much less sensitive to phloridzin but more sensitive to phloretin. This indicates that basolateral sugar transport is established by a passive, facilitated glucose transport mechanism namely, the type-2 GLUT-transporter in the early proximal tubule and GLUT1 in the late segment (S3).

Table 1.1: Transport characteristics of Na^+-dependent sugar transport in the proximal tubule

	SGLT1	SGLT2	SGLT3
$K_{0.5}$ (D-glucose)	0.4 mM	2 mM	6 mM
$K_{0.5}$ (Na^+)	3 mM	100 mM	1.5 mM
Na^+:glucose stoichiometry	2:1	1:1	2:1
K_i phloridzin	0.22 µM	1 µM	9 µM
Sugar selectivity	D-glucose ~ D-galactose	D-glucose ≥ D-galactose	D-glucose ≥ D-galactose
Na^+-uniport(*)	+	?	+
H_2O cotransport(**)	+	?	+

(*)The cotransporter can transport Na^+ in the absence of glucose with kinetics similar to the Na^+-glucose transport (Wright, 2001); (**) water can also be transported by SGLT (Loo et al., 1998; Loo et al., 1999).

Phosphate is transported by the NaPi cotransporter which is energized by the electrochemical gradient of Na^+ (Forster et al., 2006). Two types of NaPi transporters have been described in the proximal tubule. The NaPi type IIa translocates 3 Na^+ ions for 1 phosphate, while the type IIc has a Na^+/PO_4^{2-} stoichiometry of 2:1. The basolateral exit of phosphate is still controversial. Uptake of phosphate is under tight regulation of parathyroid hormone, PTH, which regulates the expression level of NaPi at the apical membrane. PTH increases phosphate excretion by endocytic removal of NaPi from the luminal membrane (Lotscher et al., 1999; Murer et al., 2002; Murer et al., 2003). Since phosphate is a major H^+ buffer in the proximal tubule, luminal and intracellular pH also determine the transport of phosphate. The NaPi cotransporter prefers to transport divalent over monovalent phosphate. Therefore, luminal acidification reduces phosphate reabsorption since the phosphate equilibrium is shifted to

H_2PO_4 On the other hand, intracellular acidification seems to drive phosphate reabsorption (Moschen et al., 2001).

The uptake of amino acids across the brush border membrane is established by secondary active, Na^+-dependent transport systems, followed by the passive exit at the basolateral membrane. Numerous transporters have been identified for the transport of neutral, cationic or anionic amino acids. Most of these transporters belong to the large family of sodium-coupled transporters (SLC) which are responsible for the uptake of several nutrients. Well-known transporters include the EAAC1-transporter (SLC1A1) and SNAT3 (SLC38A3) for glutamine, the B^0AT (SLC6A19) and $B^{0,+}AT$ (SLC7A9) transporters for the uptake of neutral or cationic amino acids, respectively, and the Na^+/proline transporter SIT (SLC6A20) (Camargo et al., 2005; Verrey et al., 2005; Broer, 2006; Moret et al., 2007). Glutamine is an important molecule for the synthesis of NH_4^+ and for gluconeogenesis. Therefore, glutamine is taken up in the proximal tubule at both the apical and basolateral membrane by a Na^+-dependent mechanism. Furthermore, also transporters for mono- and dicarboxylate (SMCT or NaDC respectively) are described in the proximal tubule (Burckhardt et al., 2005; Srinivas et al., 2005).

Since most of these transported solutes compete for the same energy source, an apparent competition could occur. This means that increasing the activity of one transporter can slow others. The mechanism for this competition can be described as follows. Sodium-coupled entry through one transporter increases locally the intracellular Na^+-concentration and thereby diminishes the Na^+-gradient for other cotransporters. Also, an electrogenic Na^+-dependent cotransporter could diminish the electrical gradient by transporting a positive charge into the cell (Murer et al., 1975).

Since, sodium-dependent solute cotransport at the apical membrane tends to depolarize the cell, Na^+ and solute reabsorption would diminish. To counteract this depolarization, K^+ is diffusing out of the cell through K^+-channels at the luminal membrane (Vallon et al., 2001).

The reabsorption of salt creates an osmotic gradient over the proximal tubule cell which attracts water to the interstitium. The proximal tubule cells are capable of transporting large amounts of water through the presence of water-channels, aquaporins, in the apical and basolateral membrane (Agre et al.,

2002). Aquaporin-1 (AQP1) is constitutively expressed in proximal tubule cells and is responsible for the majority of water reabsorption. A smaller fraction of water is transported via the tight junctions and the lateral intercellular space (LIS). The overall result is the reabsorption of large amounts of iso-osmotic fluid.

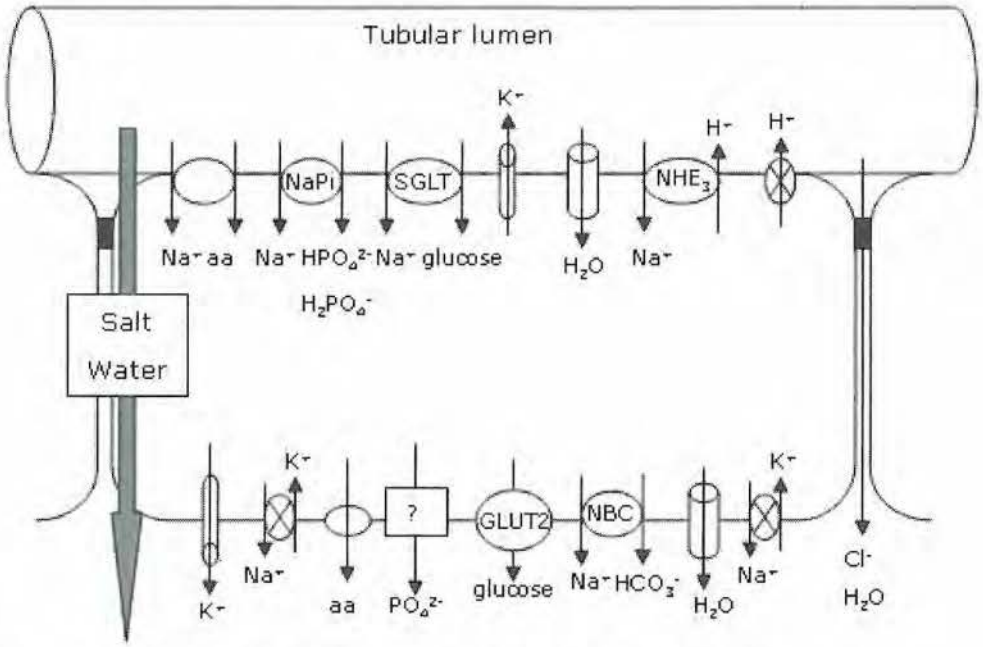

Figure 1.3: Transport of solutes and salt in the proximal tubule

At the apical membrane, solutes are taken up driven by the electrochemical gradient of Na^+, established by the Na^+/K^+-ATPase in the basolateral membrane. Electrogenic uptake of solutes depolarizes the apical membrane, enhancing the passive K^+ diffusion out of the cell. Solutes are generally transported through passive mechanisms at the basolateral side. Protons generated by the metabolism are pumped out by the V-ATPase or transported out by the Na^+/H^+-exchanger at the apical membrane. This mechanism is coupled to the uptake of HCO_3^-. Chloride (Cl^-) and water (H_2O) follow the transport of Na^+ due to the generated electrical or osmotic gradient respectively. Water reabsorption occurs either transcellularly through aquaporins, AQP1, or paracellularly. Reabsorption of Cl^- is mostly paracellular. The net result is reabsorption of water, salt and almost all solutes.

The functional differentiation of the proximal tubule is dependent upon the expression of different transcription factors. HNF-1-deficiency leads to a renal Fanconi-like syndrome characterized by polyuria, glucosuria, aminoaciduria and

phosphaturia (Witzgall, 1999; Pontoglio, 2000). Deficiency in the transcription factor, AP-2β, leads to an impaired tubular secretory function, ion homeostasis and severe hypocalcemia due to an abnormal functioning of the tubular and collecting duct epithelia (Moser et al., 2003). Other transcription factors involved in the maturation of the tubular epithelia still need to be discovered.

1.3.4 Intracellular signalling: hormone stimulated Ca^{2+}-responses

Hormones bind to their respective receptors and activate second messengers that initiate an intracellular signalling cascade resulting in their postulated response. Calcium (Ca^{2+}) is a universal second messenger used by a variety of hormones. The proximal tubule expresses various hormone receptors at its membranes. Parathyroid hormone (PTH) has multiple effects on the proximal tubule such as regulation of PO_4-transport and the metabolism of calciotropic hormones. PTH is filtered through the glomerulus, binds to megalin/cubilin at the luminal membrane of the proximal tubule and after internalization, PTH is degraded in the endosomal pathway. Deficient PTH metabolization through defects in the receptor-mediated endocytosis like in Dent's disease, often results in hyperphosphaturia and changed vitamin D plasma levels due to decreased degradation of PTH (Jentsch, 2005; Jentsch et al., 2005; Guggino, 2007). Decreased endocytosis of PTH will raise the luminal concentration of PTH in more distal segments of the proximal tubule, leading to an enhanced stimulation of the PTH-receptors and increased endocytosis of the apical Na-coupled phosphate transporter, NaPi, and hence hyperphosphaturia. Besides its effects on phosphate reabsorption, PTH also stimulates the mitochondrial enzyme 25(OH)vitaminD_3 1α-hydroxylase that is responsible for converting the inactive vitD_3 precursor to its active form, 1,25$(OH)_2$-vitD_3. Thus elevated luminal PTH will lead to enhanced production of active vitD_3. However, the inactive vitD_3 bound to vitD_3 binding protein (DBP) is also reabsorbed in the proximal tubule by receptor-mediated endocytosis. Therefore, a defect in the endocytosis process will also lead to decreased uptake of inactive vitD_3 and thus a decreased availability of the precursor hormone. The overall effect, a rise or decrease in serum levels of active vitD_3, is dependent upon a delicate balance between either the stimulation of the enzyme and the precursor scarcity (fig. 1.4).

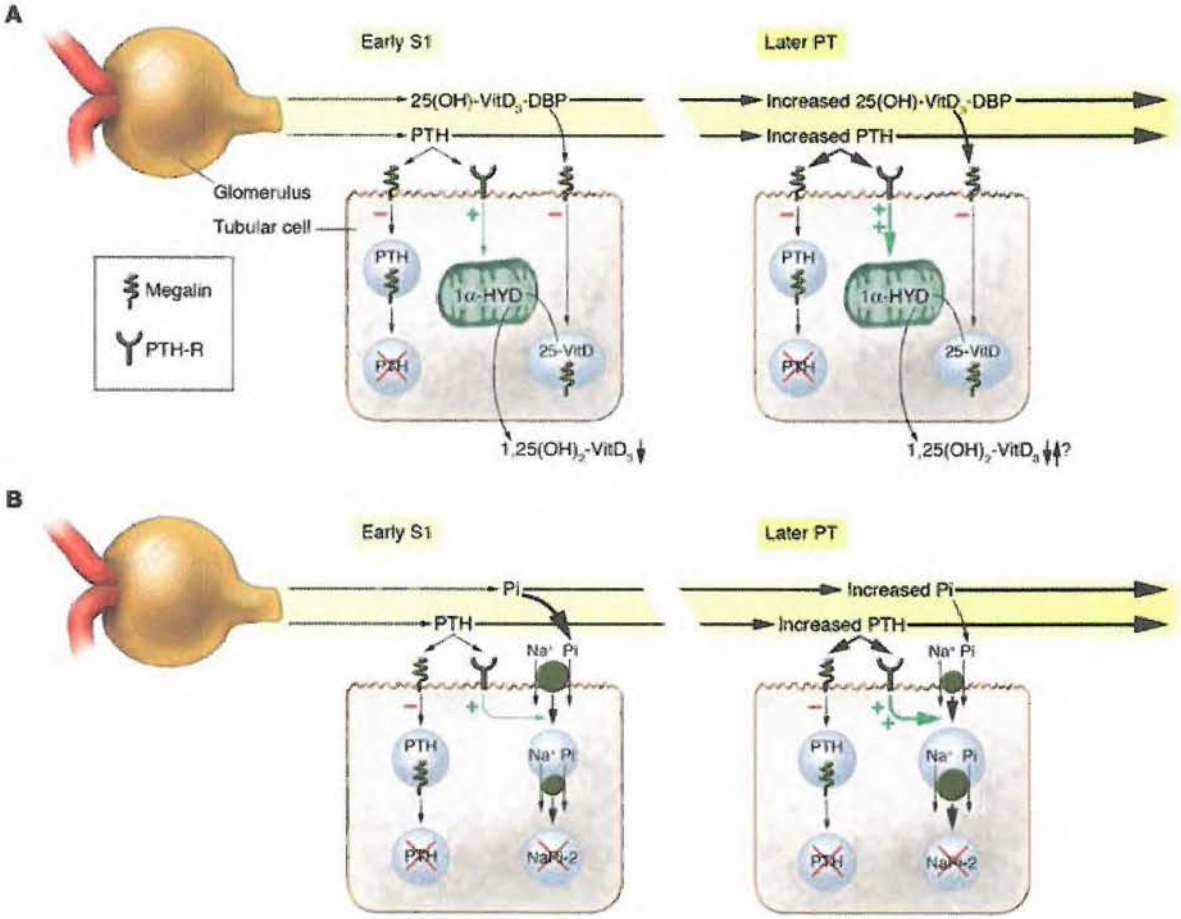
A
Early S1
Later PT
25(OH)-VitD3-DBP
PTH
Increased 25(OH)-VitD3-DBP
Increased PTH
Glomerulus
Tubular cell
Megalin
PTH-R
PTH
1α-HYD
25-VitD
1,25(OH)2-VitD3
1,25(OH)2-VitD3 ?
B
Early S1
Later PT
Pi
PTH
Increased Pi
Increased PTH
Na+ Pi
NaPi-2

Figure 1.4: Model to explain hyperphosphaturia and changed vitaminD_3 homeostasis in Dent's disease.

A: Alterations in the vitaminD_3 metabolism. B: Mechanisms causing phosphaturia. (according to Jentsch et al., 2005, with permission of Jentsch TJ)

Receptors for PTH have been localized at both the luminal and the basolateral membrane. The basolateral PTH receptor activates the adenylate cyclase/cAMP/protein kinase A (PKA) pathway, while the luminal PTH receptor activates the phospholipase C (PLC)/protein kinase C (PKC) signalling pathway. However, both pathways lead to the activation of the extracellular-signal regulated kinases (ERK)-signalling pathway that eventually results in the retrieval of the sodium-dependent phosphate cotransporter, NaPi, from the membrane and a decreased reabsorption of phosphate (Forster et al., 2006). Whereas PTH exerts its effects through intracellular signalling via cAMP after binding the basolateral receptor, angiotensin II (ATII) and bradykinin (BK) are two hormones that induce a Ca^{2+}-response in proximal tubule cells.

Angiotensin II has a receptor at both the luminal and basolateral membrane (fig. 1.5) (Douglas, 1987). However, the signalling mechanisms for both receptors are different and this explains the biphasic effect of ATII on salt and HCO_3^--reabsorption (Douglas, 1987; Romero et al., 1991). The basolateral receptor binds ATII in low (pM to nM) concentrations and inactivates via G_i-proteins (probably $G_{\alpha i}$) adenylyl cyclase which decreases the production of cAMP. Lower intracellular cAMP-concentrations in turn stimulate the Na^+/H^+-exchanger resulting in an increased Na^+-reabsorption. Usually in textbooks only the latter effect of ATII is described. However, high (nM to µM) concentrations of ATII stimulate the luminal ATII-receptor, which activates phospholipase A_2 (PLA_2) and formation of arachidonic acid (AA). In turn, AA is converted to 5,6-EET which inhibits Na^+/H^+-exchanger, Na^+/K^+-ATPase and Na^+/HCO_3^--cotransporter while increasing intracellular Ca^{2+}-concentration, $[Ca^{2+}]_i$. The net effect is an increased natriuresis.

Bradykinin binds to the B2-receptor which is present at both the apical and basolateral membrane in proximal tubule cells (fig. 1.5) (Shivakumar et al., 2005). Activation of B2 results in the activation of a Gq-protein and, consequently, in the activation of phospholipase C which catalyzes the formation of inositoltrisphosphate (IP_3) and diacylglycerol (DAG). IP_3 binds to its receptor

in the endoplasmic reticulum membrane resulting in a release of Ca^{2+} with increased $[Ca^{2+}]_i$. In a mouse proximal tubule cell line, TKPTS, and in primary cultures of rabbit proximal tubule cells, a fast and transient increase in $[Ca^{2+}]_i$ was observed, indicating that Ca^{2+} is released from intracellular stores (Tiwari and others 2005).

The increase in $[Ca^{2+}]_i$ would activate an outward rectifying chloride current in proximal tubule cells and in this way influence salt transport, however the precise mechanisms are not yet known (Tiwari et al., 2007). Furthermore, BK seems to counteract the stimulation of the Na^+/K^+-ATPase induced by low ATII concentrations (Caruso-Neves et al., 1999; Caruso-Neves et al., 2003).

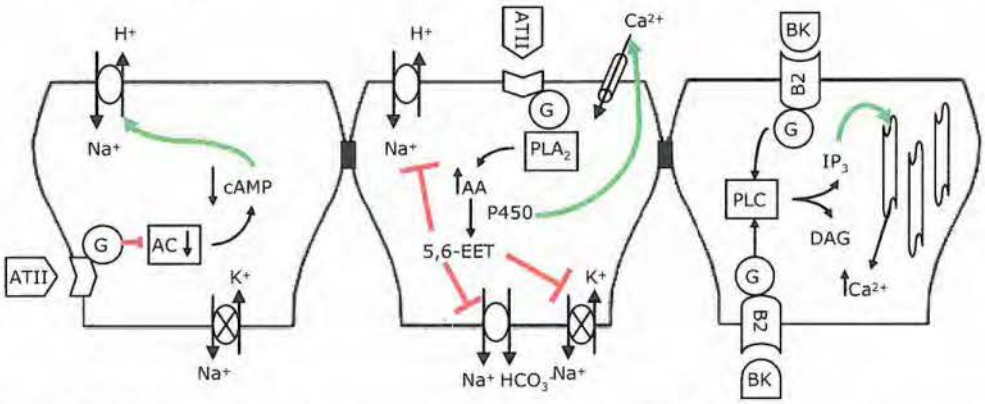

Figure 1.5: Biphasic effect of angiotensin II on salt and HCO_3^- reabsorption and bradykinin response in PTC

Left: Low concentrations of ATII (pM to nM) activate basolateral receptors leading to activation of G_i-proteins (G), decreasing adenylate cyclase (AC) activity and subsequently decreasing cAMP-concentration in the cell. Lowering [cAMP] abolishes the inhibition of the Na^+/H^+-exchanger leading to increased Na^+-influx. The net effect is thus an increased Na^+-reabsorption.

Middle: High concentrations of ATII (nM to µM) activate apical receptors leading to activation of G-proteins (G) and stimulation of phospholipase A_2 (PLA_2) and subsequent formation of arachidonic acid (AA). The P450 epoxygenase (P450) transforms AA into 5,6-epoxy-eicosatrienoic acid (5,6-EET) which inhibits the Na^+/H^+-exchanger, the Na^+/HCO_3^--cotransporter and the Na^+/K^+-ATPase while Ca^{2+}-influx is increased. The overall net effect will be an increased natriuresis.

Right: Stimulation of the B2-receptor with BK activates PLC and formation of second messengers IP_3 and DAG. IP_3 binds its receptor in the endoplasmic reticulum thereby activating Ca^{2+}-release from the ER. The net results is an increase in $[Ca^{2+}]_i$.

1.4 Electrophysiological properties of the proximal tubule

Since the two-membrane hypothesis of Koefoed-Johnson and Ussing has been postulated about a half century ago, numerous techniques and methods have been developed to elucidate the electrophysiological properties of epithelia. However the basic feature of this hypothesis, namely that opposite cell membranes of epithelial cells possess different transport properties, still stands (Lindemann, 2001; Reuss, 2001). This structural and functional asymmetry forms the basis of vectorial transport in epithelia. The electrical properties of a transporting epithelium are governed by two main pathways: (1) the transcellular pathway, which is controlled by energy-dependent transporters and channels that are asymmetrically distributed on the apical and basolateral membrane and; (2) the paracellular pathway in which tight junctions seal off the intercellular space and regulate the passive diffusion of ions and small (non)charged solutes via the paracellular space. Therefore, the electrical model of the proximal tubule can be represented as a low-resistance paracellular pathway existing in parallel with the transcellular pathway.

The low-resistance paracellular pathway indicates that tight junctions are permeable to ions. The tight junction architecture is very important in determining the resistance of the transepithelial transport. In very leaky epithelia, the tight junction is only composed out of one or two protein strands, whereas tight epithelia exhibit junctions with several strands. The leaky nature of the tight junction combined with the high amount of aquaporins in the apical and basolateral membranes in proximal tubules allows the reabsorption of large amounts of iso-osmotic fluid.

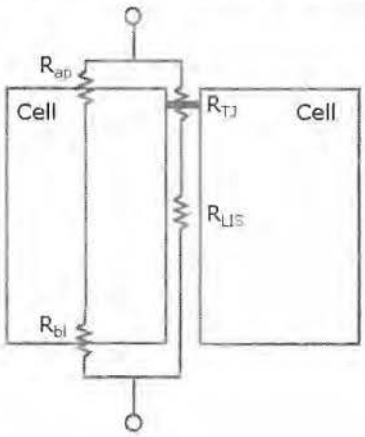

Figure 1.6: Simplified electrical model of resistance to transepithelial current flow.
The resistance of the apical membrane (R_{ap}) is in series with that of the basolateral membrane (R_{bl}). These resistances in series are in parallel with the resistance of the tight junction (R_{TJ}) and the additional series resistance generated by current flowing through the lateral membrane into the LIS (R_{LIS}). (Adapted from Madara, 1998)

The lateral intercellular space (LIS) reaches from the tight junction to the basement membrane, meaning the path depth is approximately similar to the height of the cell. In fact, the path depth may even exceed the height of the cell, since numerous folds in the basolateral membrane increase the size of the LIS. The LIS is involved in the transepithelial transport of Na^+ and water. A number of studies have shown that osmotic water flow from the lumen to the peritubular space causes a significant dilation of the LIS. This expansion in the LIS seems to be caused by augmented water flow to the LIS resulting in an increased pressure within the LIS and thus dilation (Sackin & Boulpaep, 1975; Kottra & Frömter, 1983; Kottra & Frömter, 1993; Spring, 1998). The LIS also plays a role in determining the transepithelial resistance. The LIS could account for an additional resistance, in series with the resistance of the tight junction and parallel to the resistance of the apical and basolateral membrane (fig. 1.6). Furthermore, this resistance might vary depending on the length and the volume of the LIS (Madara, 1998).

Besides the paracellular pathway, the resistance of the transcellular route is also important in characterizing the electrical properties of the epithelium. The proximal tubule possesses a large number of transporters in both the apical and basolateral membrane (as already indicated in section 1.3.3). The high transport rate of these transporters renders a large ionic conductance to the epithelium. Therefore, the proximal tubule epithelium has a very low specific epithelial resistance and a very high ion transport rate as compared to a tight epithelium (as shown in table 1.2).

The potential difference varies along the length of the proximal tubule. The lumen-negative potential difference in early proximal tubule is a result of the presence of glucose, amino acids and phosphate in the glomerular filtrate, which are cotransported with Na^+ across the luminal membrane, thereby depolarizing the luminal membrane potential difference. Furthermore, in the early proximal tubule cells protons secreted by the Na^+/H^+-exchanger and the H^+-ATPase will rapidly buffer the filtered HCO_3^- to H_2CO_3. The carbonic anhydrase (type IV) in the luminal membrane will convert H_2CO_3 into H_2O and CO_2. CO_2 will diffuse into the proximal tubule cell, while H_2O is transported through aquaporins. Intracellularly, H_2O and CO_2 will form HCO_3^- and H^+ again by an intracellular carbonic anhydrase (type II). Subsequently, HCO_3^- will be transported across the

basolateral membrane by a $Na^+/3HCO_3^-$ cotransporter (NBC). Overall, the presence of carbonic anhydrases and proton secretion across the luminal membrane, mainly via the Na^+/H^+-exchanger, result in a rapid buffering and reabsorption of filtered HCO_3^- (Boron, 2006). Combined with the reabsorption of water, the reabsorbate will mainly consist of $NaHCO_3$ in the early proximal tubule. This leads to a drop in the luminal concentration of HCO_3^-, and a rise in Cl^--concentration in the middle and late proximal tubule. A lumen-positive potential is registered as a result of the passive Cl^--reabsorption along the paracellular pathway due to a Cl^--gradient towards the blood (Barratt et al., 1974; Frömter & Gessner, 1974).

Table 1.2: Electrophysiological characteristics of leaky versus tight epithelia

	Transepithelial resistance (R_m) $\Omega.cm^2$	Transepithelial potential (V_T) mV	Ion transport rate (J_{Na}) $\mu M.cm^{-2}.hr^{-1}$	Osmolality transported fluid/ osmolality bathing fluid
Leaky epithelia:				
Proximal tubule	5 – 30	- or + 1 – 3	10 – 60	1
Gall bladder				
Small Intestine				
Tight epithelia:				
Frog skin	40 – 2000	30 – 100 (lumen negative)	2 – 10	1.5 - 5
Urinary bladder				
Collecting tubule				

(Adapted from Frömter, 1972; Maude, 1972; Lewis et al., 1996)

Leaky epithelia, like the proximal tubule, have a low resistance and transepithelial potential difference and they typically move large volumes of iso-osmotic fluid. On the contrary, tight epithelia of high resistance can generate and maintain high transepithelial electrical potentials and can create intraluminal fluids with compositions that deviate significantly from those of interstitial fluid.

1.5 Renal tubulointerstitial fibrosis

The mammalian kidney is a complex organ consisting of several tissues and a large number of distinct cell types. A multiplicity of epithelial cell types lines the fluid-filled tubules, differing morphologically and functionally depending on the segment of the tubule in which they arise. They are connected by junctional complexes which make up tissue integrity and allow intercellular communication. Asymmetry is essential to epithelial cell function since different transport systems are associated with the two membranes. Underlying the epithelial cell layer is a basement membrane, a complex network of proteins and carbohydrate-rich macromolecules, which confer a relatively static shape to the tubule. Underneath the basement membrane are fibroblasts which together with the epithelial cells participate in basement membrane biogenesis and synthesize collagens which comprise much of the extracellular matrix.

Whatever the primary insult, for instance glomerular injury, protein overload, hypertension, hypoxia, diabetes or continued toxic insults, the integrity of essentially the proximal tubular epithelium will be disrupted leading to its dysfunction. The latter is central to generate progressive chronic renal failure. Damage to the epithelium, elicited either by ATP depletion or a direct intracellular toxic insult, activates a network of cytokines and growth factors released by tubular and inflammatory cells and leading to renal tubulointerstitial fibrosis, which is considered to be the final common pathway leading to end-stage renal failure. The degree of fibrosis correlates well with the deterioration of renal function and the long-term prognosis, irrespective of the initial cause of the injury (Eddy, 1996). The process of tubulointerstitial fibrosis is characterized: (1) by the loss of renal tubules, (2) *de novo* expression of α-smooth muscle actin (α-SMA)-positive myofibroblasts and (3) the accumulation of extracellular matrix. It is widely accepted that myofibroblasts are responsible for the excessive deposit of extracellular matrix proteins and also overproduction of the profibrotic cytokine, transforming growth factor-β1 (TGF-β1). However, there is a large debate on the origin of α-SMA$^+$-myofibroblasts. They may originate from bone marrow cells, resident interstitial fibroblasts or tubular epithelial cells (Yang & Liu, 2001). Iwano et al. stated that one third of the interstitial fibroblasts originated from renal tubular epithelium via a process called epithelial-to-mesenchymal transition (EMT) (Iwano et al., 2002).

Furthermore, the pathological chain of events is not clear. Does an inflammatory response trigger the fibrotic process or do injured tubular cells send out signals that activate cells and attract the inflammatory cells? A majority of studies suggests that injured tubule cells produce and secrete chemokines and growth factors that attract mononuclear cells and macrophages, activate resident immune cells and stimulate fibroblast proliferation and production of interstitial proteins. In turn, infiltrating immune cells may stimulate renal tubule epithelial cell transdifferentiation. However, epithelial cells can also produce growth factors, such as TGF-β1, that induce transdifferentiation in an autocrine or paracrine fashion (O'Donnell, 2000; Schmitz, 2000; Klahr & Morrissey, 2002).
Proteinuria seems to have a strong predictive value in chronic nephropathies. The loss of proteins in the urine can either be the result of a diseased glomerulus resulting in an excessive filtration of proteins and subsequent overload, or due to primary failure of the uptake mechanisms for proteins in the proximal tubule. Primary or secondary impaired proximal tubule function due to for instance ATP-depletion, genetic disorders such as Dent's disease or chronic exposure to nephrotoxic substances like cisplatin, cadmium among others directly inhibit receptor-mediated endocytosis and eventually this leads to tubulointerstitial fibrosis (Choi et al., 1999; Takano et al., 2002). Protein overload caused by a primary glomerular defect induces the expression of a wide array of proinflammatory and profibrotic mediators in renal tubular cells mainly through the activation of the transcription factor NF-κB and the signal transducer and activator of transcription (STAT) signalling pathway (D'Amico & Bazzi, 2003; Nakajima et al., 2004; Abbate et al., 2006).

1.5.1 The process of epithelial-to-mesenchymal transdifferentiation

In the process of EMT, renal tubule cells lose their epithelial phenotype and acquire mesenchymal properties. During EMT, four major events can be distinguished (fig. 1.7). First, cell adhesion and cell polarity are lost due to the disassembly of tight junctions and decreased E-cadherin expression. Second, actin is reorganized into stress fibers and there is *de novo* α-SMA expression. Third, the tubular basement membrane is disrupted by enhanced activity of metalloproteinases. And finally, cells become motile through the contractile properties of the α-SMA-filaments and they migrate into the interstitium where

they are responsible for the excessive deposit of extracellular matrix (Yang & Liu, 2001; Liu, 2004).

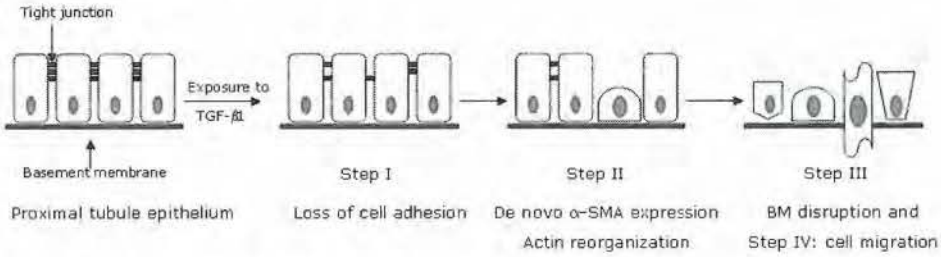

Figure 1.7: Major events during EMT

Upon exposure to TGF-β1, epithelial cells undergo EMT. The first event is the loss of cell adhesion by disassembly of the tight junction. This is followed by the change in cell morphology due to a reorganization of the actin cytoskeleton and *de novo* expression of α-SMA. Disruption of the basement membrane (BM) and enhanced contractility enables the cells to migrate to the interstitium. (Adapted from Yang & Liu, 2001)

EMT is quite interesting because the majority of renal tubules, except the collecting duct, is derived from the metanephric mesenchyme during development through the reverse process, mesenchymal-to-epithelial transdifferentiation (MET) (Horster et al., 1999; Schmidt-Ott et al., 2006). Knowing that the proximal tubule's origin is mesenchymal, the possible involvement of EMT during tubulointerstitial fibrosis is strengthened.

1.5.2 The role of TGF-β1 as inducer of EMT

Numerous studies have pointed out that proximal tubule cells can undergo epithelial to mesenchymal transdifferentiation (EMT) into α-SMA$^+$-myofibroblasts upon exposure to TGF-β1, a potent profibrotic cytokine produced by tubular epithelial cells and/or inflammatory cells following an insult or damage (Yang & Liu, 2001; Lan, 2003; Tian et al., 2003; Liu, 2004). However, a combination of cytokines is usually present in the area of tissue injury, so it is difficult to assign priorities or hierarchy. Each moiety may contribute a unique inducement of the transition or their effects may intermingle. Epithelial signalling of different cytokines and growth factors will eventually lead to the activation of transcription factors that regulate the expression of the EMT proteome (see Kalluri & Neilson, 2003). The best known transcription factors of the EMT transcriptome include Snail, Twist, HMGA2, Slug, LEF-1, FSP-1, CBF-A and Ets-1

(Fig. 1.8). However, this set of transcription factors is far from complete (Lee et al., 2006; Neilson, 2006; Teng et al., 2007; Venkov et al., 2007).

TGF-β1 is a prototypical, multifunctional cytokine with well-known physiological effects in e.g. wound-healing. The functions of TGF-β1 can be divided into three broad areas: modulation of inflammatory cell function, growth inhibition and differentiation, and control of extracellular matrix production. However, within the kidney, TGF-β1 is recognized to play the most important role in renal fibrosis and progressive kidney disease.

TGF-β1 production during kidney disease is elevated in response to numerous factors such as hypoxia, hyperglycemia, excessive protein filtration and reabsorption, mechanical and metabolic cell stress, elevated levels of angiotensin II (ATII) among others. Besides TGF-β1, angiotensin II also seems to play a central role in the progression of renal fibrosis since blockers of the angiotensin converting enzyme (ACE-inhibitors) have a renoprotective effect (Klahr & Morrissey, 2000). By binding to the ATII-type 1 (ATI) receptor, ATII induces the transcription factor NF-κB which results in vasoconstriction, growth stimulation and profibrogenic effects, as well as the production of reactive oxygen species (ROS) (Wolf et al., 2002). Oxidative stress mediates a wide range of renal impairments. ROS are generated in response to injuries caused by ischemia/reperfusion, drugs, heavy metals, glomerular damage and during chronic renal failure. Furthermore, the TGF-β1-induced response can be modulated by ROS (Rhyu et al., 2005).

During tubular injury, there is an increased expression of TGF-β1 leading to an imbalance between production and degradation of extracellular matrix. Its pathogenic effects in the kidney during chronic disease are indicated in figure 1.8 (Border & Noble, 1994; Bottinger & Bitzer, 2002).

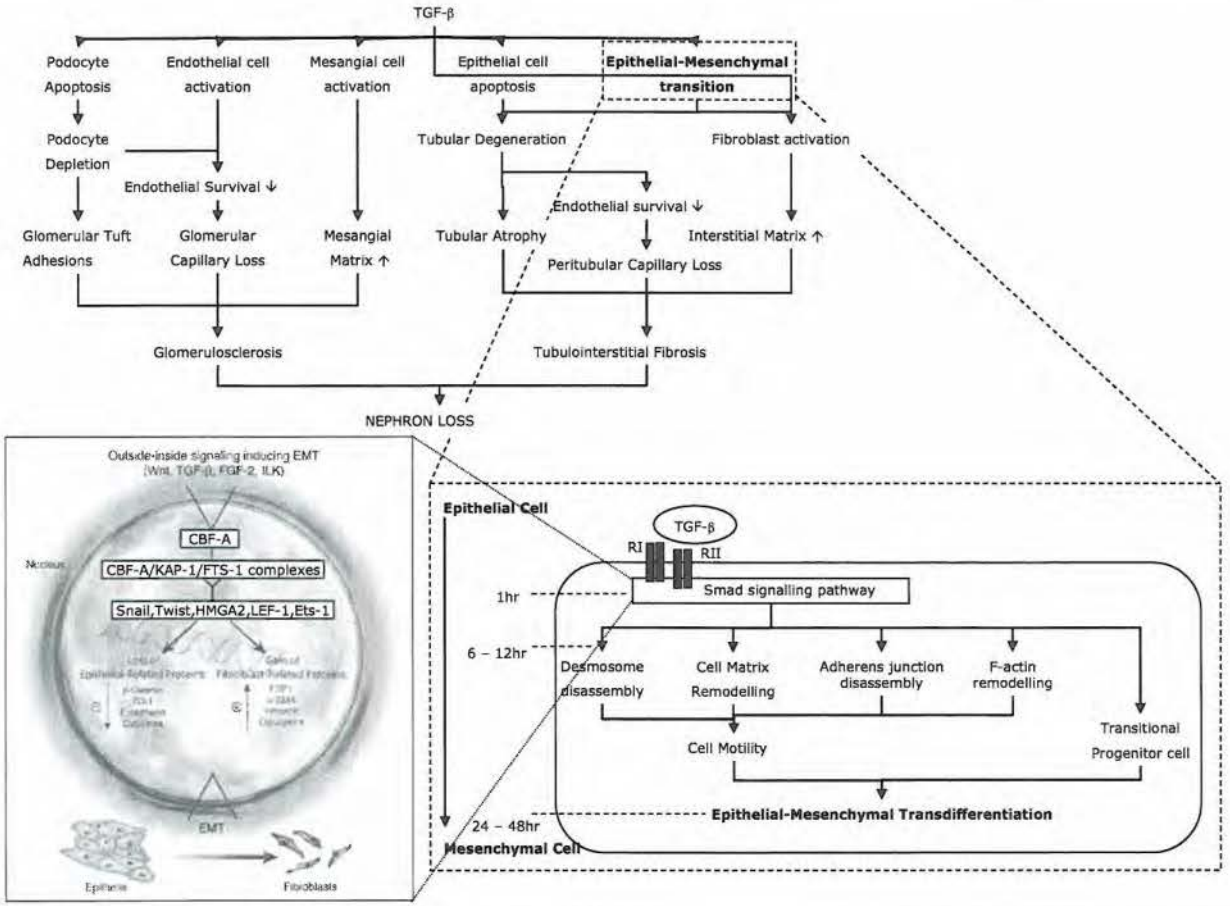
TGF-β
Podocyte Apoptosis
Endothelial cell activation
Mesangial cell activation
Epithelial cell apoptosis
Epithelial-Mesenchymal transition
Podocyte Depletion
Endothelial Survival ↓
Tubular Degeneration
Fibroblast activation
Endothelial survival ↓
Glomerular Tuft Adhesions
Glomerular Capillary Loss
Mesangial Matrix ↑
Tubular Atrophy
Interstitial Matrix ↑
Peritubular Capillary Loss
Glomerulosclerosis
Tubulointerstitial Fibrosis
NEPHRON LOSS
Outside-inside signalling inducing EMT
(Wnt, TGF-β, FGF-2, ILK)
CBF-A
CBF-A/KAP-1/FTS-1 complexes
Snail,Twist,HMGA2,LEF-1,Ets-1
EMT
Epithelial Cell
TGF-β
RI
RII
Smad signalling pathway
1hr
6 – 12hr
Desmosome disassembly
Cell Matrix Remodelling
Adherens junction disassembly
F-actin remodelling
Cell Motility
Transitional Progenitor cell
24 – 48hr
Epithelial-Mesenchymal Transdifferentiation
Mesenchymal Cell

Figure 1.8: TGF-β1-effects on renal cells during chronic renal disease
TGF-β1 exerts many effects on renal cells ultimately resulting in the loss of nephrons and a malfunctioning of the kidney. Epithelial-mesenchymal transdifferentiation is one process activated by TGF-β1 that describes the change from an epithelial cell phenotype to a mesenchymal cell. The mesenchymal phenotype is the α-SMA$^+$-myofibroblast, which is responsible for the excessive production of extracellular matrix proteins.
Inset: Cellular effects of TGF-β1. TGF-β1 binds to its receptor (RI – RII) and Smad signalling cascade is activated; that has multiple effects depending on the mediator activated downstream. Ultimately, it results in changed tubular epithelial cell morphology, due to actin reorganization and loss of epithelial cell adhesion to the matrix and neighbouring cells. The cells become motile and invade the underlying interstitium. The complete transformation of an epithelial cell to a mesenchymal cell or epithelial-mesenchymal transdifferentiation is usually complete within 48h in cultured cells *in vitro*. (Adapted from Bottinger & Bitzer, 2002; Venkov et al., 2007)

TGF-β1 is secreted by the cells as an inactive form bound to the latency-associated peptide (LAP). The so-called latent-TGF-β1 is stored at the cell surface and in the extracellular matrix. The mechanisms for the conversion to the 25-kD active dimeric protein are yet unknown. TGF-β1 binds to at least three membrane receptors, type I, II and III, which are present on virtually all cells. Receptors I and II are transmembrane serine-threonine kinases that interact with one another and facilitate each other's signalling. Receptor type III, also called betaglycan, has no signalling function but acts to present TGF-β1 to the other receptors (Border & Noble, 1994; Schnaper et al., 2003). Besides activating EMT in renal epithelial cells, TGF-β1 can also induce apoptosis. Dead tubule cells will be shed into the urine and can obstruct the tubular lumen downstream, thereby worsening the disease progression.
The imbalance between pro- and anti-fibrotic cytokine expressions is crucial in the development of tubulointerstitial fibrosis (Zeisberg et al., 2003; Zhang et al., 2005). Bone morphogenetic protein (BMP) is another member of the Transforming Growth Factor-β superfamily and plays a crucial role during renal development, where its expression correlates with the condensation of the metanephric mesenchyme to generate epithelium (Vukicevic et al., 1996). In adult kidney, BMP-7 expression is localized in the distal nefron mainly in the medullary region and in glomerular podocytes (Gould et al., 2002), where it is thought to maintain the differentiated phenotype of tubular cells (Kopp, 2002).

BMP type-7 has been described to counteract the effects of TGF-β1, as summarized in Table 1.3 (Kopp, 2002; Zeisberg et al., 2003; Neilson, 2005).

Table 1.3: Actions of TGF-β1 and BMP-7 in the kidney

TGF-β1	BMP-7
Inhibits tubule morphogenesis during kidney development	Mediator of MET in kidney embryogenesis
Increased TGF-β1 expression during the progression of chronic renal disease	Decreased BMP-7 expression during chronic renal disease
Induces EMT in chronic renal disease	Reverses EMT in chronic renal disease
Activates interstitial fibroblast to differentiate in myofibroblasts during chronic renal disease	Controls fibroblast activation

Furthermore, BMP-7 seems to induce mesenchymal-to-epithelial transdifferentiation (MET) (Zeisberg et al., 2005) in mouse models of renal injury. However, the expression of BMP-7 has been suggested to decrease in response to injury, while TGF-β1 expression is upregulated. These observations strengthen the use of BMP-7 as a therapeutic agent in the prevention or treatment of tubuinterstitial fibrosis.

1.5.3 Markers for tubulointerstitial fibrosis

Since it is still unclear which time point or degree of transdifferentiation is the point of no return for possible recovery of the epithelial phenotype, it is necessary to find good markers that are expressed early in the process of EMT. α-SMA has been widely accepted as a marker for myofibroblasts (Powell et al., 1999) and renal tubulointerstitial fibrosis. The expression of α-SMA correlates with the change in epithelial cell morphology. However, this might indicate that α-SMA is expressed in a later stage of EMT.

One could rely on the identification of the fibrosis process through detection of extracellular matrix (ECM) proteins, like fibronectin or collagens. Fibronectin is a glycoprotein secreted by α-SMA$^+$-myofibroblasts during interstitial fibrosis. Its function is to link matrix molecules to one another or to cells and in this way to provide mechanical coupling of the actin cytoskeleton to the extracellular matrix.

The binding of fibronectin to integrins in the cell membrane induces clustering of integrins, actin and actin binding protein as well as actin reorganization which results in the formation of focal adhesions (Hocking et al., 2000; Wang et al., 2005). The focal adhesion is a transmembrane complex, composed of intracellular contractile microfilaments (such as α-SMA) and the extracellular matrix protein, fibronectin, connected by the integrin receptor (Hinz, 2006) (fig. 1.10B). In myofibroblasts, multiple focal adhesions seem to cluster into a supermature focal adhesion or fibronexus (Dugina et al., 2001).

Furthermore, fibronectin seems to regulate the assembly of extracellular matrix proteins, such as collagens, and also the assembly of latent TGF-β1-binding protein-1 (LTBP1) into the ECM, which is important for the regulation of growth factor activity (Dallas et al., 2005). However, like the expression of α-SMA these specific changes come about in a later stage of the fibrotic process.

The first event to occur after tubular injury is the disruption of the epithelial integrity. Epithelial cells are, as indicated in the previous sections, connected to each other by tight junctions, that have important roles in proper cell functioning. The tight junction is composed of many different proteins, among them are claudins, occludins, junction adhesion molecule (JAM) and zonula occludens proteins 1, 2 and 3 (ZO-1, 2 and 3). Whereas claudins and occludins are transmembrane proteins that interact with proteins from neighbouring cells and form the protein strands within the tight junction, ZO-proteins have a scaffolding function and connect claudins and occludins to the actin cytoskeleton (fig. 1.9 and fig. 1.10E). ZO-proteins are members of the membrane-associated guanylate kinase homologue protein family (MAGUK) and they are important for the assembly and regulation of the tight junction, among other functions (Mitic & Anderson, 1998; Gonzalez-Mariscal et al., 2000; Van Itallie & Anderson, 2004; Van Itallie & Anderson, 2006). Their importance in the structure and function of the tight junction makes the ZO-proteins an interesting marker in following the disruption of the epithelium. Furthermore, in a study by Tian and coworkers, the tight junction was disassembled after exposure to TGF-β1 (Tian & Phillips, 2002).

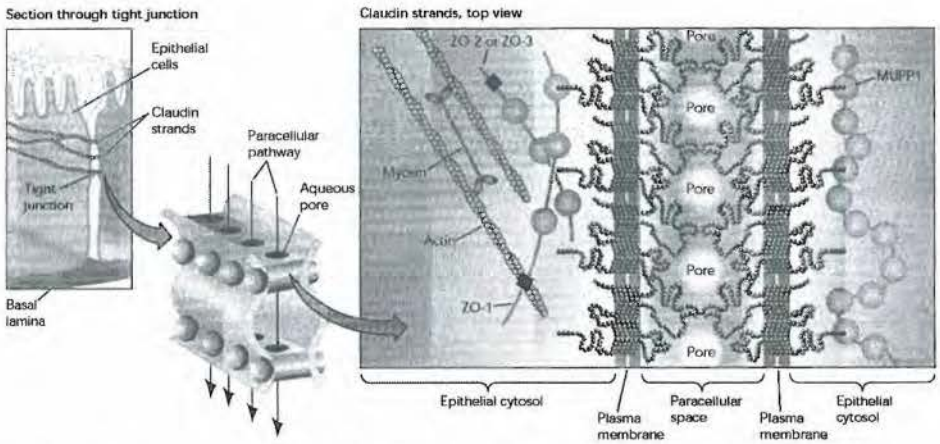

Figure 1.9: The architecture of the tight junction
Zonula Occludens proteins (ZO) 1, 2 and 3 act as scaffolding proteins that bind the transmembrane proteins, like claudins and occludins, to the actin cytoskeleton. MUPP1: Multi-PDZ-containing protein 1. (Adapted from Van Itallie & Anderson, 2004)

Another early marker for tubulointerstitial fibrosis has recently been discovered (Patschan et al., 2007; Sakairi et al., 2007). Nestin is a cytoskeleton-associated class IV intermediate filament protein. Intermediate filaments (IF) are cytoskeletal structures formed by members of a family of related proteins. Based on sequence similarities, IF can be divided into 5 major classes (Table 1.4). However, all IF proteins have a similar structure which consists of: (1) a highly conserved, 40nm long central rodlike domain that is a coiled-coil dimeric structure, formed by coiling of the α-helical sections of two polypeptides around each other; and (2) the C- and N-domains which are globular and vary widely among IF proteins. Their function is to provide mechanical support to the cell. Therefore, IF are highly abundant in the perinuclear region and around cell-cell and cell-matrix interactions (fig. 1.10). Nestin was originally identified in neuroepithelial cells. In non-neural tissue, nestin is usually expressed during embryogenesis and is very limited in adult organs. In the developing kidney, nestin is expressed by epithelial cells of immature proximal tubules, while in the mature kidney, nestin expression is only observed in podocytes. Nestin re-expression has been shown in tubulointerstitial fibrosis in mature renal tubules after injury (Patschan et al., 2007; Sakairi et al., 2007). However, its precise role and occurrence in the fibrotic process needs to be defined in detail.

Table 1.4: Classes of intermediate filaments, their tissue distribution and associated cell structures

IF protein	Tissue distribution	Associated cell structure
Type I		
Acidic keratins (*) (ex. cytokeratins 9, 10, 12 through 19)	Epithelia	Desmosomes and hemi-desmosomes (fig. 1.9B and D)
Type II		
Basic keratins (*) (ex. cytokeratins 1 trough 8)	Epithelia	Desmosomes and hem-idesmosomes (fig. 1.9B and D)
Type III		
Desmin	Muscle	Perinuclear region (frequently terminate on the nuclear membrane), desmosomes and hemidesmosomes (fig. 1.9B, D and F)
Glial fibrillary acidic protein / Peripherin	Neuronal cells Mesenchyme	
Vimentin	Epithelia (***)	
Type IV		
Low (L), Medium (M) and High (H) molecular weight Neurofilaments (NF)	Neuronal cells	Axonal microtubules
Nestin (**)	Neuroepithelial cells Developing cells	In developing cells and in some pathologic situation it is re-expressed
Type V		
Lamin	All cells	Nucleus
Laminin		Extracellular (fig. 1.9B)

(*) keratins are obligate heterodimers containing 1:1 mixture of acidic and basic IF polypeptides; either type alone cannot assemble into a keratin filament. (**) Nestin is here also categorized as a class IV IF based on its exon organization in its genes. However, sometimes nestin is identified as a class VI IF probably due to its role in the development. (***) Vimentin is associated with some epithelial cells, usually during regeneration after epithelial damage. (Adapted from Lodish et al, 1995)

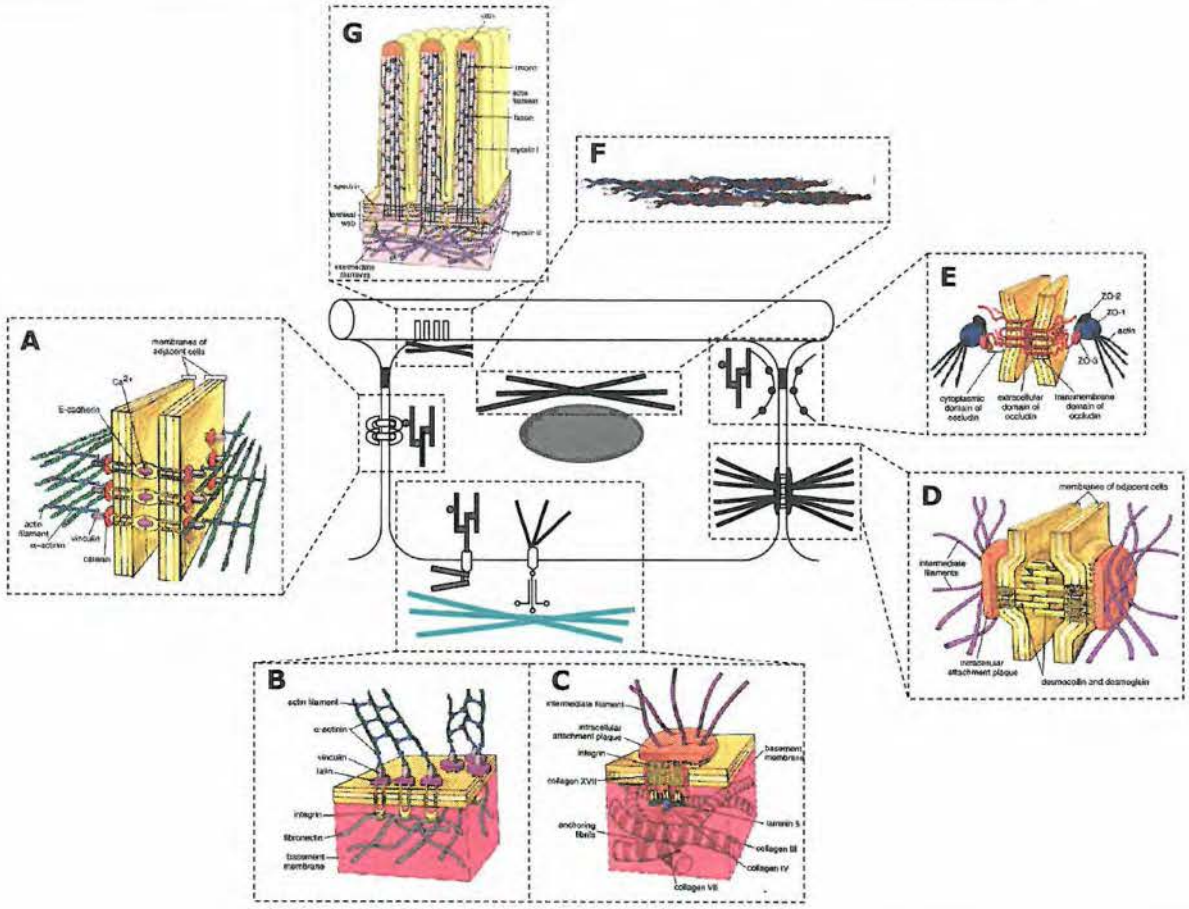
G
F
E
ZO-2
ZO-1
actin
ZO-3
cytoplasmic domain of occludin
extracellular domain of occludin
transmembrane domain of occludin
A
membranes of adjacent cells
E-cadherin
actin filament
vinculin
catenin
D
membranes of adjacent cells
intermediate filaments
desmocollin and desmoglein
B
actin filament
vinculin
talin
integrin
fibronectin
basement membrane
C
intermediate filament
intracellular attachment plaque
integrin
collagen XVII
basement membrane
anchoring fibrils
laminin 5
collagen III
collagen IV
collagen VII

Figure 1.10: Overview of cell-cell and cell-matrix contacts and the localization of intermediate filaments.

A: Zonula adherens is composed of the integral membrane protein, cadherin that links adjacent cell membranes in a Ca^{2+}-dependent manner to each other and to the terminal web of actin filaments. The zonula adherens provides mechanical coupling to sheets of cells. **B:** Focal contacts are integrin-based contacts that link the cell to the basal lamina through fibronectins. Integrins are associated with the actin cytoskeleton at the intracellular side. **C:** Hemidesmosomes link cells to the basal lamina in an integrin-based manner through the interaction with laminin which interacts with the underlying collagen-matrix. The intracellular attachment plaque binds integrins to intermediate filaments. **D:** Desmosomes or macula adherens are cell-cell contacts with similar structure as the hemidesmosome. **E:** Tight junction or zonula occludens is described in detail in fig. 1.9. **F:** Structure of an intermediate filament. **G:** The association of intermediate filaments with the apical microvilli and the terminal web of actin filaments. (Adapted from Alberts et al., 2002).

1.6 Aims of the thesis

In the past, model systems to investigate kidney function were frequently derived from rat, rabbit, Xenopus or Necturus. However, the increasing use of knock-out or transgenic mouse models, requires a good mouse model to test cellular phenotypes and physiological as well as pathological events *in vitro* in a controlled manner.

Therefore, the main goal of this thesis was to establish a morphologically and functionally differentiated primary cell culture of mouse proximal tubule cells (chapter 3). The primary cultures were extensively characterized in order to ascertain their proximal tubule origin. The expression of specific morphological features and markers for the proximal tubule were investigated. Functional characterization was done based on the presence of different transport processes like the endocytic uptake of albumin and sodium-dependent transport of glucose. Also the presence of brush-border associated enzymes was assessed.

The main advantage of our culture method as compared to previously established primary cultures is that proximal tubules were grown on transparent collagen-coated filter membranes. In this way, we were able to characterize the primary cultures electrophysiologically in an Ussing-type chamber (chapter 4) since both the apical and basolateral membranes were accessible to fluid and electrolytes, which can be changed in a controllable way. This allowed us to define the electrophysiological properties of this cultured mouse proximal tubule epithelium and compare the findings with previously reported values of leaky epithelia from rat and rabbit kidneys. Furthermore, the transport processes in the proximal tubule were characterized electrophysiologically.

Not only physiological properties were tested, a third objective was to test whether these primary cultures could be used in a study about the mechanisms underlying renal interstitial fibrosis (chapter 5). It was examined whether TGF-β1 could induce EMT in mouse proximal tubule cells. Furthermore, different markers of tubulointerstitial fibrosis such as the expression of α-SMA, fibronectin and nestin or the disappearance of ZO-1 were investigated.

Chapter 2

Materials and Methods

2.1 Animal housing and breeding

The C57/Bl6 background was chosen since these mice are mostly used for genetic manipulations. Mice were reared under constant laboratory conditions. The animals were maintained at approximately 23°C on a 12:12 h light/dark cycle and on a diet of standard rodent chow and tap water. Young mice were weaned from their parents at the age of 19 days.

The mice used for cell culture were aged 21 to 28 days. Isolated tubules from older mice were difficult to culture, possibly because the digestion time with collagenase needed to be prolonged. Only male mice were used for culture, to avoid possible influences of female hormonal cycle.

2.2 pH and osmolality of mouse plasma

2.2.1 pH of mouse plasma

The pH of plasma was measured with a standard pH-meter with a correction for temperature of the solution (Inolab 730, VWR, Heverlee, Belgium). The mean value of pH of plasma calculated from 4 male mice was 7.39 ± 0.008. The pH of all solutions and culture media was therefore adapted to 7.4 with TRIS-base.

2.2.2 Osmolality of mouse plasma

The osmolality of plasma was measured with a Knauer Halbmikro-Osmometer (Knauer ASI, Berlin, Germany). The Knauer Osmometer estimates the osmolality on the basis of the freezing-point depression of the solution. The osmometer was calibrated before each measurement with distilled H_2O and a 400mOsm/kg H_2O solution. The mean value of osmolality of plasma calculated from 4 male mice was 323.5 ± 1.3 mOsm/kg H_2O. The osmolality for all solutions and culture media used was adapted to 325mOsm/kg H_2O with mannitol.

2.3 Cell culture

The isolation and primary cell culture methods are described in detail in chapter 3. Madin-Darbey Canine Kidney cells (MDCK) were obtained from Prof. Dr. H. De Smedt (Katholieke Universiteit Leuven, Belgium). For experiments, passages 22 to 28 were used. The culture medium consists of an equal mixture (1:1) of Dulbecco's modified Eagle's medium (DMEM) and Ham's F12 supplemented with 10% heat-inactivated Fetal calf serum (FCS), 14mM L-glutamine, 25mM sodium

bicarbonate, 100IU/ml Penicillin and 100µg/ml streptomycin (the latter is a low dose, not expected to be tubulotoxic). The cells are inoculated in 25cm² tissue culture flasks and are maintained in a standard humidified incubator (95% air – 5% CO_2) at 37°C. The medium is replaced every 72 hours. Confluent cultures are trypsinized with PBS containing 0.25% trypsin and 0.2% EDTA. For experimental assays, cells are grown on cell culture inserts with 0.33 cm² collagen-coated (equimolar mixture of types I and III collagen derived from bovine placentae) polytetrafluoroethylene (PTFE) membranes, pore size 0.4 µm (Transwell-COL™, Costar™, Corning Inc., USA).

2.4 Transmission electron microscopy

Transmission electron microscopy was performed on 7-days confluent monolayers of primary proximal tubule cells grown on either permeable membranes or thermanox® coverslips. The cell-seeded support membranes and coverslips were fixed overnight in a solution of 2% glutaraldehyde in 0.05 mol/l cacodylate buffer (pH 7.3) at 4°C, postfixed in 2% osmium tetroxide in 0.05 mol/l sodium cacodylate buffer (pH 7.3) for 1h, stained with 2% uranyl acetate in 10% acetone for 20min, dehydrated in graded concentrations of acetone and routinely embedded in epoxy resin (Araldite). Semithin sections (0.5µm) were stained with a solution of thionin and methylene blue (0.1% aqueous solution) for light microscopy. Serial ultra-thin sections (60 nm) of proximal tubule cells were mounted on 0.7% formvar-coated grids, contrasted with uranyl acetate and lead citrate and examined with a Philips EM 208 transmission electron microscope operated at 80kV.

2.5 Enzyme assays

Proximal tubule cells express a wide variety of enzymes at their brush border membranes e.g. γ-glutamyl transferase, alkaline phosphatase, leucine aminopeptidase, neutral endopeptidase, dipeptidyl peptidase IV among others.

2.5.1 Alkaline phosphatase

The expression of the PT brush border enzyme, alkaline phosphatase, was assessed spectrophotometrically by the two-point method described by Walter and Schütt (Walter & Schütt, 1974). Cultures were incubated at room

temperature for 30min with 97.5 mM Diethanolamine (DEA)-HCl buffer at pH 9.8 containing 1.21mM 4-nitrophenyl-phosphate. The release of p-nitrophenol was determined by measuring absorbance at 420nm. Enzyme activity was normalized to protein concentrations in the cultures measured by the Bradford protein assay (Bradford, 1976) described in section 2.5.3. Values obtained from 7-days old cultures were compared to those of 14-days old cultures and freshly isolated proximal tubules, which resemble more closely the in vivo situation since they retain their tubular morphology. To test the adequacy of the method, MDCK-cells were used as a negative control. MDCK cells are an established cell line derived from distal tubule or cortical collecting duct and are therefore expected to have a low alkaline phosphatase activity.

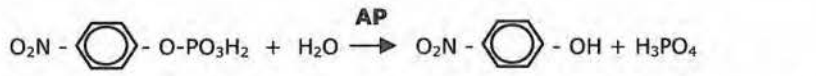

Figure 2.1: Reaction scheme of alkaline phosphatase (AP)

2.5.2 γ-glutamyl transferase

The expression of γ-glutamyl transferase was determined by the method of Szaz (Szasz, 1969). Seven-days old primary cultures and freshly isolated proximal tubules were incubated for 20 minutes with γ-glutamyl-p-nitroanilide in the presence of $MgCl_2$ and glycylglycine in TRIS buffer at 37°C and pH 8.2. The release of p-nitroaniline was measured with a spectrophotometer at 405nm. Enzyme activities were normalized to protein concentration of the culture measured by the Bradford assay (see section 2.5.3).

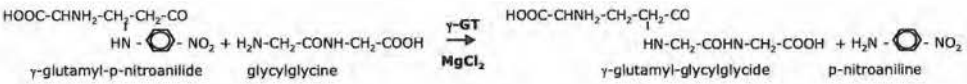

Figure 2.2: Reaction scheme of γ-glutamyl transferase (γ-GT)

2.5.3 Bradford protein assay (Bradford, 1976)

Primary cell cultures were lysed with NaOH (0.1N) for 10 min at room temperature and collected in an Eppendorf tube. Cell lysates were mixed with the appropriate amount of Bradford dye, incubated for 10 min at room temperature after which absorbance was measured at 595 nm. Protein concentration of the cell culture was determined from a standard curve of bovine serum albumin (from 10 to 100µg/ml). Protein concentration from 7-days old confluent monolayers of proximal tubule cells calculated from 55 different cultures was 42.04 ± 2.72 µg/ml proteins.

2.6 Proteomics

2.6.1 Immunoblotting

The protocol used for immunoblotting has been described previously (Jouret et al., 2004). Cells from 7-days old primary cultures were harvested by trypsinization, pooled (12 wells / sample) and centrifuged for 10 min at 1000 x g. The supernatant was discarded and the pellet was washed with phosphate-buffered saline (PBS). After another centrifugation, the pellet was snap-frozen in liquid nitrogen and stored at -80°C until further use. Frozen pellets were solubilized in ice-cold lysis buffer containing protease inhibitors (Complete Mini; Roche Diagnostics, Belgium), briefly sonicated (Branson Sonifier 250, 2 pulses at 40% intensity), and then centrifuged at 16,000 x g for one minute at 4°C. The supernatant was transferred into tubes containing 10% SDS and heated at 95°C for 90 seconds. Protein extracts were separated by SDS-polyacrylamide gels and transferred to nitrocellulose. After blocking, membranes were incubated overnight at 4°C with the first antibody, washed, incubated with peroxidase-labeled secondary antibody, and visualized with enhanced chemiluminescence (ECL). For reprobing, the membranes were rinsed, incubated for 30 minutes at 55°C in a stripping buffer (62.5 mmol/L Tris-HCl, 2% SDS, 100 mmol/L -mercaptoethanol, pH 7.4), before incubation with primary antibodies. The signal obtained on membrane extracts from an adult C57/Bl6 mouse kidney was used as positive control. All immunoblots were performed in duplicate.

2.6.2 Immunostaining

Seven-days old confluent monolayers of primary cultured PTC were fixed with 4% paraformaldehyde and then permeabilized with Triton X-100. After permeabilizing, PTC were incubated with 3% bovine serum albumin (BSA) for 1h before adding the primary antibody diluted in phosphate-buffered saline (PBS) that contained 3% BSA. After washing in PBS, cultures were incubated successively with biotinylated secondary anti-IgG antibodies, avidin-biotin peroxidase and aminoethylcarbazole (AEC) or the DAKO Envision System (Vector Laboratories). Sections were viewed under a Nikon Eclipse 80i (Nikon Co, Japan). The specificity of immunostaining was tested by incubation in the absence of primary antiserum.

2.6.3 Antibodies

Immunoblotting analyzes were performed using well-characterized (1) sheep antibodies against megalin (a gift from P. Verroust, Paris, France) (Christensen et al., 2003); rabbit affinity-purified polyclonal antibodies raised against (2) the N-terminus of the human ClC-5 (Wang et al., 2000); (3) NCC (a gift from J. Loffing, Lausanne, Switzerland) (Loffing et al., 2004); (4) AQP1 (Chemicon, Temecula, CA, USA); and (5) AQP2 (Alomone Labs, Jerusalem, Israël); (6) SGLT1 (Abcam, Cambridge, UK); (7) SGLT2 (Gentaur, Brussels, Belgium) and (8) fibronectin (DAKO) and mouse monoclonal antibodies against (9) the 31kD E1-subunit (V1 domain) of the V-ATPase (a gift from Dr. S. Gluck, University of California, San Francisco, CA, USA) (Brown et al., 1988; Wang et al., 2000); (10) alpha smooth muscle actin (Novocastra); (11) ZO-1 (Zymed laboratories, San Francisco, USA); (12) Nestin (Abcam, Cambridge, UK) and (13) β-actin (Sigma, St. Louis, MO, USA).

2.7 Transport studies

2.7.1 Assessment of sodium-dependent glucose cotransport

Large amounts of glucose are filtered every day by the glomerulus and almost none of this glucose is present in urine. The proximal tubule cells are responsible for the reabsorption of glucose. At their apical side, proximal tubules possess a secondary active transport system which is dependent upon the large sodium

gradient across the membrane. The protein responsible for this transport is called SGLT, the sodium-dependent glucose large transporter (Wright, 2001).
To study Na^+-glucose co-transport in primary PT cells, [^{14}C]-α-methyl-D-glucopyranoside (α-MG), a non-metabolizable glucose analogue, was used. Seven-days old confluent cultures were washed 3 times with standard transport buffer. To initiate uptake, transport buffer containing 20μCi/ml [^{14}C]α-MG was added at the apical side of the culture. At the basolateral side, standard transport buffer without tracer was added. After the appropriate time of incubation (5, 30 or 60 min), the uptake was stopped by aspirating the apical solution and the cells were washed rapidly with ice-cold stop solution (standard transport buffer containing 200μM phloridzin at 4°C). After the final wash, cells were solubilized with 0.1N NaOH and aliquots were sampled for liquid scintillation counting and total protein determination (Bradford protein assay, see 2.5.3). To assess the Na^+-dependence of the transport, NaCl was replaced with an equimolar concentration of choline chloride (137mM) in the standard transport buffer. Phloridzin sensitivity was determined by adding 200μM of phloridzin to the apical transport buffer containing NaCl while standard transport buffer without phloridzin was added to the basolateral side. All uptake studies were performed at 37°C. Values were expressed in pmoles of α-MG taken up per mg of proteins.

2.7.2 Uptake of albumin

Uptake of albumin was assessed as described previously (Schwegler et al., 1991). Primary PTC were incubated with fluorescein-isothiocyanate (FITC)-labelled bovine serum albumin (Molecular Probes Europe BV, Leiden, The Netherlands) in Ringer solution (see 2.10) for 15 minutes at 37°C or 4°C as indicated. After rinsing with ice-cold Ringer's solution, cells were disintrigrated with Triton X-100 (0.1% v/v in Ringer solution). Intracellular fluorescence was measured using a single-beam fluorimeter (Photon Technology International Inc., Lawrenceville, NY, USA), at an excitation wavelength of 480nm and emission wavelength at 520nm. Protein concentration was determined by the Bradford protein assay (see 2.5.3).

2.8 Fluorescence microscopy

2.8.1 Fluorescent probe, Fura-2-AM

To measure intracellular calcium concentration $[Ca^{2+}]_i$, the UV light-excitable, ratiometric Ca^{2+} indicator, Fura-2-AM, can be used. The lipophilic acetoxymethyl ester freely crosses the plasma membrane and is hydrolyzed by cytoplasmic esterases yielding the highly fluorescent but impermeant form, Fura-2 to which free Ca^{2+} will bind (Grynkiewicz et al., 1985). Fura-2 exhibits an absorption shift that can be observed by changing the excitation wavelengths from 340nm to 380nm and measuring emission at 510nm (fig. 2.3a). The major advantage of ratiometric measurements is to reduce or eliminate variations resulting from indicator concentration, excitation path length, and excitation intensity or detection efficiency. Furthermore, other artefacts like photobleaching, dye leakage, variable cell thickness or variations in loading efficiency are eliminated. The equilibrium between the free form (Fura-2) and the Ca^{2+}-bound form (Fura-2-Ca^{2+}) is giving by the dissociation constant, K_d.

$$K_d = C_f[Ca^{2+}]/C_b$$

with C_f and C_b the respective concentrations of free and bound form of Fura-2.
Fura-2 has a dissociation constant (K_d) of 135nM (Van den Bergh et al., 1995), which is close to typical basal Ca^{2+} levels in mammalian cells (~100nM). Therefore, Fura-2-AM has become the dye of choice to measure $[Ca^{2+}]_i$. However, Fura is excited with short wavelengths (near UV) enhancing autofluorescence of the cells (Lakowicz, 2006).
The fluorescent measurements were performed with a Nikon TMD 35 inverted microscope (Tokyo, Japan) that was placed in a home-built Perspex box built around the microscope (Fig. 2.3b). In the box, a constant temperature of 37°C was ensured by constant ventilation of air through an external circuit containing a heating element under control of a configurable loop controller connected to a thermocouple inside the box. The excitation light was delivered by a XBO 75 W/2 OFR Xenon lamp (Osram, Berlin, Germany). The excitation filters were connected to a computer-controlled filter wheel, Lambda-10 (Sutter Instrument Company, Novato, USA), allowing a rapid change between different excitation filters during the measurement. Neutral density filters inserted between the

microscope and the filter wheel reduce the intensity of the source. Excitation light was filtered at 340nm and 380nm by the interference filters 340DF10 and 380DF13 (Omega Optical, Vermont, USA) and reflected towards the cells by a dichroic mirror 400DCLP (Chroma technology, Brattleboro, USA) and a Zeiss Achroplane 40x/0.6 objective (LD Achroplane™, Carl Zeiss, Oberkochen, Germany). The fluorescence emission was collected by the objective, passed through a dichroic mirror type 72100 and a 535/50nm band-pass emission filter (Omega Optical, Vermont, USA) and finally detected by a Quantix CCD camera (Photometrix, Tucson, Arizona, USA) equipped with a Kodak KAF 1400 CCD (grade 2, MPP) with 849 x 609 pixels and cooled to -25°C by a thermoelectric cooler. The exposure time was 3 s at each excitation wavelength. The acquisition of pairs of images was performed every 30 seconds and was controlled by a homemade program based on the V for Windows software (Digital Optics, Auckland, New Zealand). The signals were binned (3x3). Background signal measured before cells were loaded with Fura-2-AM was subtracted, pixel by pixel, from the image of the loaded cells.

Confluent monolayers of proximal tubule cells were loaded during 1h at 37°C with 10μM (from a stock solution of 5mM in DMSO) Fura-2-AM. After loading, cells were washed 3 times with warm Ringer solution composed of (in mM): 138 NaCl, 5.33 KCl, 1.26 $CaCl_2$, 0.44 KH_2PO_4, 0.3 Na_2HPO_4, 4 $NaHCO_3$, 10 HEPES, 4 L-glutamine and 5.6 D-glucose, buffered at pH 7.4 with TRIS and osmolality of 325mOsm/kg H_20 with mannitol. After each experiment, measured Fura-2 ratios were calibrated *in vivo*. Intracellular Ca^{2+}-concentration was determined using the formula by Grynkiewicz (Grynkiewicz et al., 1985):

$$[Ca^{2+}]_i = Kd * R_{bf} * \frac{R - R_{min}}{R_{max} - R}$$

where K_d is the dissociation constant of Fura 2 for Ca^{2+} (135 nM) (Van den Bergh et al., 1995); R_{bf} is the maximum fluorescence intensity due to excitation at 380 nm (in the absence of Ca^{2+}) divided by the minimum fluorescence intensity at 380 nm (in the presence of saturating Ca^{2+}); R is the fluorescence ratio, F_{340}/F_{380}; R_{max} and R_{min} are the fluorescence ratios, F_{340}/F_{380}, in the presence of saturating Ca^{2+} and in the absence of Ca^{2+}, respectively; R_{max} was obtained by permeabilizing the cells with the Ca^{2+} ionophore ionomycin (10 μM from a 1 mM stock solution in ethanol) in the presence of 5 mM extracellular Ca^{2+}. To obtain

the minimum ratio R_{min} subsequently, the cells were exposed to a Ca^{2+}-free Ringer solution containing 10 mM EGTA, with 10 µM ionomycin and BAPTA-AM (10 µM from a stock solution of 10 mM in DMSO) to buffer intracellular Ca^{2+}. After each experiment, a calibration was done unless calibration was impossible due to disappearance of the cells from the filter. In this case, calibration was done with averaged values of all other calibrations.

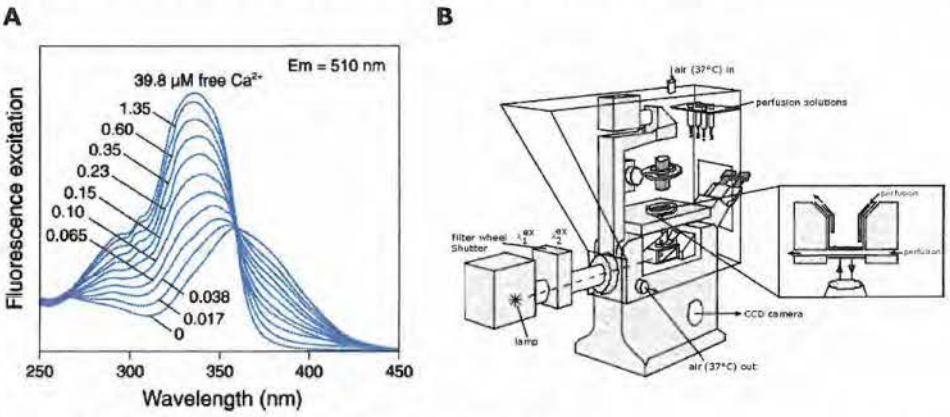

Figure 2.3: Measurement of $[Ca^{2+}]_i$ with Fura-2-AM.

A: Fluorescence excitation spectra of Fura-2 in solutions containing 0 to 39.8µM Ca^{2+} (Molecular Probes, Handbook). Dual-excitation at 340nm and 380nm, emission at 510nm. B: Nikon Fluorescence setup.

2.8.2 The ZO-1 and Nestin antibody

The tight junctional complex between adjacent cells can be visualized by the marker for the zonula occludens protein-1, ZO-1. Nestin is an early fibrotic marker and was used to visualize epithelial-to-mesenchymal transition in PTC exposed to TGF-β1 (as described in chapter 5). Confluent monolayers of PTC were fixed by immersion in ice-cold (-20°C) ethanol, permeabilized and incubated with a rabbit anti-Nestin directed against the tail of the protein (Abcam, Cambridge, UK) and subsequently incubated for 1h at 37°C with rabbit anti-ZO-1 directed against the N-terminus (Zymed laboratories, San Francisco, USA). The specificity of the staining was tested by incubation in the absence of primary antiserum. Visualization of Nestin was done with a secondary Cy-5-conjugated goat anti-rabbit IgG (Abcam, Cambridge, UK). ZO-1 was visualized using a FITC-conjugated goat Anti-rabbit IgG (H+L) (ZyMax Grade, Zymed laboratories, San Francisco, USA). Collagen-coated filters with PTC were cut out

and placed on a glass coverslip which was mounted upside down on the stage of the Zeiss LSM 510 META laser-scanning confocal microscopic (LSCM) system attached to an Axiovert 200 (motorized) frame (Zeiss, Jena, Germany). Fluorescence measurements were performed with an x63/1.4 Plan-Apochromat oil-immersion objective (Zeiss). The FITC-conjugated Ab was excited by the Ar laser (488-nm line). A 633nm-line (He laser) was used to excite the Cy5-conjugated Ab. Laser intensity was set at only 2% of the maximum level for FITC and 12% for Cy5 to minimize dye bleaching and to protect the cells against possible photodamage (Koenig, 2001). Fluorescence emission of FITC was collected, via the NFT490 dichroic mirror and the 500-550 barrier filter, that came with the confocal microscope. Fluorescence emission of Cy5 was collected via the NFT545 dichroic mirror and the 650-710 barrier filter. The scanning speed was set to a pixel dwell time of 102.4 μs. Each 12-bit 512 x 512-pixel image was averaged twice via software-selected repeated line scan mode to ameliorate the signal-to-noise ratio. The effective frame collection time was ~100 s. The thickness of the optical slices was <1.0 μm in all experiments. The pinhole was set at 1 airy unit.

2.9 Statistical analysis

All values are expressed as means ± standard error of the mean (SEM). Data from control experiments were fitted with Origin 6.0 (Micoral Software, Northampton, USA) using the best-fit function. For the albumin uptake experiments, data were fitted according to the Michaelis-Menten kinetics. Significance of differences between two means was calculated using the GraphPad InStat software (demo version, graphpad Software, San Diego, USA). For the alkaline phosphatase experiments, significance was calculated with the One-way ANOVA with Bonferroni correction. For the glucose uptake experiments, significance was calculated by the Kruskal-Wallis test (nonparametric ANOVA) with the Dunn's Multiple Comparison test. Significance level of the differences of the means (p-value) is indicated in the legend of each figure.

2.10 Solutions and chemicals

The control Ringer solution used for the primary proximal tubule cells for all experiments except in the study of glucose transport had the following composition (in mM): 138 NaCl, 5.33 KCl, 0.41 $MgSO_4$, 1.26 $CaCl_2$, 0.44 KH_2PO_4, 0.5 $MgCl_2$, 0.3 Na_2HPO_4, 4 $NaHCO_3$, 10 HEPES, 4 L-Glutamine, 1 alanine, 5 glycine and 5.6 D-glucose buffered to pH 7.4 with TRIS-base and an osmolality adjusted to 325mOsm/kg H_2O with mannitol.

Changes in the composition of this Ringer solution in experiments described in the following chapters are indicated in the Materials and Methods section of that particular chapter.

The transport buffer used to assess sodium-dependent glucose cotransport in primary proximal tubule cells had the following composition (in mM): 137 NaCl, 5.4 KCl, 1.2 $MgSO_4$, 2.5 $CaCl_2$, 10 HEPES and 4.0 L-glutamine buffered to pH 7.4 with TRIS-base and osmolality adjusted to 325mOsm/kg H_2O with mannitol.

Chapter 3

Primary cell culture

The results of this chapter are described in:

A primary culture of mouse proximal tubular cells, established on collagen-coated membranes.

Sara Terryn, François Jouret, Frank Vandenabeele, Inge Smolders, Marjan Moreels, Olivier Devuyst, Paul Steels and Emmy Van Kerkhove. (2007). Am J Physiol 293:F476-F485.

3.1 Introduction

Primary cell culture is an essential and powerful tool to investigate kidney cell function (Bello-Reuss & Weber, 1986), transport processes as well as hormone actions or mechanisms of cytotoxicity (Elliget & Trump, 1991; Sheridan et al., 1993) under well-defined conditions. Furthermore, the increasing use of transgenic and knock-out mice needs an *in vitro* model to study the cellular phenotype. Previously established techniques are often time-consuming, have low yields of starting material or expose the cells to mechanical or chemical aggression that influence cell differentiation. Mostly, these techniques work well for more distal nephron segments, like thick ascending limb (TAL) or collecting duct (CD) (Jans et al., 2000) but usually fail in the isolation of viable proximal tubules (Wagner et al., 2003). Proximal tubule cells rely on an oxidative metabolism that provides energy for the Na^+-K^+-ATPase that drives their high transport rates (Mandel, 1985). They are therefore especially sensitive to damage due to low oxygen availability. Our goal was to establish a simple and fast method avoiding aggressive manipulations and with limited oxidative stress to culture PTC and preserve a high degree of differentiation. In the past, cells were cultured on solid surfaces, like plastic or glass, allowing access from the apical side only. We attempted to culture the cells on permeable collagen-coated filters, giving access to physiological saline at both the apical and the basolateral side, so they can grow in a polarized state resembling more the in vivo situation.

3.2 Solutions and chemicals

For optimal survival during dissection, HEPES buffered balanced salt solutions (Hank's balanced salt solution, HBSS without phenol red) were used with additions (in mM: 10 glucose, 5 glycine, 1 alanine, 15 HEPES, final pH brought to 7.4 with TRIS base and osmolality to 325 mOsm/kg H_2O with mannitol).

The cell culture medium was optimized for primary cultures of mouse proximal tubule cells and consisted of DMEM/Ham's F12 (1:1) without phenol red and supplemented with heat-inactivated fetal calf serum (FCS) 1% (v/v), HEPES 15 mM, L-glutamine 2 mM, hydrocortisone 50 nM, insulin 5 µg/ml, transferrin 5 µg/ml, selenium 50nM, sodium pyruvate 0.55 mM, 100x non-essential amino acids 10ml/l, penicillin 100 IU/ml and streptomycin 100 µg/ml buffered to pH 7.4 with TRIS and osmolality of 325 mOsm/kg H_2O.

DMEM/ Ham's F12 without phenol red, HBSS without phenol red, MEM non-essential amino acids (liquid, 100x), sodium pyruvate, L-glutamine and penicillin/streptomycin were purchased from Invitrogen Life Technologies, Paisley, Scotland. Hydroxyethylpiperazine-N'-2-ethanesulphonic acid (HEPES) and mannitol were obtained from Acros Organics, Geel, Belgium. D-glucose and nylon strainer were obtained from Merck Eurolab, Leuven, Belgium. Collagenase class 2 was purchased from Worthington Biochemical Corporation, Lakewood, NJ, USA. Cell culture inserts were 0.33 cm^2 collagen-coated polytetrafluoroethylene (PTFE) membranes, pore size 0.4 µm and accessory 24-well tissue culture-treated cell culture plates were obtained from Corning Costar Corporation, Cambridge, MA, USA. Plastic thermanox® coverslips were from Electron Microscopy Sciences, Hatfield, PA, USA. All other hormones and chemicals were purchased from Sigma, St.Louis, MO, USA.

3.3 Isolation and primary cell culture of mouse proximal tubule cells

Primary proximal tubule cells were cultured under sterile conditions by a modification of previously described methods (Sheridan et al., 1993; Jans et al., 2000). Male C57/Bl6-mice (aged 21-30 days) were killed by decapitation. Rapid exsanguination ensured an almost complete removal of blood from the kidneys, causing a clear distinction between the pale cortex and the red medulla. In this way, renal cortices could be separated visually from the medulla.

After decapitation of the mice, kidneys were dissected out and rapidly transferred to ice-cold dissection solution (DS, HBSS with supplements). During the following steps of the dissection, DS was kept at 4°C and frequently refreshed. The capsule from each kidney was removed with fine forceps. Using a bistoury, kidneys were first cut longitudinally into 2 identical pieces and then coronally, starting from the hilus, into small slices approximately 1 mm thick. Finally, cortices were separated from the medulla and cut into small pieces. These cortical pieces were transferred into a glass vial containing collagenase solution (DS with 0.1% (w/v) type-2 collagenase and 96µg/ml soybean trypsin inhibitor) at 37°C and digested for 30min. After digestion, the supernatant was sieved through two nylon sieves (pore size 250µm and 80µm). The 250µm sieve retained undigested tissue blocks while the longer proximal tubule (PT) fragments remained in the 80µm sieve. Blood cells, distal and other small

nephron fragments, glomeruli and cellular debris passed through the 80µm sieve. To resuspend the PT fragments, the sieve was flushed in the reverse direction with warm DS (37°C) containing bovine serum albumin (BSA) 1% (w/v), to block all collagenase activity. The PTs present in the BSA-solution were centrifuged for 5min at 170xg, washed and then resuspended into the appropriate amount of culture medium. The PT fragments were seeded onto collagen-coated permeable PTFE-filter supports (Costar™) and left unstirred for 48h at 37°C and 95% air/5% CO_2 in a standard humidified incubator (Jouan, USA) after which the culture medium was changed for the first time. The medium was then replaced every 2 days. After 7 days, cell cultures were organized as a confluent monolayer. PTC were also grown on plastic thermanox® coverslips under the same culture conditions for transmission electron microscopy to evaluate whether the morphology was different from cells grown on PTFE-filter supports.

3.4 Results

3.4.1 Primary cell culture

Each cell culture was initiated from the isolation of PT fragments from 2 kidneys (1 mouse). To avoid substantial oxidative stress to the proximal tubule cells, the total time of isolation was less than 2h from dissecting the kidney until seeding the tubule fragments onto the collagen-coated filter and dissection was performed at 4°C. The number of viable proximal tubules was correlated with the duration of the isolation. Furthermore, addition of glycine and alanine to the dissection solution seemed to have a protective effect, as described previously (Baines et al., 1990; Jans et al., 2000). High amounts of glycine are found in the cytoplasm through an active transport mechanism. Hypothermia during isolation results in the rapid loss of the amino acid because an inhibition of the Na^+/K^+-ATPase. Therefore, extracellular administration of glycine seems to be necessary to preserve cell integrity (Garza-Quintero et al., 1993). Glycine cytoprotection has been postulated to delay membrane disruption through the blockage of a glycine-sensitive death channel, responsible for the leakage of macromolecules. Alanine seems to have a similar cytomembrane protective effect (Pan et al., 2005). The amount of collected tubules was usually sufficient for 12 collagen-coated PTFE-filter supports. First, PT fragments (fig. 3.1A) were left unstirred for

48h. At this time, cellular outgrowth was observed at the open ends of the tubular fragments. After 7 days, islands of cellular outgrowth became progressively larger to form a confluent monolayer of (epithelial) polygonal cells (fig. 3.1B and C).

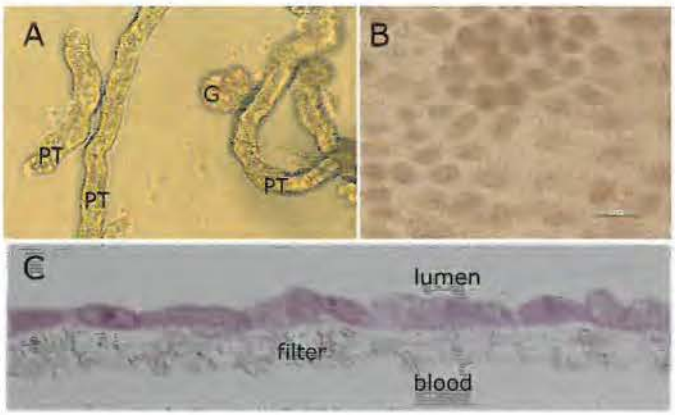

Figure 3.1: light microscopic images of proximal tubules

A: freshly isolated proximal tubules (PT) and an occasional glomerulus (G) at initiation of cell culture. The proximal tubules can be identified by their diffuse appearance and collapsed lumen.

B: 7-days old confluent monolayer of PTC (bar: 20µm, 100x)

C: transverse section of confluent monolayer of PTC

3.4.2 Transmission Electron Microscopy

Proximal tubule cells are polarized epithelial cells with distinct properties at the apical and basolateral membrane. At low magnification, the transverse section revealed that single cells grew as a homogeneous monolayer of cells with cobblestone-like appearance on the PTFE-filter (fig. 3.2A and I). The cells were structurally polarized: the apical pole, facing the free surface, differed from the basal pole, toward the underlying support layer. We observed that the apex of the cells exhibited numerous short, regularly oriented microvilli (fig. 3.2B and G). The apical cytoplasm possessed clear vacuoles of varying size, some vacuoles being associated with the apical membrane (fig. 3.2F and H). Coated vesicles were regularly found (fig. 3.2H). Well-defined tight junctions interconnected the cells at their apical poles (fig. 3.2B, E and F), whereas the basolateral side of the cells showed membrane invaginations (fig. 3.2D and E). Mitochondria were diffusely distributed in the cytosol as observed in primary

cultures of medullary thick ascending limb cells (Jans et al., 2000). Also, a primary cilium was present at the apical membrane (fig. 3.2C).

When PT cells were grown on a solid surface like thermanox® slides (fig. 3.2J), cellular growth was slower compared to the filter supports (fig. 3.2I), since confluency was not reached after 7 days. Furthermore, cells became more elongated instead of being polygonal but they still showed differentiated characteristics like microvilli and tight junctions, although they were less confined to the apical pole.

Figure 3.2: Proximal tubule cells morphology (TEM)

A: TEM-image of cobblestone-like cells grown on a collagen-coated filter (bar: 10µm). B: TEM-image showing the presence of apical microvilli, numerous mitochondria and apical tight junctions (bar: 2000nm). C: Detail TEM-image of a primary cilium at the apical membrane and the nucleus with heterochromatin (bar: 1000nm). D: detail of basolateral infolds (bar: 500nm). E: apical tight junction (TJ) and basolateral infolds (BI) and mitochondria (M) (bar: 1000nm). F: Detail of TEM-image showing a vacuole (V) and apical tight junction (TJ).

G: Detail of apical microvilli and glycialbodies (arrow). H: Detail of a TEM-image showing a coated vesicle (CV) associated with the apical membrane. I: Tangential section of confluent monolayer of PTC cultured on collagen-coated membranes (bar: 10µm). J: Tangential section of primary PTC cultured on thermanox® (bar: 10000nm).

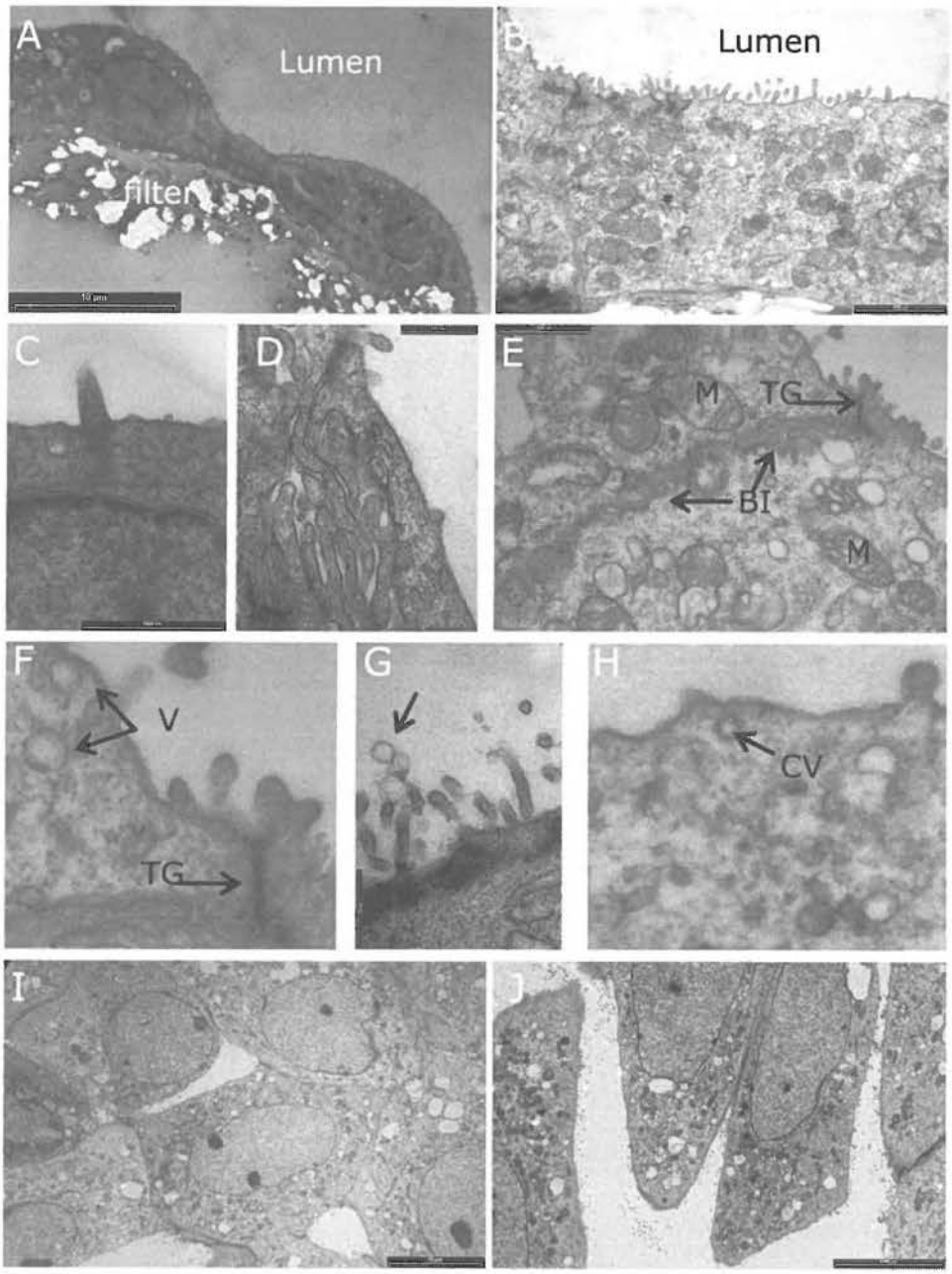
A
Lumen
filter
B
Lumen
C
D
E
M
TG
BI
M
F
V
TG
G
H
CV
I
J

3.4.3 Immunoblotting and Immunostaining analysis

Well-characterized antibodies against proximal and distal tubule markers were used to establish the state of differentiation of the primary cultures derived from PT segments (fig. 3.3). The water channel, AQP1, provides the high water permeability in the proximal tubule and is present at both the apical and basolateral membrane (Agre et al., 2002). Immunoreactivity for AQP1 showed two specific bands, which correspond to the core (~28 kD) and the glycosylated (~35-50 kD) forms of the protein, in all samples. By contrast, no signal was detected in the same samples for the thiazide-sensitive NaCl co-transporter (NCC) and for AQP2, established markers of the early distal convoluted tubule and the collecting duct, respectively (Kim et al., 1999; Campean et al., 2001; Loffing et al., 2001). To further characterize the PT cells, immunoblotting for major components of the receptor-mediated endocytosis were performed. The renal chloride channel, ClC-5, which plays a key role along the endocytic pathway in PT cells (Christensen et al., 2003), was clearly detected in all samples, as well as its functional partners, the V-ATPase, and the multiligand receptor, megalin. Note that the molecular mass of ClC-5 was slightly higher in cultured PT cells than in the positive control kidney, which might reflect a differential post-translational processing, e.g. N-glycosylation, of ClC-5 in cultured PT cells (Jouret et al., 2004).

Immunoblotting experiments were confirmed by immunostaining (fig. 3.4). Almost all cells stained positive for AQP1 (fig. 3.4C and D), ClC-5 (fig. 3.4G and H) and megalin (fig. 3.4I and J) while practical no cells stained for AQP2 (fig. 3.4E and F) nor did cells incubated in PBS with 3% BSA without primary antibody (control, fig. 3.4A and B).

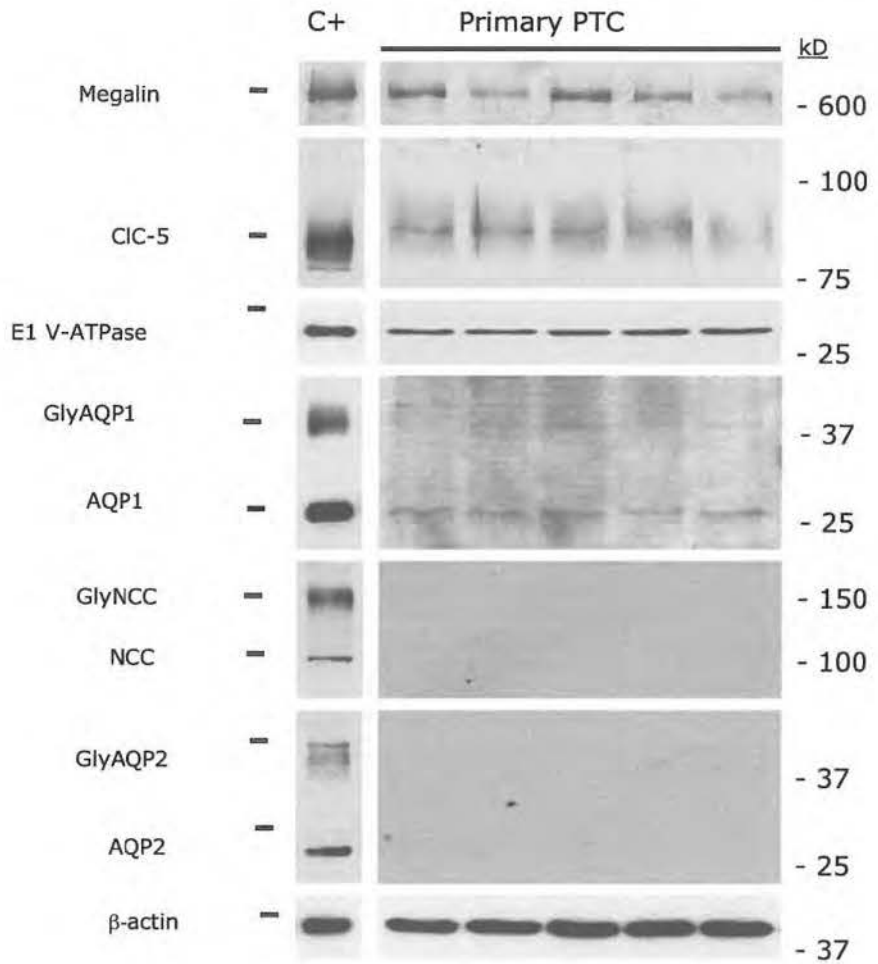

Figure 3.3: Representative immunoblottings for proximal tubule, early distal convoluted tubule and collecting duct markers

Protein extracts from mouse control kidney (C+) and from 5 pooled 7-days old primary cultured PT cells (12 wells/sample) were run on SDS-PAGE, transferred to nitrocellulose and probed with antibodies against megalin (1:4000), ClC-5 (1:1000), E1 subunit of the V-ATPase (1:100), AQP1 (1:20.000), NCC (1:2000) and AQP2 (1:1000). Membranes were stripped and reincubated with a monoclonal antibody against β-actin (1:10.000). In all samples, PT markers, i.e. megalin, ClC-5, V-ATPase and AQP1, are present, whereas no specific signal is detected for NCC and AQP2, even after longer film exposure (up to 2 hours).

Figure 3.4: Immunostaining for AQP1, AQP2, ClC-5 and megalin primary PTC
Immunostaining of 7-days old primary PTC with primary antibodies raised against AQP1 (1/200) (**D, E and F**), AQP2 (1/200) (**G, H and I**), ClC-5 (1/100) (**J, K and L**) and megalin (1/10000) (**M, N and O**). The proximal tubule cells stained for AQP1, and endocytosis markers, ClC-5 and megalin, while staining for AQP2, a distal tubule marker, was very rare. No staining was detected in primary PTC incubated in PBS with 3% BSA without primary antiserum (**A, B and C**). Magnification A-D-G-J-M: 10x (bar: 200µm), B-E-H-K-N: 40x (bar: 50µm) and C-F-I-L-O: 100x (bar: 20µm). Image quality was not optimal due to interference of the filter (striped aspect).

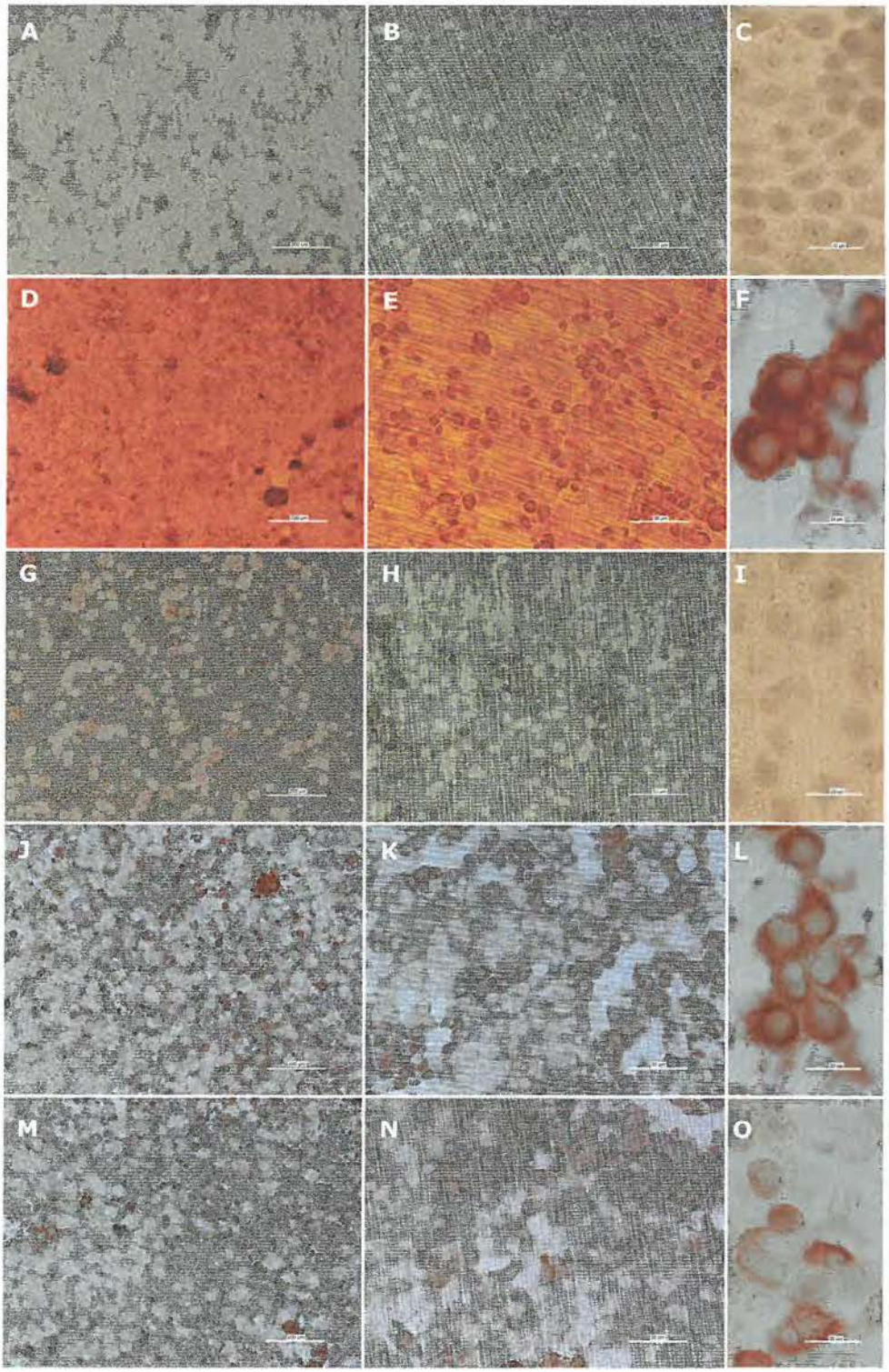
A
B
C
D
E
F
G
H
I
J
K
L
M
N
O

3.4.4 Uptake of albumin

In PTC, albumin is taken up at the apical side by receptor-mediated endocytosis using the multiligand receptors, megalin and cubulin (Christensen & Birn 2002). The fluorescent probe, FITC-albumin is routinely used to measure receptor-mediated endocytosis and the uptake process is characterized by saturation kinetics. In our cells, uptake of FITC-albumin at 37°C saturates as a function of dose (fig. 3.5, squares). Due to the large variability in the analysis, the Lineweaver-Burk plot (figure 3.5, inset) for the cell cultures sets with lowest uptake data (triangles) and highest uptake (spheres) was assessed and compared to the mean (squares). Both experiments as well as the mean show the same apparent K_m (intercept with X-axis) but different V_{max} (intercept with Y-axis). Using the Michaelis-Menten kinetics (fig. 3.5) and the Lineweaver-Burk plot (fig. 3.5, inset), the mean maximal uptake (V_{max}) was calculated to be 1.5 ± 0.6 ng/µg protein/15min and the apparent K_m (concentration for half-maximum uptake) was estimated at 36 ± 0.9 mg/l. At 4°C, the uptake represents the cell-bound fluorescence and should therefore not increase as a function of dose. Indeed, at this low temperature, the uptake process is delayed and does not increase with higher doses (fig. 3.5, open spheres).

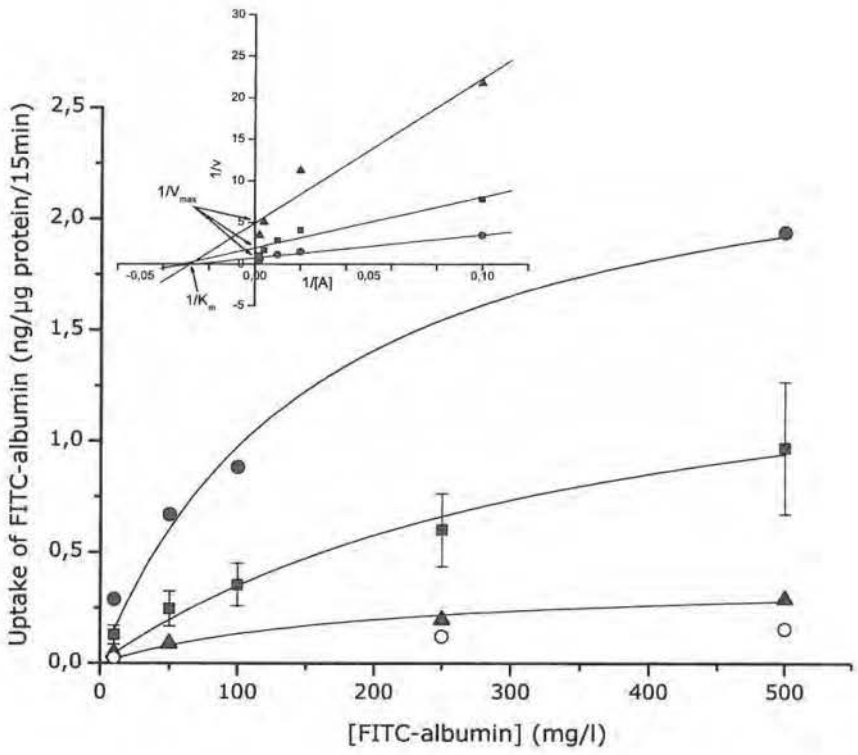

Figure 3.5: Uptake of FITC-albumin in primary PTC

Uptake of FITC-albumin assessed in 7-days-old primary PTC at 37°C (squares, n=12) and at 4°C (open spheres, n=1) for 15min. The uptake at 37°C clearly rises as a function of the dose but gradually saturates at higher doses while at 4°C there is no dependence on dose. V_{max} was calculated to be 1.5 ± 0.6 ng/µg protein/15min and the apparent K_m was 36 ± 0.9 mg/l. The large error in the analysis is due to heterogeneity between different sets of cultures. The uptake data from the culture set with the lowest (triangles) and highest (spheres) uptake are also shown. The inset shows the Lineweaver-Burk plot of the experiment with the lowest (triangles) uptake data and the experiment with the highest (spheres) uptake data. The Lineweaver-Burk plot of the mean uptake is presented by squares. The intercept with the X-axis (y=0) is $1/K_m$ and the intercept with the Y-axis (x=0) is $1/V_{max}$. From the 3 data sets, the $1/V_{max}$-value is different while the $1/K_m$-value is similar. Each value is the mean ± SEM of the different determinations (n=12), except for determinations at 4°C and the highest and lowest uptake culture set.

3.4.5 Alkaline Phosphatase and γ-glutamyl-transferase Assay

Alkaline phosphatase and γ-glutamyl-transferase (γGT) are enzymes expressed at the brush border of PTC. Their activity can be classically assessed by spectrophotometrical methods based on the colour conversion of respectively p-nitrophenyl phosphate to p-nitrophenol in an alkaline solution or γ-glutamyl-p-nitroanilide to the yellowish p-nitroaniline. To localize the enzymes in our cultures, we tested the solution containing p-nitrophenyl phosphate or γ-glutamyl-p-nitroanilide at both apical and basolateral sides of the cells. Enzyme activity for the apical side is presented in figure 3.6. Enzyme activity was also assessed at the basolateral side, but no activity was measured. For alkaline phosphatase, the activity in 7-days old primary PTC was about 20 times higher than in 14-days old primary cultures, indicating the degree of differentiation is dependent on time in culture (fig. 3.6, open bars). In isolated PT, enzyme activity was about 4 times lower than in primary PTC. To test whether the two-point method (Walter & Schütt, 1974) we used was adequate to evaluate the presence of alkaline phosphatase in our culture system, we compared MDCK cells with 7-days old primary PTC. MDCK cells are from a distal tubular origin and are therefore assumed to have a low alkaline phosphatase activity, as indeed documented here. MDCK cells displayed an alkaline phosphatase activity that was ~ 5000 times lower than that of 7-days old primary PT cells and still ~ 200 times lower than that of 14-days old primary PT cells (fig. 3.6, open bars). For γ-GT, the activity in 7-days old primary PTC amounted to 172,5 ± 13,9 mU/mg protein which was higher than the values reported by Cummings B. et al. (Cummings et al., 2000) in primary cultures of human proximal tubule cells but lower than the values reported for whole mouse kidney (275 mU/mg protein) (Hanigan et al., 1999). In freshly isolated PT, enzyme activity was about 2 times lower than in primary PTC (fig. 3.6, striped bars).

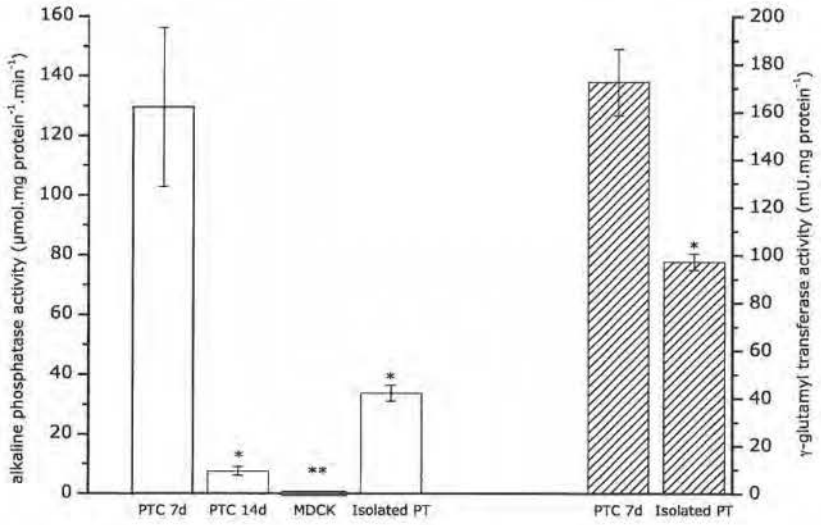

Figure 3.6: Alkaline phosphatase and γ-glutamyl-transferase activity in primary PTC
Alkaline phosphatase (AP) activity (open bars) measured in 7-days old (PTC 7d), 14-days old primary cultures of PTC (PTC 14d), MDCK-cells and freshly isolated proximal tubules (isolated PT). Values (mean±SEM) are in µmol.mg protein^{-1}.min^{-1}: 129.6 ± 26.6, 7.5 ± 3.2, 0.026 ± 0.004 and 33.7 ± 6.6 for 7-days old PTC (n=16), 14-days old PTC (n=4), MDCK-cells (n=8) and isolated PT (n=16), respectively. Gamma-glutamyl-transferase (γGT) (striped bar) activity was measured in 7-days old primary cultures of PTC (n=21) and isolated PT (n=16). Each value is the mean of different determinations ± SEM and is expressed as mU.mg protein^{-1}. Significance was determined by One-way ANOVA with Bonferroni correction and P-values are: $p<0.001$(*) and $p<0.0001$(**).

Figure 3.7: α-MG uptake in primary cultures of PTC

The uptake of α-MG reaches a maximum after about 60min (squares). Glucose transport is sensitive to omission of Na^+ (spheres) and can be blocked by phloridzin (triangles). Values are mean ± SEM, each value is the mean of 5 to 7 determinations. Significance was analysed by Kruskal-Wallis test (nonparametric ANOVA) with the Dunn's Multiple Comparisons test and p-value was $p<0.05$(*), $p<0.01$(**) and $p<0.001$(***).

3.4.6 Na^+-dependent transport of glucose

Transport of glucose is a highly differentiated function of renal PT cells localized at the apical membrane (Wright, 2001). To test if our primary cells still displayed this function, we evaluated the uptake of [^{14}C]-α-methyl-D-glucopyranoside (α-MG). To localize the transport of glucose, α-MG was tested at both apical and basolateral sides of the cells. When α-MG was added to the basolateral side, we did not observe any uptake into the cells (data not shown). Therefore, we evaluated α-MG uptake under various conditions at the apical side. The time-course of α-MG uptake was saturable since it slowly reached a maximum transport rate after 60 min (fig. 3.7, squares). Addition of phloridzin (200μM), a competitive inhibitor of glucose reabsorption, resulted in a significant reduction of the α-MG uptake after 30 and 60 min in the presence of Na^+ (fig. 3.7, triangles). The uptake of α-MG was only 12% of control after 60 min in the presence of phloridzin. When Na^+ was omitted from the transport buffer and replaced by an equal amount of choline, uptake of α-MG without Na^+ was significantly reduced after 30 and 60 min (fig. 3.7, spheres). The maximum rate was only 18% of the control after 60 min. Still a small amount of α-MG was taken up under Na^+-free conditions. Immunostaining for the sodium-dependent glucose cotransporter type 1 (SGLT1) and type 2 (SGLT2) is shown in figure 3.8. Primary cultures of 7-days old PTC expressed both SGLT1 and SGLT2.

Figure 3.8: Immunostaining for SGLT1 and SGLT2 in primary PTC.

Immunostaining of 7-days old PTC with antibodies raised against SGLT1 (1/200) and SGLT2 (1/50). Primary PTC stained positive for both SGLT1 (A and C) and SGLT2 (B and D) while cells incubated without primary antibody showed no staining (data not shown). Magnification A-B: 10x (bar: 200μm) and C-D: 40x (bar: 50μm).

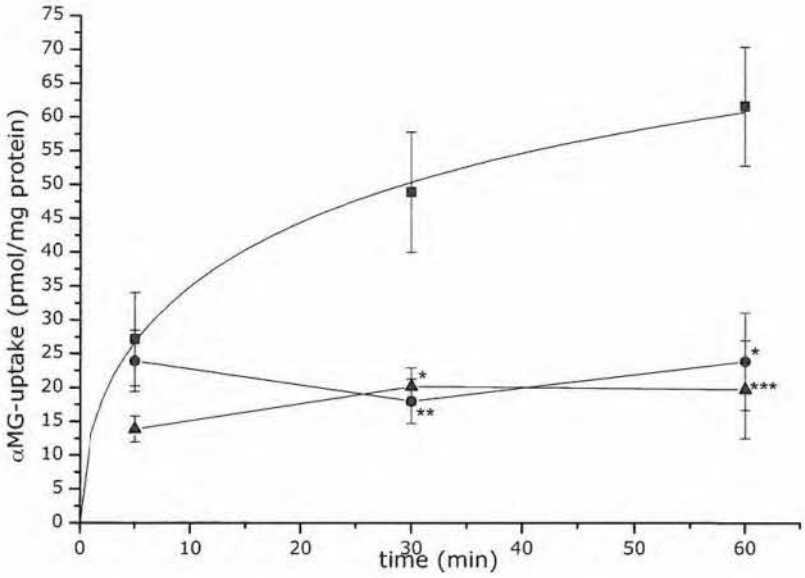
αMG-uptake (pmol/mg protein)
time (min)
0
5
10
15
20
25
30
35
40
45
50
55
60
65
70
75
0
10
20
30
40
50
60
*
**
*
***

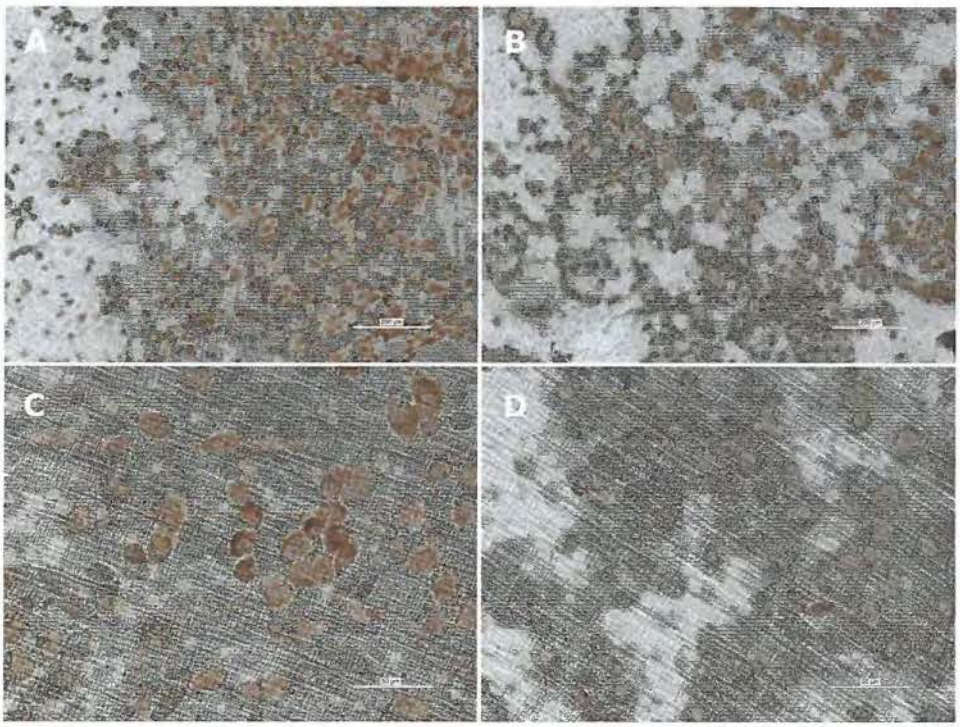
A
B
C
D

3.4.7 Hormone-induced intracellular Ca^{2+}-responses

The intracellular Ca^{2+} concentration ($[Ca^{2+}]_i$) in response to the hormones bradykinin (BK) and angiotensin II (ATII), was investigated. Both hormones were applied simultaneously at both sides of the epithelium since we did not test the exact localization of the receptors. It has been reported that the ATII-receptor is present at both the apical and basolateral side (Douglas, 1987). In MDCK, LLCPK and rat kidney cells, the B2-receptor for bradykinin was present at both membranes (Simmons, 1992; Figueroa et al., 1995; Shivakumar et al., 2005). In primary cultured PTC, we observed a basal $[Ca^{2+}]_i$ of 82.5 ± 2.6 nM. As shown in fig. 3.9, stimulation with BK or ATII resulted in an increase in $[Ca^{2+}]_i$. In response to 100nM ATII or 1µM ATII, a 57% or 84% increase respectively could be observed. Higher doses of BK seemed to reduce the Ca^{2+}-response: a 229%, 114% and a 90% increase with 1nM, 10nM and 100nM, respectively. Furthermore, when cells were stimulated with ATII, $[Ca^{2+}]_i$ increased towards a plateau (fig. 3.10A). The response observed with ATII is different from the response to BK. BK induced a transient increase in $[Ca^{2+}]_i$ after which Ca^{2+}-levels returned to baseline and then, in the continuous presence of BK, increased again towards a plateau (fig. 3.10B).

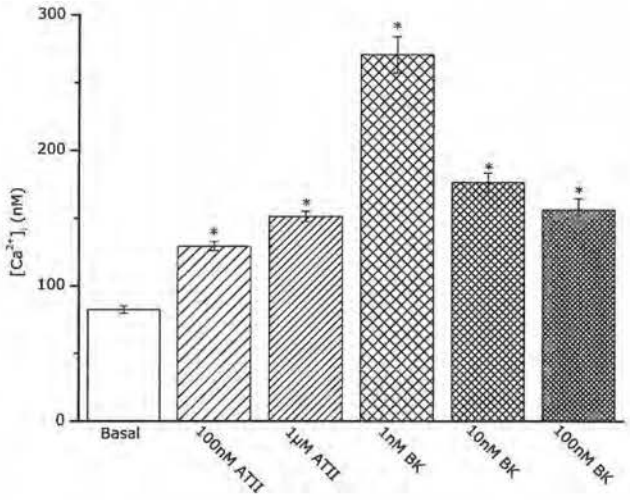

Figure 3.9: Intracellular Ca^{2+} responses after hormonal stimulation
Increases in $[Ca^{2+}]_i$ after stimulation with 100nM or 1µM angiotensin II (ATII, striped bars, n=3) or 1, 10 or 100nM bradykinin (BK, checked bars, n=3). Stimulated conditions are compared to basal levels of $[Ca^{2+}]_i$ (Basal, n=7). Overall basal $[Ca^{2+}]_i$ is given by the open bar. Values are given as mean ± SEM. Each value is the mean of different determinations. Significance was determined by One-way ANOVA with Bonferroni correction and P-values are: $p<0.001$(*).

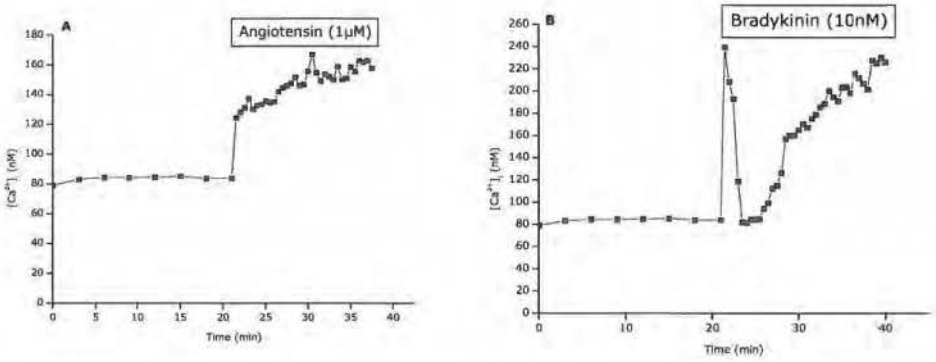

Figure 3.10: Ca^{2+}-response after stimulation with Angiotensin II or Bradykinin.
A: In confluent monolayers of PTC, ATII rapidly increased $[Ca^{2+}]_i$ to a plateau. B: In PTC, BK induced a transient increase in $[Ca^{2+}]_i$ after which Ca^{2+}-levels returned to baseline. In the continuous presence of BK, $[Ca^{2+}]_i$ increased again towards a plateau. Both figures show representative traces of the experiment (n=3).

3.5 Discussion

Microdissection of individual nephron segments was used to culture PT cells from mouse kidney. The microdissection technique has the major advantage of providing pure starting material (Jans et al., 2000). However the yield is rather low and it is a time-consuming method exposing the cells to oxidative or mechanical aggression. PT cells have been shown to be very susceptible to membrane and oxidative damage during the isolation method compared to tubular fragments of a more distal origin (Baines et al., 1990; Weinberg et al., 1990; Wagner et al., 2003). Thus, to properly culture PT cells we need a fast isolation method with a minimum of aggressive manipulations.

The method described here is a combination of careful dissection of the kidney, enzymatic digestion and sieving. This low cost procedure is characterized by a rather high yield, and it enables a rapid isolation of a large number of PT fragments. When brought into culture, cellular outgrowth is observed at the open ends of the tubular fragments within a few days. After 7 days, a monolayer of polygonal PTC is formed. Taub et al. (Taub et al., 1989) reported the use of hormonally defined serum-free medium to culture differentiated PTC, with restricted outgrowth of fibroblasts or glomeruli. In our hands, the absence of serum caused a restricted growth of the PT cultures, and a concentration of 1% FCS was necessary to obtain confluent cultures within a reasonable time. No fibroblast overgrowth was observed.

Electron microscopic analysis revealed that confluent monolayers grown on collagen-coated membranes had a cobblestone-like appearance and were polarized. The tight junctions were confined to the apical poles. Coated vesicles were also observed in the PTC and are known to be involved in the endocytic uptake mechanism of reabsorption of low-molecular weight proteins that have been filtered across the glomerulus. Moreover, the cytosol contained numerous mitochondria and also basolateral invaginations were observed, both characteristic features of PTC *in vivo*. We also show that PTC cultured in our conditions show a primary cilium at the apical membrane, which is another indicator of their differentiation (Pan et al., 2005). These results indicate that PTC when cultured on permeable collagen-coated filter membranes retain a high degree of morphologic differentiation. When grown on a solid support, cells were flatter, elongated and the apical tight junctions were less defined. The PTC

developed typical ultrastructural characteristics of myofibroblasts, such as stress fibers. Furthermore, cell growth was retarded.

The presence of specific markers, like transporter proteins or brush border enzymes, was established to characterize these primary cultures (Agre et al., 2002). In particular, we evaluated the expression of the PT water channel, AQP1, in comparison to NCC and AQP2, which are mostly expressed in the early distal tubule and in the collecting duct, respectively. The PTC cultured in our conditions showed a clear immunoreactivity against AQP1, while no positive signal for AQP2 or NCC was obtained. These results indicate that our primary cell cultures originated from PT cells, without significant contamination of cells from other parts of the nephron. Moreover we investigated whether specific markers of the endocytic apparatus were present in our primary cultures. The multiligand receptor, megalin, is located at the brush border of PT cells and participates in protein reabsorption from the primitive urine. The chloride channel, ClC-5, and the vacuolar proton pump, V-ATPase, are both localized in endosomes (Devuyst et al., 1999; Sakamoto et al., 1999; Jouret et al., 2004) ensuring correct endosomal acidification and protein trafficking in PT cells (Christensen et al., 2003). All of these components of the endocytic apparatus were detected in our primary PT cells, indicating that these cells possess functional markers of the PT. Since essential components of the endocytic apparatus were detected in our primary PT cells, we then investigated whether receptor-mediated endocytosis (RME) could be performed by these cells. The quantitative analysis of the uptake process of FITC-albumin showed that the uptake was saturable as a function of dose and decreased at 4°C. The calculated apparent K_m (36 ± 0.9 mg/l) was comparable with those described in the literature (Park & Maack, 1984; Schwegler et al., 1991; Gekle et al., 1996; Lazzara & Deen, 2007) indicating the presence of a functional endocytic apparatus characterized by a high affinity and low capacity in our cells. The large variability in the analysis is due to the heterogeneity among different sets of cell cultures. Lineweaver-Burk analysis of cell cultures with high uptake and low uptake as compared to mean values (fig. 3.5, inset) shows that the different sets of cell cultures possess different V_{max}-values but the same K_m-value meaning that the same transport system is present but that the expression level at the brush border membrane is different.

In the immunoblotting experiments, a difference in level of expression of megalin between different sets of cultures was observed. Therefore, the difference in rate of uptake (different V_{max}-values) could be explained by the difference in expression levels of megalin, the receptor responsible for binding and internalizing albumin in proximal tubule cells (Christensen & Birn, 2001). As all uptake data are normalized for the amount of protein in each cell culture and all experiments are conducted on 7-days confluent monolayers, we believe that factors like age of cell cultures and cell density as well as number of cell divisions can be ruled out to play a role in the differences observed in V_{max}.

Thus, the method enables us to isolate and grow highly differentiated primary cultures, which express distinct essential PT transport proteins.

By a simple spectrophotometric assay, we demonstrated the presence of alkaline phosphatase, an enzyme that catalyzes the hydrolysis of phosphate monoesters, and γ-glutamyl-transferase, an enzyme that catalyses the transfer of a γ-glutamyl moiety of glutathione to a variety of α-amino acids. Freshly isolated proximal tubules were also analyzed since they resemble more closely the *in vivo* situation and thus enzyme activity should be preserved as well. For both enzymes, the activity was lower in isolated PT as compared to 7-day old PTC. This difference might be due to the collapse of the tubular lumen during isolation (Rodeheaver et al., 1990) and therefore, only enzyme activities at the open endings are measured. However, surface markers, like brush border enzymes, are known to be unstable during the transition from *in vivo* to *in vitro* (Van der Biest et al., 1994).

In order to characterize our cells functionally, we evaluated the transport of glucose at the apical membrane, another specific cellular function of PT cells. PT cells possess at their apical membrane a sodium-dependent glucose transport system (Del Valle et al., 2002) ensured by the SGLT-protein (Wright, 2001). Using [^{14}C]-α-methyl-D-glucopyranoside (α-MG), a stable glucose analogue transported by SGLT, we demonstrated that our primary cultures were capable of transporting glucose. The uptake of α-MG, strictly observed at the apical side of the cells, was saturable as a function of time, and almost completely inhibited by phloridzin, a non-transportable competitive inhibitor of the SGLT-proteins as observed by Schaaf et al. (Schaaf et al., 2001). When sodium was omitted from the transport buffer and replaced by choline chloride, sugar uptake was only

18% of control values after 60 minutes, indicating that the observed α-MG transport is indeed sodium dependent. Note that a small amount of α-MG was still taken up in Na^+-free conditions, which might represent passive diffusion of α-MG (Sakhrani et al., 1984). Immunostaining showed the presence of both SGLT1 and SGLT2 in primary PTC. These subtypes of the SGLT family are expressed at different segments of the proximal tubule with SGLT1 being preferentially expressed in the S3 segment and SGLT2 in the S1/S2 segment (Wright, 2001). In our primary cultures, proximal tubule cells from both segments are present. These results demonstrate the presence of a sodium-dependent glucose transport at the apical membrane of our primary cultured cells.

Proximal tubule cells possess a variety of hormone receptors at their apical and/or basolateral membrane. Intracellular Ca^{2+}-signalling has been described after stimulation of the B2-receptor with bradykinin (BK) and after stimulation of the angiotensin type 1 receptor (AT1-receptor) with angiotensin II (ATII) (Aboolian & Nord, 1988; Miyata et al., 1999; Tiwari et al., 2007). In our primary cultures of PTC, an increase of $[Ca^{2+}]_i$ was observed after stimulation with both ATII and BK. The high concentration of ATII necessary to elicit an increase in $[Ca^{2+}]_i$ is consistent with findings in the literature: Concentrations in the micromolar range are necessary to obtain ATII-induced Ca^{2+}-releases (Douglas, 1987; Romero et al., 1991). Low concentrations of ATII (in the picomolar to nanomolar range) inhibit cAMP production in the proximal tubule cells and thereby enhance fluid reabsorption. High ATII concentrations (in the micro- to millimolar range) seem to have the opposite effect (Douglas, 1987). Furthermore, ATII induced a small increase in $[Ca^{2+}]_i$ towards a plateau. This is consistent with findings obtained by Welsh et al. (Welsh et al., 1988). In contrast with ATII, BK induced a transient increase, which was followed by a slower increase towards a plateau, if BK remained present. Furthermore, a concentration of 1nM bradykinin seems to elicit the highest Ca^{2+}-response in our primary PTC. Higher doses of BK might cause a desensitisation of the B2-receptor and therefore, the Ca^{2+}-response is lower. These observations are similar to findings in primary cultures of rabbit proximal tubule cells by Aboolian et al. (Aboolian & Nord, 1988) and in the mouse proximal tubule cell line, TKPTS (Tiwari et al., 2005). Tiwari et al. have reported that activation of the B2-

receptor with BK and the subsequent increase in $[Ca^{2+}]_i$ induces a chloride conductance in proximal tubules (Tiwari et al., 2007). A basal $[Ca^{2+}]_i$ of 82.5 ± 2.6 nM was measured in our primary cultures of PTC. This is in the same range of values found by others (Bonventre & Cheung, 1986; Goligorsky et al.,1986; Suzuki et al., 1989).

In conclusion, we have described a novel method to culture mouse PT cells on collagen-coated membranes with a reasonable yield. Electron microscopic analysis displayed a differentiated morphology of polarized cells with characteristics of PT cells. Furthermore, the presence of PT-specific proteins, such as water-, ions- or glucose-transporters, a receptor-mediated endocytosis of proteins and efficient brush border-associated enzymes demonstrated that these primary cells retained the differentiated functions of their *in vivo* counterparts for at least 3 to 4 days after reaching confluence (day 7). Since these cultures were established on collagen-coated membranes, this method represents a useful tool to study a variety of proximal transport systems and the influences of different substances like hormones at both the apical and the basolateral sides of the PT cell. Moreover, used in an Ussing chamber, the confluent monolayer allows to study and follow the electrogenic transport characteristics online (described in chapter 4).

Chapter 4

Electrophysiology of the proximal tubule

The results of this chapter are described in:

Electrophysiological properties of mouse proximal tubule cells in primary culture.

Sara Terryn, Willy Van Driessche, Paul Steels and Emmy Van Kerkhove. *In preparation*

4.1 Introduction

Electrophysiological analysis of the proximal tubule epithelium is a powerful tool for the study and characterisation of the epithelial transport processes. Not only can the electrical properties like short-circuit current (I_{SC}), transepithelial conductance (G_T), resistance (R_T) and capacity (C_T) be continuously recorded but also the relative contribution in total transport of different ions or substrates coupled to the ion transport can be assessed. Furthermore, the effects of different hormones, toxins, etc. on the electrical properties and transport processes of the epithelium can be analyzed. However, it is essential to culture proximal tubule cells on permeable supports in order to measure and follow electrophysiological properties in an Ussing-type chamber since both the apical and basolateral membranes need to be accessible by an electrolyte solution of known composition. As indicated in chapter 3, proximal tubule cells grown on filters are polarized cells and they possess tight junctions at the apical pole. Both polarity and tight junctions are fundamental features of the transporting epithelium. Polarity creates the necessary gradient for vectorial net transport of substances across epithelia. Tight junctions form the major intercellular barrier between luminal side and lateral intercellular space (LIS) and seal the paracellular transport route in a variable, dynamic manner (Cereijido et al., 1998; Madara, 1998; Guo et al., 2003). In the proximal tubule, the tight junctional complexes connecting neighbouring cells are highly permeable to different ions and solutes. Therefore, the electrophysiological properties of the proximal tubule are characteristic for a leaky epithelium (Boulpaep & Seely, 1971; Barratt et al., 1974; Lapointe et al., 1984). The high transepithelial transport rates, established by the numerous transport systems in both apical and basolateral membranes, combined with the permeability of the tight junctions are characterized by a high conductance (G_T), a low transepithelial resistance (R_T) and a high short-circuit current (I_{SC}).

Contrary to tight epithelia, measuring the electrophysiological properties of a leaky epithelium is complicated by the very low R_T-values that are in the same order of magnitude as the series resistance (R_S, resistance of the solution and support). Usually the R_S amounts to values up to 40 – 50 $\Omega.cm^2$, while the R_T of leaky epithelia is around 5 to 30 $\Omega.cm^2$ and tight epithelia show a few $k\Omega.cm^2$ (as previously indicated in chapter 1, section 1.4). It is therefore necessary to

perform impedance measurements that allow distinguishing the R_S from the R_T and correcting the recorded I_{SC} accordingly. Impedance measurements are also done to determine transepithelial membrane capacitance (C_T).
In this chapter, electrophysiological properties of proximal tubule cells in primary culture were investigated. The role of Na^+ and Na^+-coupled solutes in the transport processes of proximal tubules were determined.

4.2 Electrophysiological measurements

4.2.1 Ussing chamber

The Ussing-type chamber was especially designed for the measurement of leaky epithelia at 37°C. Because cells were cultured on small Costar® filters (6.5mm diameter), the very flexible PTFE membrane with the epithelium could not be removed from the filter holder. Cutting out the membrane would have damaged the epithelium. Therefore, a vertical chamber in which the entire Costar® transwell fitted, was designed (as shown in figure 4.1). The apical, cylindric part was oriented upwards thus avoiding that air bubbles, which are continuously generated when working at 37°C, were trapped at the apical membrane surface. However, with this arrangement, air bubbles could accumulate near the basolateral side of the filter. Therefore, a space in the basolateral compartment that extended up to 4mm above the filter membrane was provided. Outflow of solution, and possible air bubbles, occurred through an outflow tube that was forseen in the upper corner of the compartment extension. The inflow tubing in the basolateral compartment was located perpendicularly under the outflow. In this way, air bubbles in the inflow immediately moved to the outflow. Also, the chamber was mounted under an angle of 6° with the outflow tubing facing upwards. Furthermore, in this setup the apical and basolateral voltage electrodes are positioned very close to the epithelium. This is a prerequisite to generate accurate measurements of the transepithelial capacitance (C_T) and resistance (R_T). The closer the voltage electrodes are positioned to the epithelium, the lower the series resistance (R_S). The current electrodes are placed at 15mm from the epithelium to ensure a uniform distribution of the current through the epithelium. The Ag/AgCl current and voltage electrodes are connected with the bath solutions by agar bridges containing 3% agar in 3M KCl medium. The offset potential of the electrodes was measured at the beginning

and the end of each experiment and was always smaller than 1mV. This manoeuvre is important to prevent wrong I_{SC} measurements based on an attribution of the voltage clamp feedback due to unequal dilution potentials of the electrodes.

The Ussing-type chamber was placed on a support built in a home-made transparent box in which the air was kept at 37°C by constant ventilation through a heating element under control of a thermostat and a thermocouple inside the box. Perfusion solutions (Table 4.1) were also placed inside the box and kept at a constant temperature of 37°C.

Table 4.1. Composition of Ringer solution for electrophysiological experiments (in mM)

	Control	$-Na^+$	$-PO_4^{2-}$	-glucose	-substrates
NaCl	140	-	140	140	140
NMDG	-	140	-	-	-
$CaCl_2$	1.5	1.5	1.5	1.5	1.5
Hepes	10	10	10	10	10
KCl	5	5	5	5	5
$MgSO_4$	1	1	1	1	1
KH_2PO_4	3.67	3.67	-	3.67	-
K_2HPO_4	-	0.5	-	-	-
Na_2HPO_4	3.0	-	-	3.0	-
Glucose	5.5	5.5	5.5	-	-
Sucrose	-	-	-	5.5	5.5
L-glutamine	2	2	2	2	2
Pyruvate	0.55	0.55	0.55	0.55	0.55
Alanine	1	1	1	1	-
Glycine	5	5	5	5	-

pH: 7.4 with TRIS-base and osmolality: 325mOsm/kg H_20 with mannitol

Figure 4.1: Vertical assembly of the Ussing-type chamber

The Ussing-type chamber consisted of an apical and a basolateral part made of transparent Plexiglas. The filter containing the primary cultures was placed in the apical part. The filter extended into the basolateral part. In both parts, Ag/AgCl voltage electrodes were placed in the proximity of the epithelium, while Ag/AgCl current electrodes were positioned on a certain distance from the epithelium. The two parts were tightly sealed with screws and placed on the support mounted in a perfusion box at 37°C.

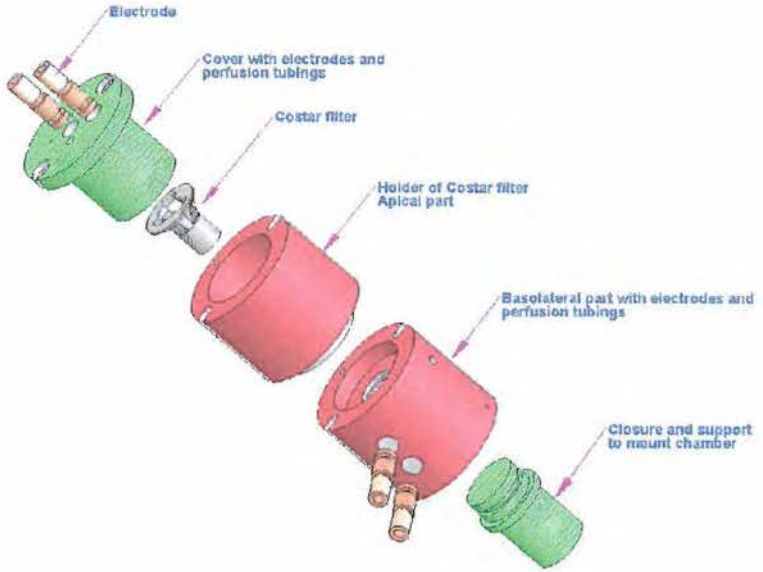
Electrode
Cover with electrodes and perfusion tubings
Costar filter
Holder of Costar filter Apical part
Basolateral part with electrodes and perfusion tubings
Closure and support to mount chamber

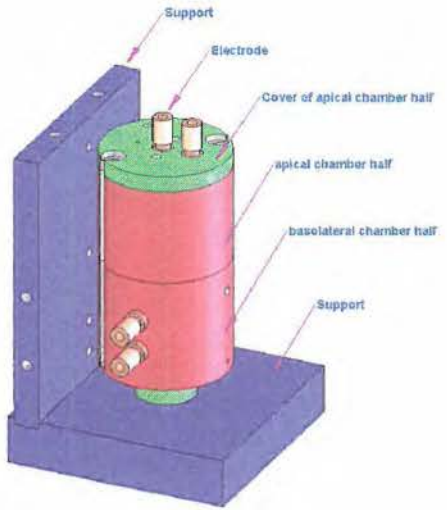
Support
Electrode
Cover of apical chamber half
apical chamber half
basolateral chamber half
Support

4.2.2 Electrical measurements and impedance analysis

Seven- to 10-days old confluent primary cell cultures were gently placed in the Ussing-type chamber (described above in section 4.2.1). During the measurements, cultures were constantly perfused at both sides with warm (37°C) Ringer solution (see control Table 4.1) unless stated otherwise. Transepithelial voltage was continuously clamped to zero with an automatic voltage-clamp apparatus connected with Ag/AgCl voltage and current electrodes. The short-circuit current (I_{SC}) was the current through the external electrical circuit that was necessary to clamp the transepithelial potential to zero. For leaky epithelia, it is essential that the voltage electrode offset potential is close to 0 mV because it will also be clamped to zero and results in an erroneous current generated by the clamp circuit. Otherwise, the current electrodes will indicate an erroneous I_{SC}, due to the multiplying of difference in electrode potential. I_{SC} was registered by the current electrodes. The transepithelial conductance (G_T) and capacitance (C_T) were registered simultaneously. G_T can be calculated from the I_{SC}-deflection induced by a brief voltage-deplacement according to Ohm's law. C_T is calculated from the impedance data as described below.

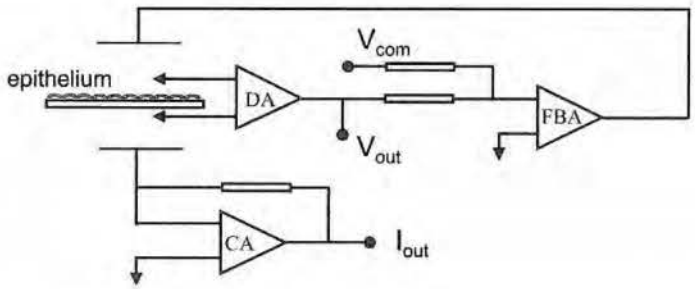

Figure 4.2: Voltage clamp and transepithelial current and resistance recording
Ag/AgCl voltage electrodes are placed in the proximity of the epithelium, connected to a differential amplifier (DA) that records the voltage across the epithelium. The DA in turn is connected to a feedback amplifier (FBA), which is set to change continuously the voltage to zero transepithelial potential. Ag/AgCl current electrodes are placed on a distance of the epithelium and connected to a current amplifier that registers the current through the epithelium.

Impedance analysis takes advantage of the capacitance formed by the lipid bilayer (fig. 4.3A). This capacitor is located in parallel with the ion channels which behave electrically as a conductive pathway. Consequently the electrical equivalent circuit of cell membrane consists of a parallel arrangement of a resistor and capacitor (fig. 4.3C). At low frequencies, the impedance (ratio of voltage (V) by current (I)) of the membrane is determined by the ion conductive pathway because the capacitor behaves as a very low conductive pathway. This becomes obvious from the following reasoning: The amount of electrical charge on the capacitor (Q) perfectly follows the voltage across the membrane: Q=C.V (fig. 4.3B). If the voltage changes slowly, only small currents (I) are needed to adjust the slowly changing Q. Thus, at low frequencies, the impedance (V/I) of C_m will be large. However, at high frequencies, voltage changes rapidly and large currents are required to guarantee that Q follows V. Consequently, at very high frequencies the impedance of the capacitor becomes small and even will vanish. Due to the fact that membrane conductance and capacitance are arranged in parallel, also the membrane impedance will be decreased to zero. On the other hand, at low frequencies (and DC), the membrane impedance equals R_m.

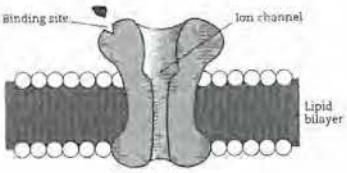

Figure 4.3A: The cell membrane as a capacitor
The lipid bilayer of the cell membrane acts as a capacitor (C) that charges electrical current. The presence of ion channels defines the conductance (G) or resistance (R) of the cell membrane.

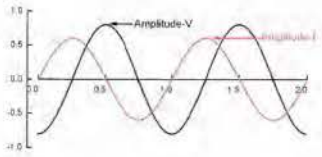

Figure 4.3B: Electrical behaviour of capacitance
Voltage is delayed to current flow because current provides the charge on the capacitor. Voltage is directly proportional to charge: $V=Q/C_m$. If the capacitor is not shunted by a parallel resistance, as in the illustration, the phase shift is 90°.

$I(t) = I_m \sin(\omega t + \varphi)$

$V(t) = V_m \sin(\omega t - \varphi)$ with $\omega = 2\pi f$ and $\varphi = 90°$

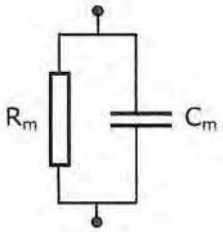

Figure 4.3C: Electric equivalent circuit of the plasma membrane.
R_m represents the ion conductive pathway. Cm represents the capacitance of the lipid bilayer.

When studying epithelia in Ussing chambers, voltage is recorded with 2 electrodes that are located at a small distance from the membrane. In our chambers, the solution layer between an electrode and the epithelium has a resistance of about 25 Ω. So, the sum of the resistances of the apical and basolateral solution layer will be approximately 50 Ω. This series resistance is larger than the transepithelial resistance (R_T) of monolayers of proximal tubular cells. From DC measurements in the Ussing chamber, we will obtain the total resistance between the voltage electrodes, which is the sum of R_s and R_T ($R_{total} = Z_{total}(DC) = R_s \pm R_T$). Thus, DC measurements of the transepithelial resistance are hampered by the presence of the comparatively large series resistance.
As explained above, at high frequencies the impedance of the apical and basolateral cell membrane will vanish. Consequently, due to the presence of the membrane capacitances, transepithelial impedance at high frequencies will approach zero and the impedance of the preparation including the bathing solution, will approach the series resistance. So, the fact that cell membranes have an electrical capacitance enables us to measure R_s with a high frequency sine wave. From R_{total} (DC) and R_s we can determine R_T (fig. 4.4C).
The presence of the relatively large solution resistance not only masks the transepithelial resistance, but it also leads to an underestimation of the short circuit current (I_{SC}). Indeed when the resistance between the voltage electrodes is increased, less current is required to clamp the open circuit potential (V_{oc}) to zero. Indeed with $R_s=0$, I_{SC} and V_{oc} are related by:

$I_{SC} = V_{oc}/R_T$. With $R_s>0$, $I_{sc} = V_{oc}/(R_T + R_s)$. Consequently:

$$I_{sc}^{corrected} = I_{sc}^{recorded} \cdot \frac{R_s + R_T}{R_T}$$

Taking into account the above reasoning, we can build up a profound mathematical analysis based on the equivalent electrical model of the epithelium depicted in Figure 4.4A. The electrical equivalent circuit of the passive components of an epithelium can be represented by a model depicted in figure 4.4A. It consists of two RC networks (R_aC_a and R_bC_b) that represent the resistance and capacitance of the apical (a) and basolateral (b) membrane. Furthermore, in this model the resistance of the paracellular pathway is represented by R_p. R_s represents the solution resistance discussed above. For this model the transepithelial capacitance equals:

$$\frac{1}{C_T} = \frac{1}{C_a} + \frac{1}{C_b} \quad (1)$$

Unfortunately, from transepithelial impedance data it is not possible to determine the individual values of C_a and C_b (Gordon et al., 1989). Van Driessche et al. (1999) demonstrated that at high frequencies, C_T equals the capacitance obtained from model calculations based on the simple R_T-C_T model depicted in figure 4.4B. With this model we can calculate R_s from impedance data recorded at two frequencies well above the characteristic frequency of the RC circuit: $f_c=1/(2.\pi.R_T.C_T)$.

$$R_S = \frac{R_{Z1}\frac{I_{Z2}}{\omega_2} - R_{Z2}\frac{I_{Z1}}{\omega_1}}{\frac{I_{Z2}}{\omega_2} - \frac{I_{Z1}}{\omega_1}} \quad (2)$$

Our system used 5 sine waves with frequencies in the range of 2 to 8 kHz. R_S was calculated as mean value of 10 possible combinations of the set of 5 frequencies. With this value of R_S we could determine C_T and R_T as:

$$C_T = \frac{-I_Z}{\omega\left((R_Z - R_S)^2 + I_Z^{\,2}\right)} \quad (3)$$

and

$$R_T = \frac{(R_Z - R_S)^2 + I_Z^{\,2}}{(R_Z - R_S)} \quad (4)$$

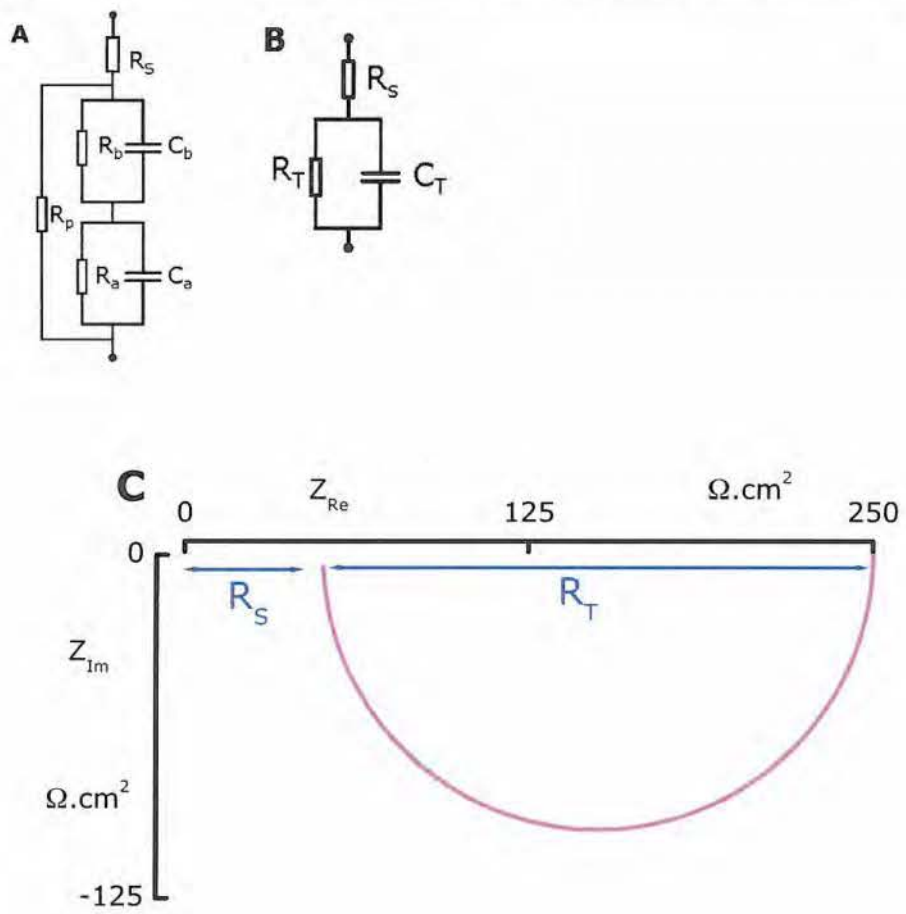

Figure 4.4: Models for the analysis of membrane impedance

A: Electrical equivalent circuit for the lumped model representing an apical and a basolateral membrane. The transepithelial capacitance equals an equivalent capacitance of a series arrangement of the apical (C_a = capacitance apical membrane and R_a = resistance apical membrane) and basolateral membrane (C_b = capacitance basolateral membrane and R_b = resistance basolateral membrane). The series arrangement of apical and basolateral membrane is shunted by a paracellular resistance (R_p) which represents the conductive properties of the paracellular pathway. **B**: Electrical equivalent circuit for a single membrane used to calculate transepithelial capacitance (C_T). R_T is the transepithelial resistance. **C**: Nyquist plot of an epithelial membrane displays one semicircle from which the transepithelial resistance (R_T), series resistance (R_S) and capacitance can be determined. Since there is a time-dependent factor in the formula (ω), impedance data can be represented by an imaginary (Z_{Im}, Y-axis) and a real (Z_{Re}, X-axis) part.

4.3 Results

4.3.1 The role of sodium transport

Proximal tubule cells are characterized electrophysiologically by low transepithelial resistance (R_T) resulting in a high transepithelial flow. Steady-state values show that our primary cultures of proximal tubule cells possess a short-circuit current (I_{SC}) of about 14.0 ± 0.4 μA/cm² and a R_T of 53.8 ± 0.9 Ω.cm² (n=7). Transepithelial capacitance (C_T) measured 1.13 ± 0.02 μF/cm². Since proximal tubule cells reabsorb about 67% of total filtered Na^+, they are predominantly Na^+-transporting cells. Therefore, I_{SC} should be almost completely carried by Na^+ and show a positive deflection on the recording. Only a small fraction is expected to be due to the electrogenic H^+ secretion into the luminal fluid via the H^+-ATPase, which should result in a negative current. To investigate this, Na^+ was replaced with $NMDG^+$ in the Ringer solution and Na^+-free Ringer was perfused at both sides of the epithelium.

In all experiments, changes in Ringer solutions were done simultaneously at both sides of the epithelium to avoid passive concentration-dependent diffusion potentials or back-leak through the tight junctions resulting in mixtures of both perfusion solutions. As shown in figures 4.5 to 4.8, removal of Na^+ resulted in an instant drop of I_{SC} to a value of -6.0 ± 0.3 μA/cm² (n=9). Removal of Na^+ also resulted in a decrease in the conductance (G_T), expressed by an increase in R_T to 145.5 ± 5.9 Ω.cm² (fig. 4.6). The increase in R_T was also observed in the Nyquist plot (fig. 4.9). A small drop (about 12%) in C_T to 0.99 ± 0.03 μF/cm² was also observed. In some experiments, the change in C_T was transient with a sudden drop immediately after Na^+ removal followed by a return to steady-state levels and then a plateau at lower C_T-values compared to steady-state (fig. 4.5). In other experiments, no transient change in C_T was observed. Here, C_T dropped immediately after Na^+ removal and values remained low until epithelia were perfused with control Ringer again (fig. 4.6 and 4.7).

4.3.2 The role of solute transport

A large part of total sodium transport in the proximal tubule is carried by sodium-dependent co-transporters. Here, the role of glucose, phosphate and amino acids was investigated in relation to the total transport of sodium. Different substrates of sodium-dependent cotransporters were omitted from the Ringer solution and the changes in I_{SC}, G_T and C_T were compared with the respective changes after a Na^+-omission. In fig. 4.5, glucose was replaced with equimolar amounts of sucrose and glucose-free Ringer superfused the epithelium at both sides. Omission of glucose resulted in an immediate drop in I_{SC} with ~28%. Also, R_T increased to 102.7 ± 2.6 Ω.cm² and a small decrease in C_T similar as observed in Na^+-free conditions could be seen (fig. 4.5).

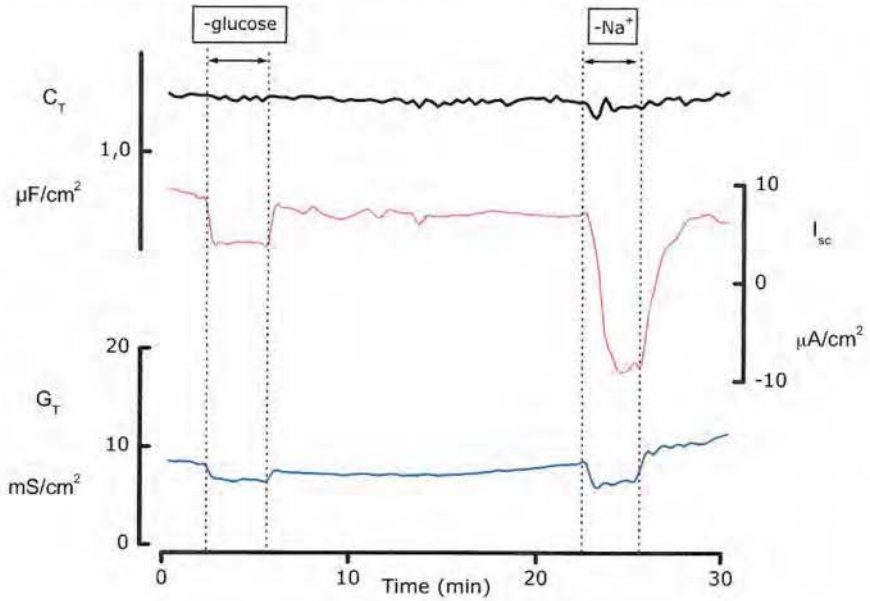

Figure 4.5: The effect of glucose replacement on I_{SC}, G_T and C_T.
Comparison of the time course of I_{SC}, G_T and C_T after omission of glucose or Na^+ from the perfusion solution. Seven-days old primary PTC were perfused at both sides with control Ringer solution. At indicated times control Ringer was replaced by: a) glucose-free Ringer in which glucose was replaced with equimolar concentration of sucrose (-glucose) or b) Na^+-free Ringer with equimolar replacement of $NMDG^+$ for Na^+ (-Na^+). Representative trace of 3 individual experiments (n=3).

Omission of phosphate from the Ringer solution, as shown in fig. 4.6, resulted in a ~30% drop in I_{SC} similar to the decrease in I_{SC} observed after omission of glucose from the Ringer solution. Also a small decrease in both G_T and C_T could be observed. Thus R_T increased to a value of 89.1 ± 2.5 Ω.cm² (fig. 4.6).

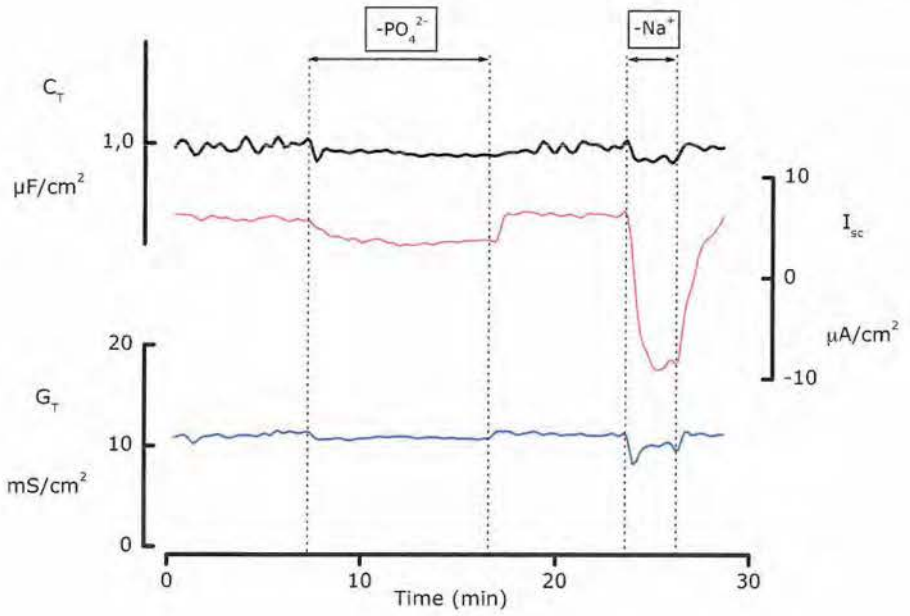

Figure 4.6: The effect of phosphate omission on I_{SC}, G_T and C_T.
Time-courses of I_{SC}, G_T and C_T after omission of phosphate ($-PO_4^{2-}$) or replacement of Na^+ with $NMDG^+$ ($-Na^+$) at indicated times on both sides of the epithelium. Under control conditions, PTC were perfused with control Ringer solution on both sides. Representative trace of 3 individual experiments (n=3).

When all substrates i.e. glucose, phosphate and amino acids, were removed from the Ringer solution, I_{SC} decreased to about 76% decrease of the I_{SC} compared to control conditions, as shown in figure 4.7. The drop in I_{SC}, when all substrates were removed, was larger than when only phosphate (30%) or glucose (28%) was omitted from the Ringer solution, as indicated in fig. 4.8. Furthermore, under these conditions, C_T decreased in parallel with an increase in R_T to a value of 100.6 ± 2.4 Ω.cm² (fig. 4.7).

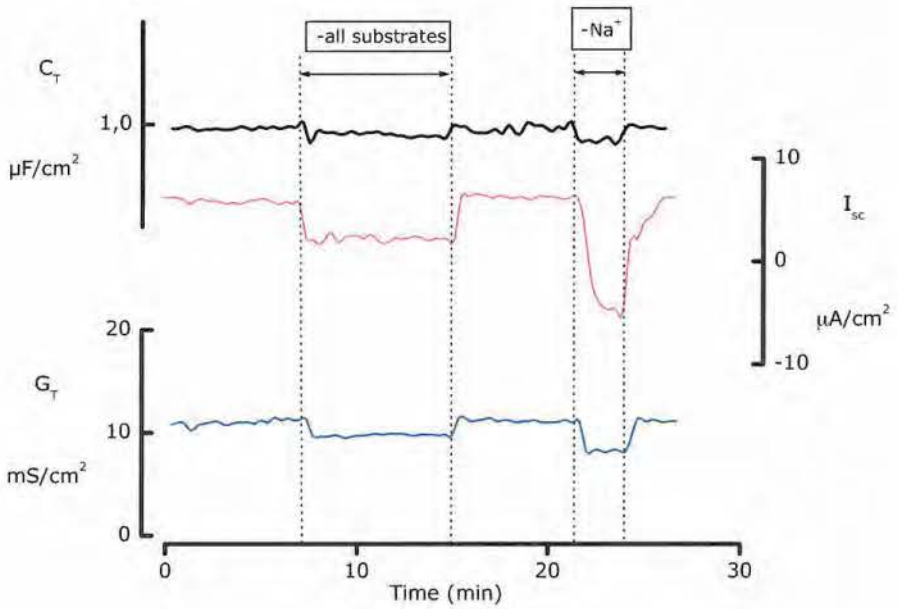

Figure 4.7: The effect of omission of all substrates on I_{SC}, G_T and C_T.

Time-course of I_{SC}, G_T and C_T after omission of all substrates (-all substrates) or replacement of Na^+ with $NMDG^+$ ($-Na^+$). Under control conditions, PTC were perfused with control Ringer on both sides of the epithelium. At indicated times, control Ringer was replaced on both sides of the epithelium with: a) substrate-free Ringer in which glucose was replaced with equimolar concentration of sucrose and phosphate and amino acids were omitted or b) Na^+-free Ringer in which Na^+ was replaced with equimolar concentrations of $NMDG^+$. Representative trace of 3 individual experiments (n=3).

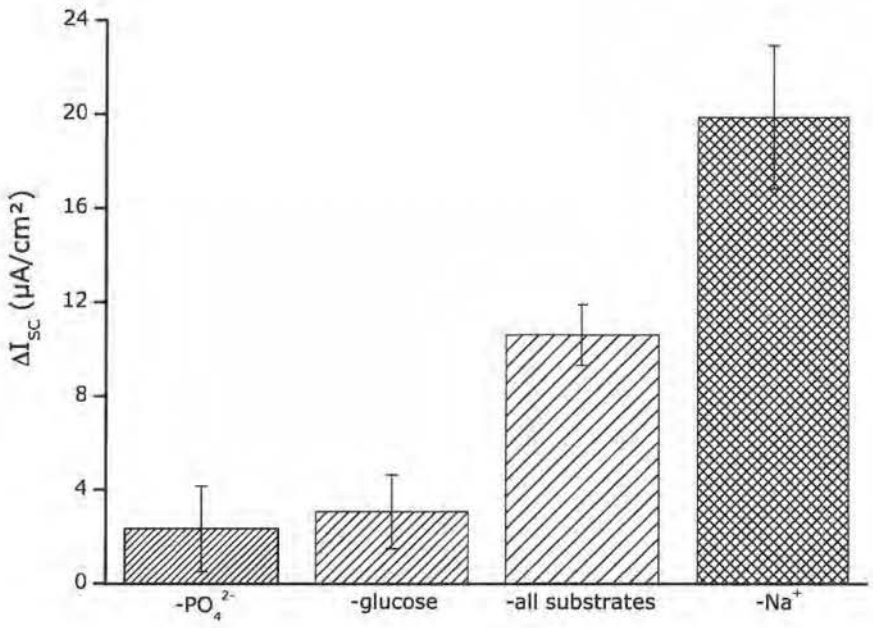

Figure 4.8: ΔI_{SC} under different conditions.

Difference in short-circuit current measured in primary PTC after omission of phosphate (-PO_4^{2-}), glucose (-glucose), all substrates (-substrates = -glucose, -phosphate and – amino acids) or Na^+ (-Na^+) as compared to steady-state conditions in normal Ringer solution. Values are expressed as mean ± SEM of different experiments (n=3 except for Na^+-removal, n=9).

4.3.3 Impedance measurement

The values obtained by the calculation from the Nyquist plot (fig. 4.9) using the formulas (1), (2) and (3) from section 4.2.2, are given in figure 4.10.

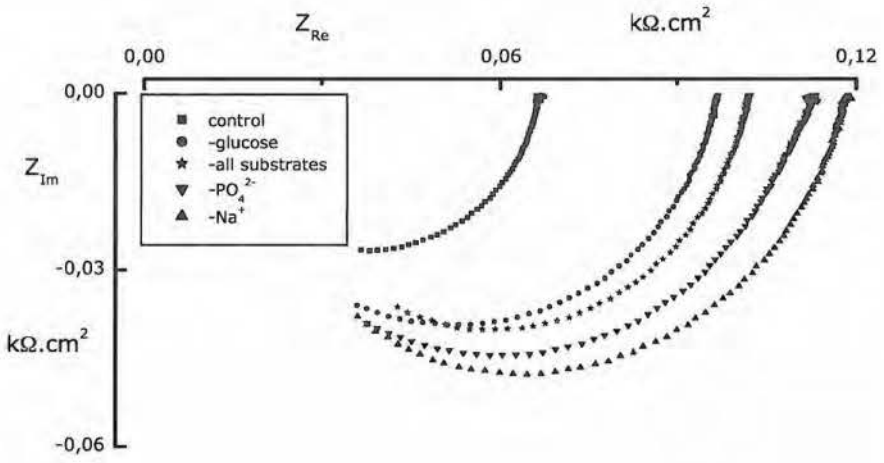

Figure 4.9: Impedance measurement of a representative experiment
Impedance data under control conditions (■) and after omission of glucose (●), phosphate (▼), all substrates (★) or sodium (▲) from the Ringer solution. C_T, R_T and R_S values were calculated from the curves according to the equations described in section 4.2.2.

The series resistance (R_S) was 18.4 ± 0.5 Ω.cm² in control conditions and remained unchanged under the other experimental conditions. However, transepithelial resistance (R_T) changed drastically when solutes or Na^+ were omitted from the Ringer solution. Under control conditions, a R_T of 53.8 ± 0.9 Ω.cm² was measured and a 2-fold (after removal of solutes) or even 3-fold increase after Na^+ removal could be observed. The transepithelial capacitance (C_T) amounted to 1.13 µF/cm² under control conditions and decreased slightly although not significantly after removal of either solutes or Na^+. An overview of all data is given in table 4.2.

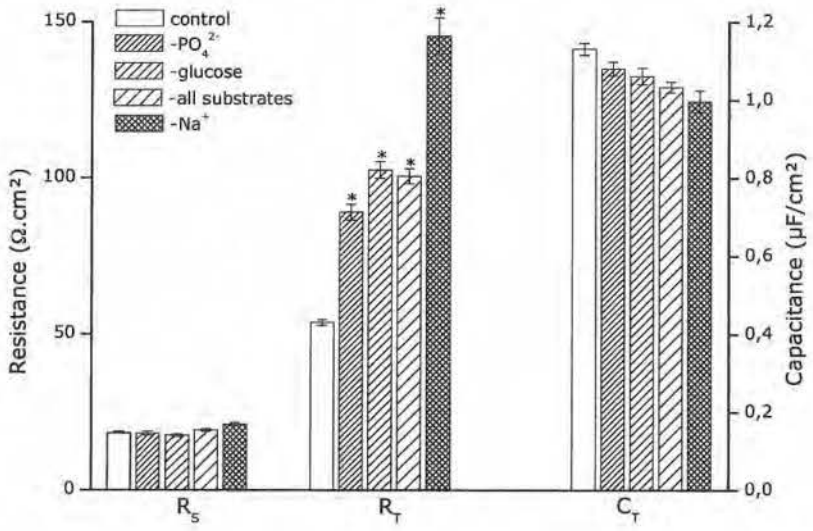

Figure 4.10: Values for series (R_S) and transepithelial resistance (R_T) and transepithelial capacitance (C_T) calculated from the impedance data

In control conditions (open bars), R_S amounted to 18.4 ± 0.5 Ω.cm² and was not significantly different in the other experimental conditions. Transepithelial resistance (R_T) was 53.8 ± 0.9 Ω.cm² under control conditions and increased significantly when phosphate (89.1 ± 2.5 Ω.cm²), glucose (102.7 ± 2.6 Ω.cm²), all substrates (100.6 ± 2.4 Ω.cm²) or Na^+ (145.5 ± 5.9 Ω.cm²) were omitted from the Ringer solution. Transepithelial capacitance (C_T) decreased in all experimental conditions ($-PO_4^{2-}$: 1.08 ± 0.02 µF/cm²; -glucose: 1.06 ± 0.02 µF/cm²; -all substrates: 1.03 ± 0.01 µF/cm²; $-Na^+$: 0.99 ± 0.03 µF/cm²) as compared to control (1.13± 0.02 µF/cm²). Values are mean ± SEM of different experiments (n=9 for control and Na^+-removal, n=3 for all other experimental conditions). Significance was determined with One-way ANOVA with Bonferroni correction (*p<0.001).

Table 4.2: I_{SC}, R_T and C_T-values under different experimental conditions

	(Δ)I_{SC} (µA/cm²)	R_T (Ω.cm²)	C_T (µF/cm²)
Control	14.0 ± 0.4	53.8 ± 0.9	1.13 ± 0.02
$-Na^+$	Δ I_{SC} = 13.6 ± 3.1	145.5 ± 5.9	0.99 ± 0.03
-glucose	Δ I_{SC} = 2.3 ± 1.8	102.7 ± 2.6	1.06 ± 0.02
$-PO_4^{2-}$	Δ I_{SC} = 3.1 ± 1.6	89.1 ± 2.5	1.08 ± 0.02
- all substrates	Δ I_{SC} = 10.6 ± 1.9	100.6 ± 2.4	1.03 ± 0.01

4.4 Discussion

Little is known about the electrophysiological behaviour of mouse proximal tubule cells in primary cell culture. Possible explanations might be attributed to the technical difficulties connected to this kind of study. First, proximal tubule cells are difficult to culture due to their oxidative metabolism and sensibility to different kinds of stress generated during isolation (as described in chapter 3). Furthermore, a complete confluent monolayer is essential for measurements in an Ussing chamber. Secondly, the electrophysiological measurements are hampered by the leaky nature of the epithelium (Weinstein, 2000). Confluent proximal tubule cells show a typical low transepithelial resistance (R_T) which is in the same range as the series resistance (R_S) of the bathing solution and submucosa. In our vertical assembly setup, voltage electrodes are placed very close to the epithelium in order to keep R_S as low as possible. However, to evaluate changes in R_T, one must measure R_S as well. Furthermore, in leaky epithelia, I_{SC} is usually underestimated. We applied impedance measurements to calculate R_S, R_T and C_T and correct I_{SC} accordingly to these values. The series resistance, R_S, amounted to a mean value of 18.9 ± 0.3 Ω.cm². However, R_T and C_T changed in function of the composition of the Ringer solution. These changes will be discussed in detail below.

4.4.1 Dissecting I_{SC}

In our primary cultures of PTC, a high short-circuit current (I_{SC}) was measured which dropped immediately after replacing Na^+ for $NMDG^+$ in the Ringer solution indicating that the current was completely carried by Na^+ and that the Na^+-K^+-ATPase in the basolateral membrane is present and should be active. This coincides with the generally accepted view of the proximal tubule as a leaky Na^+-transporting epithelium. Since the measured I_{SC} is carried by Na^+, the transport rate of sodium per square area (J_{Na}) could be calculated from the I_{SC} (summarized in table 4.2). Doing so, a J_{Na} of 1.39 x 10^{-10} mol/s.cm² was obtained in our primary cultures. The J_{Na} *in vivo* can be calculated from the single nephron glomerular filtration rate (snGFR equals ~11nl/min in mice), plasma concentration of Na^+ ([Na^+] ~153mM) and the knowledge that about two thirds of filtered Na^+ is reabsorbed by the proximal tubule (Meneton et al., 2000). Given a total mean proximal tubule length of 4.57mm and a mean

luminal diameter of 14.4µm, the J_{Na} can be calculated at 47.8 x 10^{-10} mol/s.cm² (Zhai et al., 2003). However, in the calculation of the surface area, the apical membrane is assumed to be a flat sheet. *In vivo*, the apical membrane is extensively enlarged by the presence of an elaborate brush border, which augments the surface area by a factor 36 in the convoluted tubule and a factor 15 in the pars recta (Welling & Welling, 1975). This means that the transport rate of Na^+ (J_{Na} per square cm) should decrease with the same factor. By taking a mean factor of 25.5, J_{Na} *in vivo* decreases to 1.87 x 10^{-10} mol/s.cm². The J_{Na} calculated in our primary cultures is quite comparable with the *in vivo* situation. However, the J_{Na} from our cultures is also overestimated since the I_{SC} measurements were assumed over a surface area of 0.33cm², the area of the filter membrane; thus not taking the brush border into account. Furthermore, under voltage clamp conditions, I_{SC} is overestimated since the transepithelial potential is continuously clamped to zero. However, the lower J_{Na} in our cultures can be the result of four aspects. First, there are fewer microvilli and a less defined brush border present at the apical membrane (as observed by TEM, chapter 3). Thus, fewer transporters should be present since they are mainly located within the microvilli. Second, total transport rate of Na^+ should be reduced since the bicarbonate (HCO_3^-)/CO_2 system is not present in our setting. Na^+/HCO_3^- transport plays a major role in the total Na^+-reabsorption in the proximal tubule (Chan & Giebisch, 1981; Chan et al., 1982; Preisig et al., 1987; Preisig & Rector, 1988). Third, the I_{SC} measured under steady-state conditions is lowered by the secretion of H^+. This final statement is underlined by the fact that omission of Na^+ resulted in a reversal of the I_{SC} to a negative value of -6.0 ± 0.3 µA/cm². This means that either an anion was transported from the apical to the basolateral side or a cation was secreted at the apical membrane. Since, chloride passively follows the movement of Na^+ in the proximal tubule; the transepithelial uptake of Cl^- in the absence of Na^+ seems unlikely. On the other hand, protons (H^+) are continuously generated by the cellular metabolism and need to be secreted in order to maintain cellular pH at a constant level. Protons can be secreted by the Na^+/H^+-exchanger type 3 (NHE_3) which has been studied in detail in the proximal tubule (Preisig et al., 1987; Preisig & Rector, 1988). However, this transporter can be ruled out since its driving force, namely the uptake of Na^+, is not present. Another possibility might be the extrusion of

protons via the V-type H^+-ATPase, which actively pumps H^+ out of the cell at the apical membrane (Nakhoul & Hamm, 2002). We already indicated the presence of a V-ATPase by immunoblotting in chapter 3. Fourth, *in vivo* the colloid osmotic pressure in the peritubular capillaries is high. In the glomerulus, water and solutes are filtered thereby concentrating proteins which are not filtered. The high colloid osmotic pressure attracts water and solutes to the peritubular capillaries. In our primary cultures, there was no change in colloid osmotic pressure between the apical and basolateral compartment. Therefore, the J_{Na} should be lower than the J_{Na} calculated from the in vivo situation, where colloid osmotic pressure differences influence transepithelial water and salt transport.

After replacing glucose for sucrose in the Ringer solution, a small drop in I_{SC} was observed indicating that glucose is transported over the apical membrane in an electrogenic way, achieved by the presence of a sodium-dependent glucose cotransporter (Wright, 2001). As indicated in chapter 3 by immunostaining, the SGLT type 1 and 2 are present in our primary proximal tubule cells. Also, radiotracer uptake experiments indicated the presence of a sodium-dependent glucose cotransporter in the apical membrane. The drop in I_{SC} after glucose omission which was smaller than the decrease in I_{SC} after Na^+ deletion implies that other electrogenic Na^+-cotransporters are present as well.

Therefore, phosphate and amino acids were omitted from the perfusion solution, since both solutes were present in the Ringer solutions and are transported via a sodium-dependent cotransporter (Hoyer & Gogelein, 1991; Silbernagl, 1988; Forster et al., 2006). In proximal tubule cells, phosphate is transported across the apical membrane by the NaP_i type IIa and IIc cotransporters. NaP_i-IIa is an electrogenic transporter that couples the uptake of 3 Na^+ ions to the uphill movement of one divalent P_i per transport cycle. NaP_i-IIc is electroneutral and exhibits a 2:1 stoichiometry. In adult mice kidneys, NaP_i-IIa has been indicated as the major transporter for P_i, while NaP_i-IIc plays a dominant role in weaning animals (Forster et al., 2006). Omission of phosphate resulted in a drop in I_{SC} with 30% compared to control Ringer. The decrease in I_{SC} after omission of glucose or phosphate was comparable, i.e. 28% when glucose was replaced with sucrose and 30% after PO_4^{2-}-depletion. However, the decrease in I_{SC} might be underestimated. It has been reported that there is a mutual interaction between phosphate and sugar transport (Ullrich, 1979). Since both solutes use a common

driving force, i.e. the electrochemical gradient of Na^+ at the apical membrane, the omission of one substrate, might elicit a partial compensatory increase of transport by the other substrate. Therefore, the decrease in I_{SC} might be less than expected (Murer et al., 1975).

When amino acids, glucose and phosphate were omitted from the Ringer solution, an even larger drop in I_{SC} (76%) could be observed indicating that all these solutes are transported at the apical membrane. However, omission of all solutes did not result in a complete suppression of I_{SC}. A small component (about 3µA/cm²) remained present. This might reflect the uptake of Na^+ through the Na^+/H^+ exchanger at the apical membrane. NHE_3 plays a major role in the reabsorption of HCO_3^- and NaCl (Chan & Giebisch, 1981; Preisig et al., 1987; Preisig & Rector, 1988) and is also involved in the receptor-mediated endocytosis of proteins (Gekle, 2001). Another possibility could be the uptake of either sulphate (SO_4^{2-}) which is Na^+-dependent on the apical membrane with a stoichiometry of 3:1 (Aronson, 2006; Markovich & Aronson, 2007). The uptake of pyruvate through the Na^+-dependent monocarboxylate transporter is another candidate (Halestrap & Price, 1999). It might also relate to a secretion of Cl^- through an apical Cl^--channel. A possible candidate is the ClC-5-channel that is involved in receptor-mediated endocytosis of LMW-proteins (as described in chapter 1). However, the activation kinetics of ClC-5 describes the channel as an outward-rectifier, meaning that the positive outward current or the influx of an anion (Cl^-) is stimulated (Steinmeyer et al., 1995; Jentsch, 2002). This counteracts a secretion of Cl^-. However, proximal tubule cells also express a CFTR-channel which is also involved in the receptor-mediated endocytosis (Jouret et al., 2007). Cl^--secretion by the CFTR-channel should be possible.

4.4.2 Impedance analysis

The proximal tubule epithelium is characterized by a typical low transepithelial resistance (R_T). In our cultured cells, R_T was about 53.8 ± 0.9 Ω.cm². This value is higher than the R_T of about 5 Ω.cm² measured *in vivo* in rat proximal tubule (Frömter & Gessner, 2001) or of a R_T of 8 Ω.cm² in dog proximal tubule (Boulpaep & Seely, 1971). The reason for this discrepancy might be the influence of the filter support on the electrical properties of our PTC. In the past, several studies on A6 or MDCK cells have indicated a role of the culture support

on either I_{SC} or R_T (Helman & Liu, 1997; Lo et al., 1999). These studies show that although the filters are permeable, the transport of ions is usually lower than in native tissues and the R_T is usually higher. The higher R_T might result from the decrease in transcellular ion transport or from the increased resistance of the paracellular pathway. The decrease in ion transport is already evident from the lower J_{Na} calculated from the I_{SC} in section 4.4.1. This might reflect a decrease in number of transporters present at the apical membrane since the brush border is less elaborate. The increased resistance of the paracellular pathway might be due to a less pronounced basolateral membrane, i.e. fewer folds. Thus culturing conditions seem to determine the resistance of the monolayer, probably through a shift in the proportion between sealing and conductive elements.

The transient small drop in capacitance after omission of Na^+ or other substrates (phosphate, glucose or all substrates) might be due to a drop in transport, resulting in a closure of the lateral intercellular spaces as has been described previously by Van Driessche et al. (Van Driessche et al., 1999) and Spring et al. (Spring & Hope, 1979). However, we believe that the closure of the LIS is not due to swelling of the cells like in A6 cells, but rather to a decreased transport of Na^+ and subsequently water to the LIS. Several models for solute and water transport across the proximal tubule (Weinstein et al., 2007) indicate that the LIS behaves like a middle compartment. This refers to active transport of solutes across the lateral membrane into the LIS, creating a region of local hypertonicity that acts to pull water from the cell and the lumen hereby opening the LIS as indicated in fig. 4.11 (Sackin & Boulpaep, 1975). Therefore, when the transport of Na^+ or solutes over the apical membrane drops, less ions and water are transported into the LIS and the LIS closes. This results in a decreased surface area of the basolateral membrane and by that a decreased capacitance of the basolateral membrane. According to the formula (1) pg 77, C_T decreases will decrease.

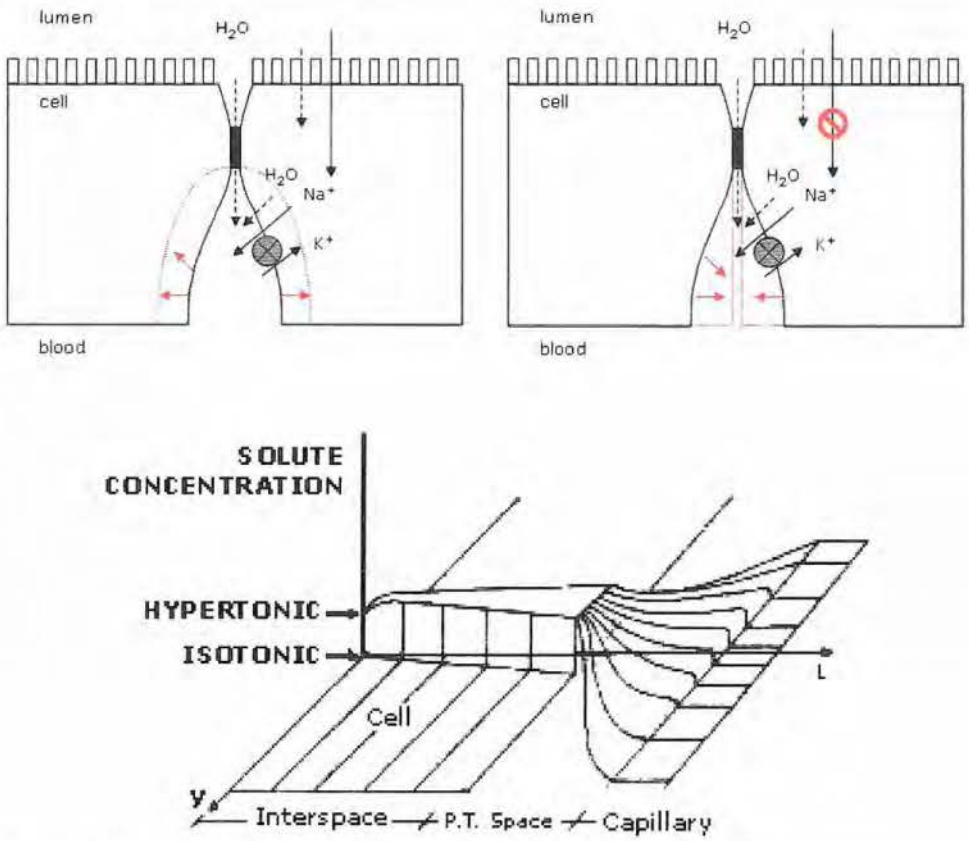

Figure 4.11: Model for the role of the LIS in transepithelial capacitance

Left: During control conditions, Na^+ is transported across the apical membrane and through the Na^+/K^+-ATPase into the LIS (full arrows) where it creates hypertonicity that attracts H_2O (dashed arrows), resulting in an opening of the LIS (red arrows, red dashed lines).

Right: After omission of Na^+ from the Ringer solution, the apical Na^+ falls and less Na^+ and H_2O are transported to the LIS resulting in a closure of the LIS (red arrows, red dashed lines) and a resulting drop in C_T. Bottom: Solute concentration profile according to Sackin H and Boulpaep EL (Sackin & Boulpaep, 1975) suggesting the LIS (interspace) is hypertonic compared to the tubular fluid or blood. Hypertonicity drops to nearly iso-osmotic values in the peritubular space (PT).

4.4.3 Conclusion

Electrophysiological analysis revealed that the PTCs in primary culture possess typical characteristics of a leaky proximal tubule epithelium with a high Na^+ transport rate, transport of solutes at the apical membrane and a low transepithelial resistance (R_T). The capacitance measurements revealed a dynamic state of the LIS in function of the transepithelial Na^+- and H_2O-transport.

Chapter 5

EMT in proximal tubule cells

The results of this chapter are described in:

Mouse proximal tubule cells in primary culture transdifferentiate in α-SMA$^+$ myofibroblasts after exposure to TGF-β1.

Sara Terryn, Frank Vandenabeele, Paul Steels and Emmy Van Kerkhove. *In preparation*

5.1. Introduction

Chronic renal injury most often results in the onset of interstitial fibrosis leading to end stage renal disease (Remuzzi & Bertani 1998). Myofibroblasts are believed to play a key role in the development of interstitial fibrosis. They are responsible for the excessive deposit of extracellular matrix proteins. Myofibroblasts are, besides injured tubule cells and activated immune cells, also a source of TGF-β1 production, a potent profibrotic cytokine. Several lines of evidence indicate that about one third of renal interstitial myofibroblasts are derived from renal tubule epithelial cells via a process called epithelial-to-mesenchymal transition (EMT) and that transforming growth factor-β1 (TGF-β1) is the most potent inducer of EMT (Yang & Liu, 2001; Iwano et al., 2002; Lan, 2003). Previous studies using human renal epithelial cells in primary culture (Tian et al., 2003; Forino et al., 2006) have failed to show a definite conversion of epithelial cells into myofibroblasts since α-smooth muscle actin (α-SMA) staining, the most important marker for myofibroblasts and EMT (Badid et al., 2001) was not observed. The expression of α-SMA microfilaments is associated with a reorganization of the cytoskeleton and thus related to the change in morphology from a classical cuboid epithelial cell with apical and basolateral polarity to a spindle-shaped, elongated fibroblast-like cell with front-end to back-end polarity. The change in morphology coincides with loss of cell-cell contacts and the disappearance of a confluent cell monolayer. The tight junctional complex is disassembled and dense focal adhesions between intracellular stress fibers and extracellular matrix proteins are formed (Tian & Phillips, 2002). The ECM-protein, fibronectin (FN), plays an important role in the formation of focal adhesions and the composition and assembly of the ECM (Hocking et al., 2000; Mosher, 2001; Wang et al., 2005). The focal adhesions of a myofibroblast are also called fibronexus and are characterized by a close alignment of actin bundles and FN fibers. This complex structure arises from the fusion of several focal adhesions (Dugina et al., 2001). Disassembly of the tight junction was assessed by staining for the tight junction associated protein, ZO-1, which is important for the interaction between the tight junctional proteins, claudin and occludin, and the actin cytoskeleton (Van Itallie & Anderson, 2004). The intermediate filament protein, nestin, is normally transiently expressed by epithelial cells of the developing kidney. However, re-expression of nestin has

been observed in pathologic situations such as tubulointerstitial fibrosis, thereby establishing a role for nestin as a novel marker for tubulointerstitial injury (Sakairi et al., 2007; Patschan et al., 2007). During EMT, the cell has an increased biosynthetic activity, which is reflected by nuclear hypertrophy and the presence of numerous polyribosomes in the cytoplasm.

Two main mediators have been shown to aggravate the disease progression of tubulointerstitial fibrosis, namely hypoxia and TGF-β1. The peritubular capillary bed is a dynamic structure which shows a rapid decline in capillary density in chronic kidney disease. Capillary loss and hypoperfusion lead to a rapid decline in oxygen levels resulting not only in an impaired energy generation but it might also influence cellular functions and induce certain hypoxia-inducible genes by hypoxia-inducible transcription factors (HIFs). HIF is considered a master regulator of gene expression in response to hypoxia. The majority of HIF-induced genes are involved in adaptation and protection against hypoxia. However, HIF-induced gene expression may also promote renal fibrosis by induction of the expression of collagens and tissue inhibitors of metalloproteinases, the activation of TGF-β and the promotion of EMT. In turn, interstitial fibrosis may lead to local ischemia by increasing the diffusion distance from the capillary to the tubule. In this way, a positive feedback system is generated which aggravates the disease progression. (Fine et al., 2000; Bottinger & Bitzer, 2002; Kang et al., 2002; Eckardt et al., 2005; Nangaku, 2007). However, there is still debate on what comes first, hypoxia or TGF-β1, or do they occur simultaneously? In this thesis, we studied the effects of TGF-β1 on proximal tubule cells with a focus on the process of epithelial-to-mesenchymal transdifferentiation.

5.2. Assessment of epithelial-to-mesenchymal transdifferentiation (EMT)

5.2.1 Transmission electron microscopic analysis of TGF-β1 exposure

Seven-days old confluent monolayers of primary proximal tubule cells grown on either collagen-coated membranes or on thermanox® slides (culture details described in chapter 3) were exposed to different concentrations of human recombinant TGF-β1 (Sigma, St.Louis, MO, USA) from 1ng/ml to 50ng/ml for 48h and analyzed by transmission electron microscopy in the same way as described in section 2.4.

5.2.2 Immunostaining for α-SMA and fibronectin

Proximal tubule cells were grown to confluence on glass coverslips or collagen-coated membranes, treated with TGF-β1 (1ng/ml to 50ng/ml) for 24 or 48h and then analyzed for the expression of alpha smooth muscle actin (α-SMA) or fibronectin (FN). TGF-β1 treated and untreated cell cultures were fixed with 4% paraformaldehyde and then permeabilized with Triton X-100. After permeabilization, cells were incubated with diluted (1/40) primary antibody against α-SMA or diluted (1/1000) primary antibody against fibronectin with 1% BSA in PBS. Then non-specific binding was blocked with 5% BSA before incubation with 5% goat anti-serum. The DAKO Envision System was used to visualize α-SMA or fibronectin.

5.2.3 Staining for ZO-1 and the intermediate filament protein, nestin

TGF-β1 treated and untreated confluent monolayers of proximal tubule cells were analyzed for the expression of ZO-1, a specific marker for the tight junctional complex. Cells were fixed with ice-cold ethanol for 20 sec and incubated with diluted (1/200) primary antibody raised against ZO-1 with 3% BSA in PBS. The non-specific binding was blocked with 3% BSA. Visualization of ZO-1 was done with FITC-conjugated anti-serum using the confocal microscope. The specificity of immunostaining was tested by incubation in the absence of primary antiserum. Staining for nestin was essentially the same as for ZO-1 except that visualization was done with a Cy5-conjugated secondary antibody.

5.2.4 Quantification of nuclear hypertrophy

Cell contours were delineated by free hand and nuclear diameter was assessed using the ImageJ software. Different nuclei from primary cultured proximal tubule cells under control conditions or after exposure to different concentrations of TGF-β1 (from 1 to 50ng/ml) were analyzed. All values are expressed as the mean ± standard error of the mean (SEM). Significance of differences between two means was calculated using the GraphPad InStat software (demo version, graphpad Software, San Diego, USA). Significance was calculated with the one-way ANOVA with post test. The significance level is indicated in the legend of the figure.

5.3 Results

5.3.1 Ultrastructural changes after a TGF-β1-exposure

Transmission electron microscopy (TEM) was used to analyze proximal tubule morphology after exposure to 1ng/ml (fig. 5.1B1-4), 10ng/ml (fig. 5.1C1-4) or 50ng/ml (fig. 5.1D1-4) TGF-β1 for 48h. Proximal tubule cells were either cultured on collagen-coated membranes (1 & 2 of fig. 5.1A-D) or on thermanox® slides (3 & 4 of fig. 5.1A-D). Proximal tubule cells (PTC) cultured in the absence of TGF-β1 (fig. 5.1A1-4) formed a confluent monolayer of cells with a classic epithelial morphology with apical to basolateral polarity and different characteristics of proximal tubule cells like apical microvilli, defined tight junctions and numerous microvilli as described in chapter 3. However, cells cultured on coverslips grew slower since confluency was usually not reached at day 7 and tight junctions were less defined (fig. 5.1A4). In TGF-β1-treated cultures (fig. 5.1B-D), cells gradually (as a function of dose) lost the typical proximal phenotype and developed a spindle-shaped, fibroblastic morphology characterized with prominent actin filaments coalescing into focal densities, front-end to back-end polarity and a cytoplasm containing numerous polyribosomes. Changes in morphology were more pronounced in cells grown on coverslips compared to EMT induced in PTC seeded on filter supports. Culture in 1 ng/ml TGF-β1 caused only minor changes in morphology (fig. 5.1B1-4). The PTCs retained their normal morphology with apical tight junctions and some microvilli but a reorganization of the actin microfilaments into stress fibres could be observed (fig. 5.1B2 & B4). Also, more dense vacuoles and numerous

polyribosomes could be detected in the cytoplasm. Higher concentrations of TGF-β1 (10 and 50 ng/ml, fig. 5.1C & D) caused profound changes with elongated, spindle-shaped fibroblastic cells that lost epithelial characteristics such as microvilli and tight junctions. Prominent bundles of actin microfilaments that interact with focal contacts (focal densities) to either adjacent cells or to the extracellular matrix or substratum could also be observed. These changes were more evident in cells grown on coverslips. Furthermore, TGF-β1-treated cells showed signs of high metabolic activity, i.e. large euchromatin-rich nucleus with prominent nucleoli, as well as nuclear hypertrophy and numerous polyribosomes and dense vacuoles in the cytoplasm.

Figure 5.1: Changes in proximal tubule phenotype assessed with TEM

Morphology of proximal tubule cells grown on PTFE filter (**1&2**) or thermanox® slides in control conditions (**3&4**) or exposed to 1 ng/ml TGF-β1 (**B**), 10 ng/ml TGF-β1 (**C**) or 50 ng/ml TGF-β1 (**D**) as assessed by transmission electron microscopy (TEM). **A**: Under control conditions, a confluent monolayer of cobblestone-like cells is formed. Untreated cultures show characteristics of proximal tubule cells, like microvilli (MV), tight junctions (TJ) and numerous mitochondria (M). **B**: Cultures treated with 1ng/ml TGF-β1 show only minor changes in morphology. Microvilli (MV) and tight junctions were still present at the apical membrane. However, some bundles of actin filaments could be observed (SF). **C**: Exposure to 10 ng/ml TGF-β1 caused major changes in morphology, especially for cells cultured on coverslips. Cells became elongated and typical proximal tubule characteristics like microvilli and tight junctions disappeared. Also the number of mitochondria decreased while numerous polyribosomes and dense vacuoles can be observed. Focal contacts and densities could be observed at the junctions between adjacent cells (FD) or with the substratum (FC). **D**: Exposure to 50ng/ml TGF-β1 further augments the formation of stress fibers (SF) and dense vacuoles and the loss of the proximal tubule phenotype. For all concentrations of TGF-β1 used, EMT is more pronounced in cells grown on coverslips as compared to cells grown on collagen-coated membranes.

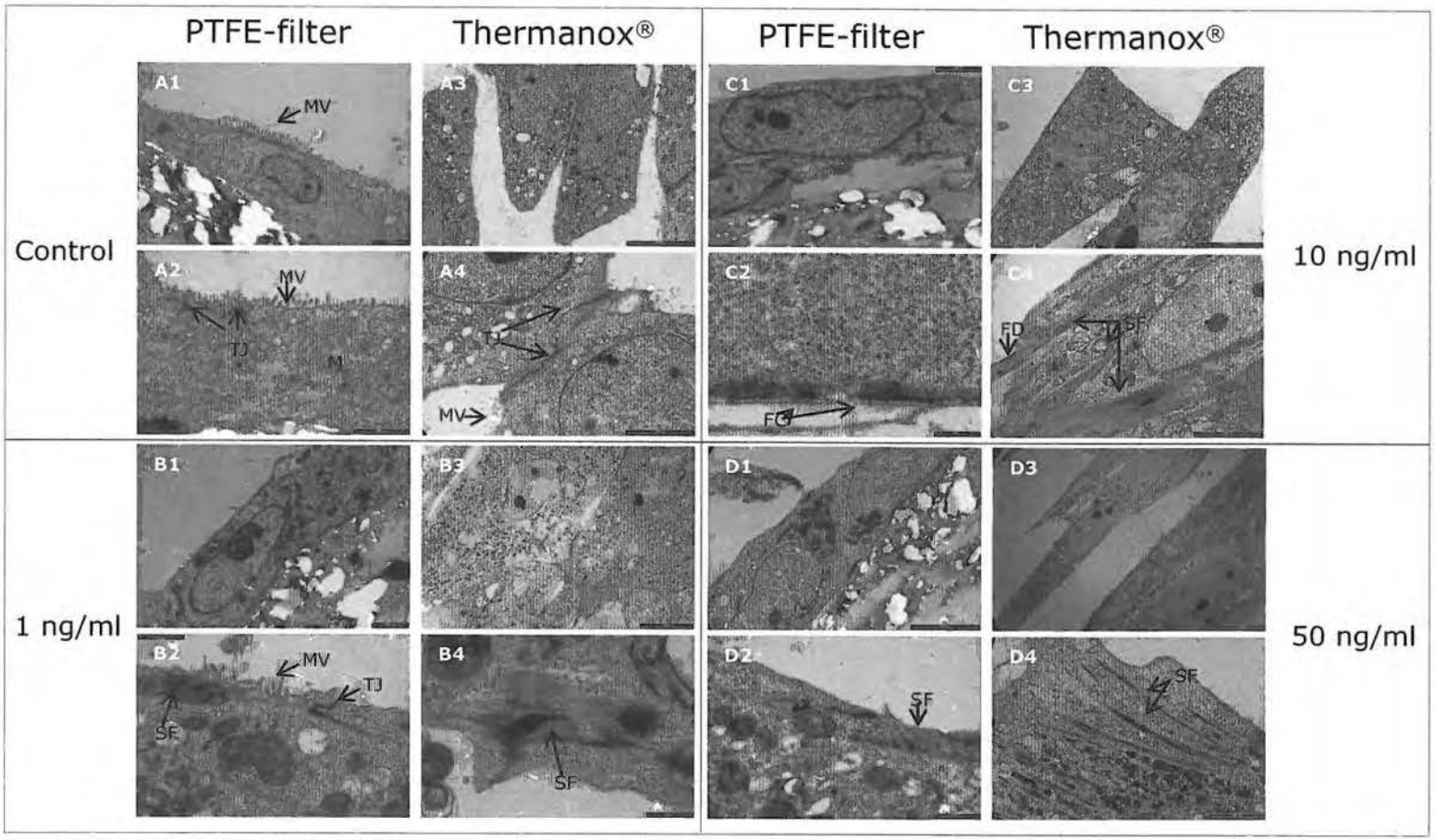
PTFE-filter
Thermanox®
PTFE-filter
Thermanox®
Control
10 ng/ml
1 ng/ml
50 ng/ml
A1
MV
A3
C1
C3
A2
MV
TJ
M
A4
TJ
MV
C2
FC
C4
FD
TJ
SF
B1
B3
D1
D3
B2
MV
TJ
SF
B4
SF
D2
SF
D4
SF

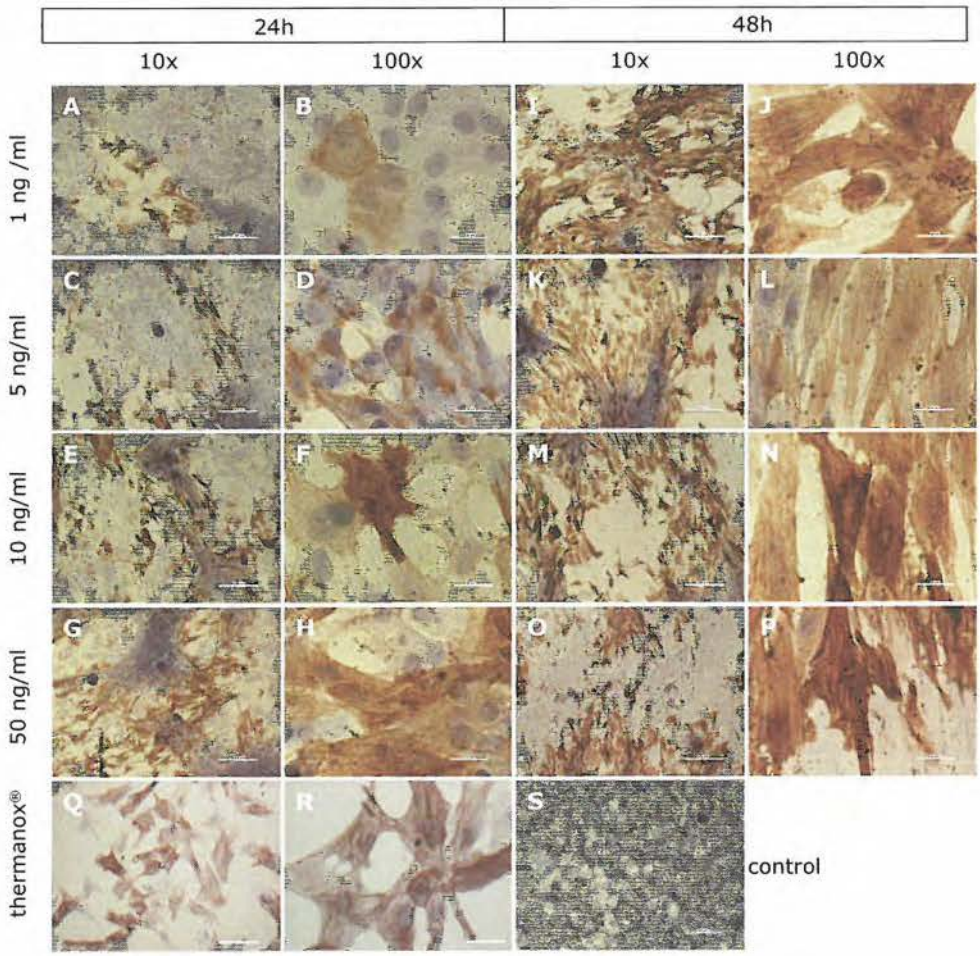

Figure 5.2: De novo expression of α-smooth muscle actin

Proximal tubule cells grown on thermanox® slides (**Q & R**) or on permeable PTFE-supports (**A-P & S**) were grown under control conditions (**S**) or exposed to 1 ng/ml (**A-B, I-J, Q-R**), 5 ng/ml (**C-D, K-L**), 10 ng/ml (**E-F, M-N**) or 50 ng/ml TGF-β1 (**G-H, O-P**) for 24h (**A-H**) or 48h (**I-R**). The expression of α-SMA was assessed by immunostaining with the mouse monoclonal antibody raised against alpha smooth muscle actin. Magnification: 10x (bar: 200μm) or 100x (bar: 20μm) except Q: bar: 50μm.

5.3.2 Expression of α-smooth muscle actin after TGF-β1-exposure

α-Smooth muscle actin (α-SMA) is the most important marker for myofibroblasts (Badid et al., 2001). In normal quiescent proximal tubule cells, no α-SMA is expressed. Several reports show a *de novo* expression of this microfilament in proximal tubule cells after exposure to TGF-β1 (Ng et al., 1998; Fan et al., 1999). In untreated cultures (fig. 5.2S) no staining for α-SMA could be observed. Treatment of proximal tubule cells with 1, 5, 10 or 50 ng/ml TGF-β1 (fig. 5.2 A through R) resulted in an expression of α-SMA-positive microfilaments in the cytoplasm. The expression of α-SMA was time- and dose-dependent (fig. 5.3) ranging from only 15% positive cells with 1ng/ml TGF-β1 exposure for 24h to a 100% α-SMA positive cells after 48h exposure to the highest dose. The majority of cells stained positive after 48h (fig. 5.2 I-R). Furthermore, epithelial morphology was lost, the monolayer became disorganized and fibroblast-like spindle-shaped cells appeared. Occasionally, in cultures treated with the lowest doses of TGF-β1 for 48h (fig. 5.2 I-L), a group of unstained cell could be observed. However, when cells were grown on thermanox® slides (fig. 5.2 Q and R), all cells became fibroblastic and expressed α-SMA after 48h even with the lowest dose of TGF-β1 (1ng/ml, fig. 5.2Q and R). When cells were treated for 24h with TGF-β1, a dose-dependency could be clearly observed (fig. 5.2A-H). With the lowest dose of TGF-β1, expression of α-SMA could mostly be observed at the gaps that occurred occasionally in the monolayer (fig. 5.2A and B). The majority of cells (85%) however still retained their epithelial morphology and did not express α-SMA. With higher doses of TGF-β1, more gaps appeared in the monolayer, more cells stained positive and the transformation into a fibroblast-like cell became more evident (fig. 5.2 C-H). The detachment of cells from the monolayer is even clearer when the cultures were treated for 48h with the highest dose (fig. 5.2O and P). These data indicate that a clear conversion into an α-SMA$^+$-myofibroblast-like phenotype was already evident with exposure to 10 ng/ml TGF-β1. Incubation with 50 ng/ml TGF-β1 did not augment the response. Therefore, exposure to 50 ng/ml TGF-β1 was not further investigated, also because our first objective was to assess the early events of EMT.

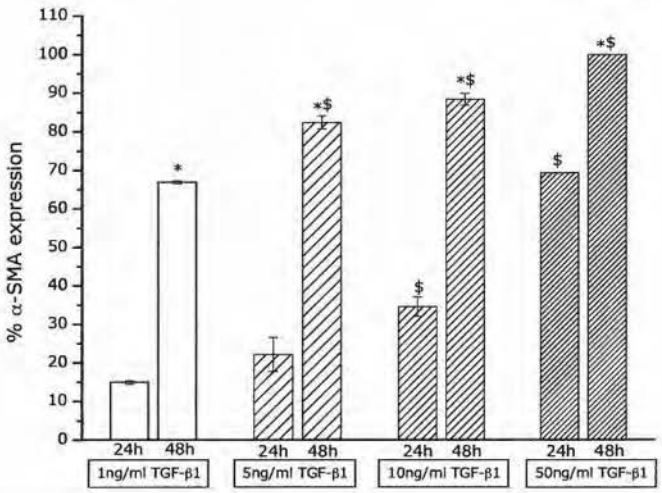

Figure 5.3: Time and dose-dependency of α-SMA expression
Number of cells that express α-SMA after 24h and 48h after exposure to increasing concentrations of TGF-β1. α-SMA expression increased significantly within time (*) and also with dose ($). Values are expressed as mean ± SEM (n=3), $^{*,\$}$ $p<0.001$.

5.3.3 Expression of fibronectin after TGF-β_1-exposure

Fibronectin (FN) is an extracellular adhesion molecule which is expressed by fibroblast-like cells during EMT (QI et al., 2006). Under control conditions (fig. 5.4K and L), proximal tubule cells stained negative for FN. Treatment with TGF-β1 caused a dose- and time-dependent expression of FN, similar to the expression of α-SMA. Exposure to 1ng/ml TGF-β1 for 24h caused a mild expression of fibronectin without profound changes in cell morphology (fig. 5.4A and B). Increasing the dose of TGF-β1 resulted in a denser expression of fibronectin combined with a changed cell morphology. Also, the expressed fibronectin was more filamentous and dense around the focal densities (indicated by arrow). Furthermore, in unexposed proximal tubule cells (fig. 5.4K and L) a confluent monolayer of polygonal cells is formed, while in cultures treated with TGF-β1, confluence is gradually lost and cells become fibroblastic. The expression of fibronectin in cells grown on thermanox® after exposure to TGF-β1 (fig. 5.4M-O) was more pronounced compared to cells grown on filter. A similar observation was made for the expression of α-SMA (fig. 5.2).

5.3.4 ZO-1 and nestin staining

Cell-to-cell contacts seem to play a major role in the function and differentiation of proximal tubule cells (Bergin et al., 2000). To test the hypothesis that the disassembly of the tight junction occurs during EMT, confluent monolayers were exposed to various concentrations of TGF-β1 (ranging from 1 to 10ng/ml) for 24h and subsequently stained for the tight-junctional protein, ZO-1 (fig. 5.5B,D,F,H). In untreated cultures, ZO-1 staining showed a honey-comb-like staining of the cell membranes (fig. 5.5B). Treatment of PTC with 1 ng/ml TGF-β1 resulted in a decreased expression of ZO-1 at the membrane (fig. 5.5D arrow) and in some cells, an increased intracellular expression was observed. Exposure to higher concentrations of TGF-β1 (fig. 5.5F and H) decreased membrane staining of ZO-1 even further and augmented cytosolar staining. Staining of ZO-1 after incubation with 10 ng/ml TGF-β1 was only occasionally observed at the membrane (fig. 5.5H arrowheads), while cytoplasmic staining dominated. Furthermore, ZO-1 staining could only be observed in cells that still resided in a monolayer. In transformed cells or at gaps in the monolayer, ZO-1 staining was abolished.

Nestin has been addressed as an early marker for tubulointerstitial fibrosis. Therefore, confluent monolayers of 7-days old PTC were exposed to TGF-β1 for 24h and stained for nestin (fig. 5.5A,C,E,G). In untreated cell cultures, very faint staining for nestin could be observed (fig. 5.5A). Exposure to TGF-β1 resulted induced the expression of nestin in a dose-dependent manner (fig. 5.5C,E,G). When cellular morphology changed, nestin-positive filaments in the cytoplasm could be observed and staining was dense at the cell contacts to the substrate or neighbouring cells (fig. 5.5G arrow).

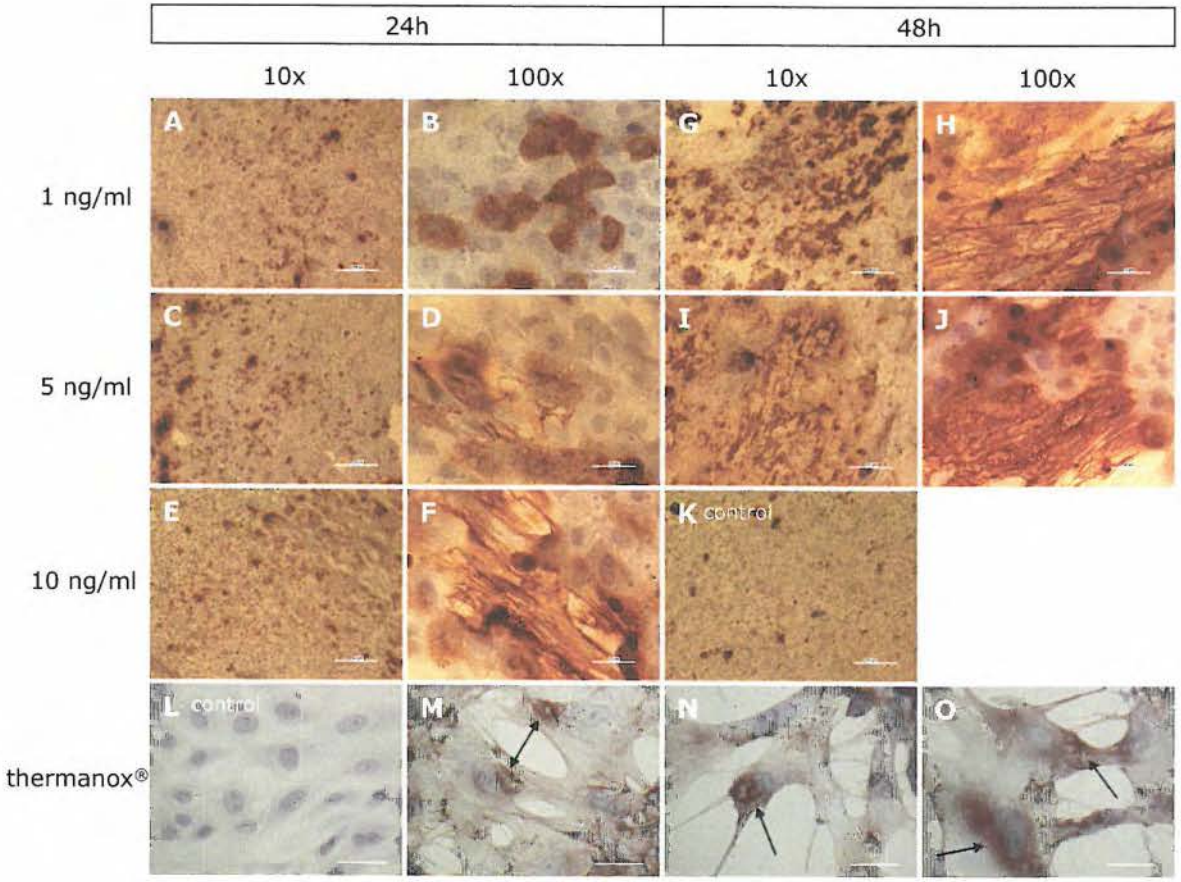
24h
48h
10x
100x
10x
100x
1 ng/ml
5 ng/ml
10 ng/ml
thermanox®
A
B
G
H
C
D
I
J
E
F
K control
L control
M
N
O

Figure 5.4: The expression of fibronectin

Light microscopic images of primary cultured proximal tubule cells grown on PTFE-supports (**A through K**) or on thermanox® coverslips (**L through O**) for 24h (**A through F**) or 48h (**G through O**) under control conditions (**K & L**) and after exposure to 1 ng/ml TGF-β1 (**A,B,G,H,M**), 5 ng/ml TGF-β1 (**C,D,I,J,N**) or 10 ng/ml TGF-β1 (**E,F,O**) and stained with the rabbit polyclonal antibody raised against fibronectin. Dense staining was observed at the fibronexus (indicated by arrow). Magnification: 10x (bar: 200μm) or 100x (bar: 20μm).

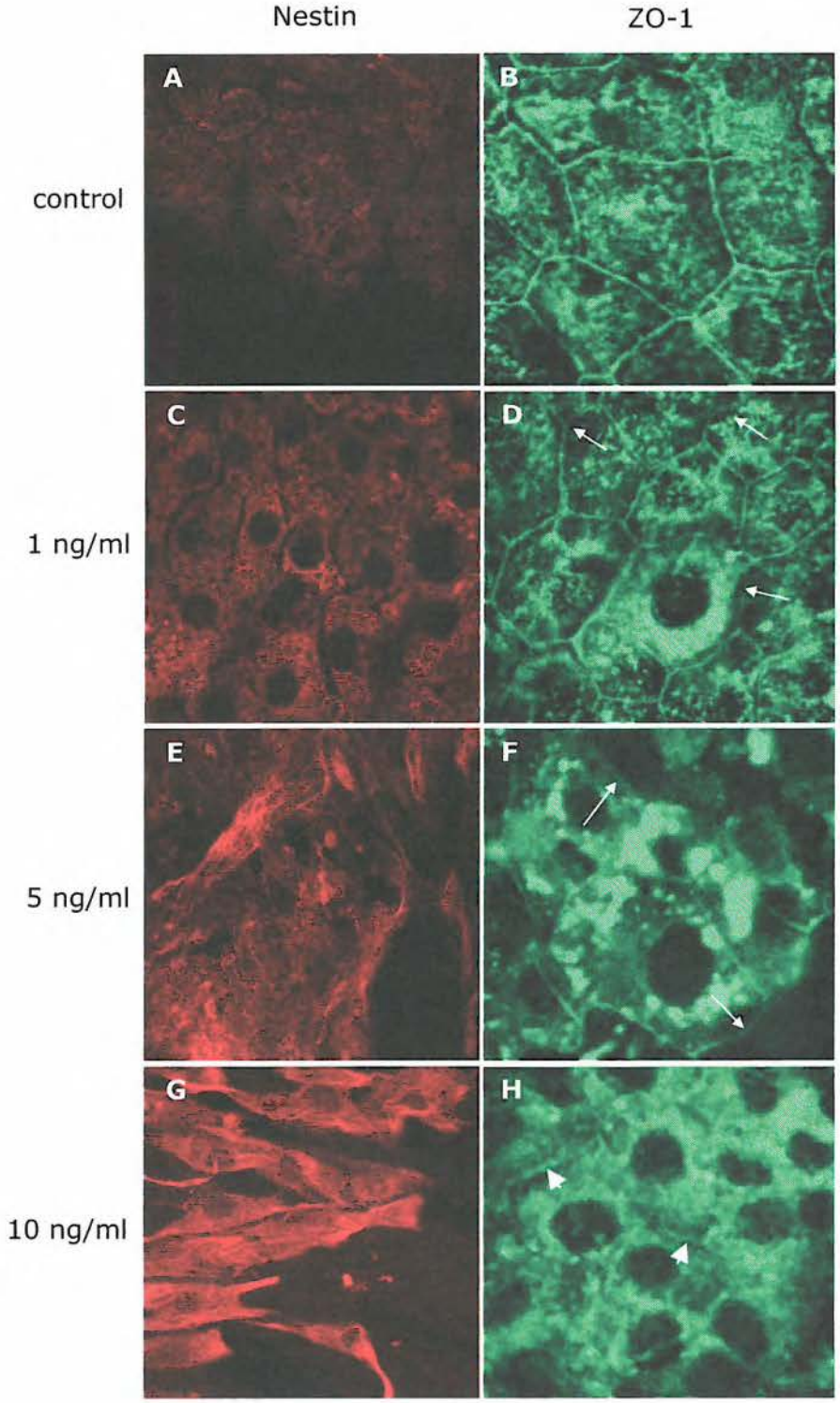
Nestin
ZO-1
control
1 ng/ml
5 ng/ml
10 ng/ml
A
B
C
D
E
F
G
H

Figure 5.5: The expression of Nestin and ZO-1

Untreated and TGF-β1-treated confluent primary cell cultures were stained for either nestin (**A,C,E,G**) or ZO-1 (**B,D,F,H**) and analyzed by confocal microscopy. In control conditions, faint nestin staining (**A**) and dense honey-comb-like staining for ZO-1 at the cell membrane (**B**) could be observed. Incubation with 1ng/ml TGF-β1 (**C,D**) resulted in an increased expression of nestin (**C**) while ZO-1 expression was interrupted at the cell membrane (**D, long arrows**). Exposure to 5ng/ml TGF-β1 resulted in a filamentous staining of nestin in the cytoplasm of cell with changed morphology (**E**). ZO-1 staining further decreased at the cell membrane, while cytoplasmic staining increased (**F**). Similar effects were observed with 10 ng/ml TGF-β1 (**G,H**). Nestin staining became dense at the cell-cell and cell-matrix contacts (**G**) while ZO-1 staining at the membrane was only occasionally observed in cells that were still located in a group of cells (**H, arrowheads**).

5.3.5 Assessment of nuclear hypertrophy

Nuclear hypertrophy reflects an increased biosynthetic activity which is present in transforming cells (Koda et al., 2006). The nuclei of different cells were analyzed (fig. 5.6). In control conditions, proximal tubule cells have a nuclear diameter of 5.5 ± 0.3 µm or 5.5 ± 0.2 µm when grown on thermanox® coverslips or collagen-coated membrane respectively. Exposure to TGF-β1 resulted in a dose-dependent increase in the nuclear diameter. On coverslips, low concentrations of TGF-β1, 1 and 5ng/ml, increased nuclear diameter to 7.6 ± 0.2 µm and 6.9 ± 0.9 µm, respectively, or a 38% and 25% increase compared to control. High concentrations of TGF-β1, 10ng/ml, caused a significant increase in nuclear diameter to 8.4 ± 0.7 µm or a 53% increase compared to control. When cells were grown on collagen-coated membranes, 1ng/ml TGF-β1 did not cause an increase in nuclear diameter after 24h incubation. At 48h, an increase of 11% in nuclear diameter could be observed with 1ng/ml TGF-β1. However, the increase was not statistically significant. For all other concentrations of TGF-β1, the enlargement of the nucleus was similar after 24h or 48h incubation. A gradual increase to a nuclear diameter of 8.4 ± 0.2 µm with 10ng/ml TGF-β1 was observed. In cells grown on thermanox® coverslips, the nuclear enlargement of cells grown on collagen-coated membranes was comparable.

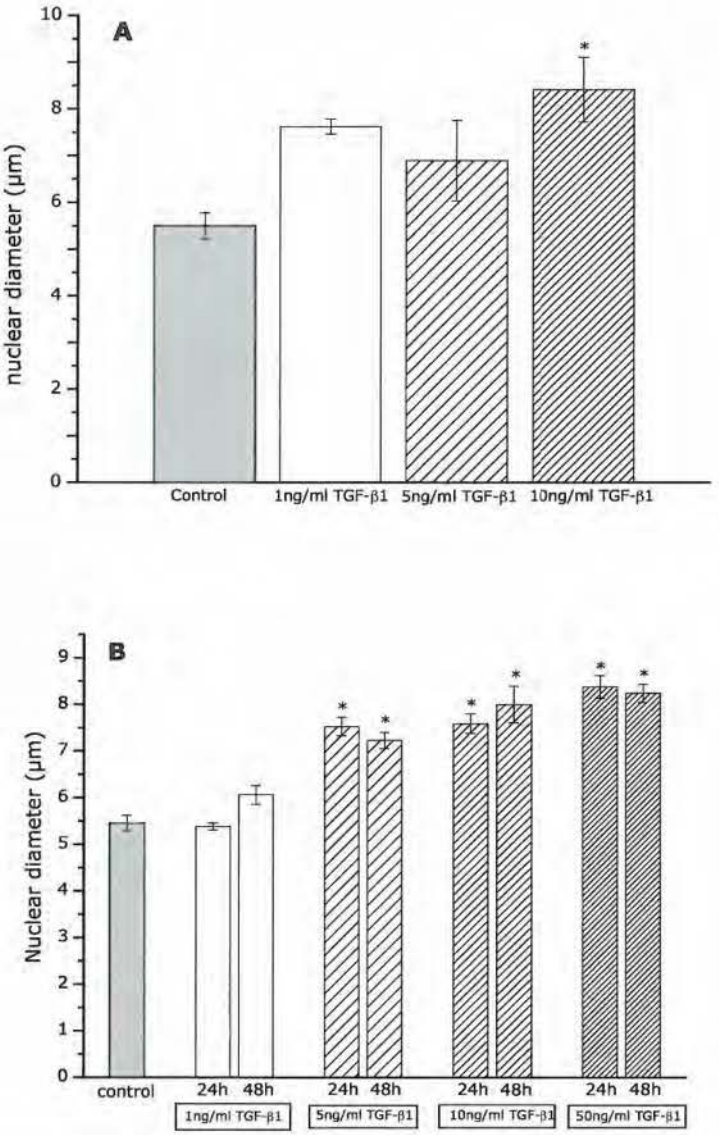

Figure 5.6: Assessment of nuclear hypertrophy

The nuclear diameter was assessed by free hand and calculated using the ImageJ software. The nuclear diameter of proximal tubule cells grown on thermanox® coverslips (A) or collagen-coated membranes (B) and challenged with TGF-β1 (1 to 50ng/ml) was compared to untreated cells (control). Values are expressed as mean ± SEM (n = 12 for control cells and n = 9 for 1 or 50ng/ml TGF-β1). Treatment with TGF-β1 was compared to control (*$p<0.01$).

5.4 Discussion

During EMT, proximal tubule cells loose their epithelial phenotype and transdifferentiate into a mesenchymal cell type, which is characterized by *de novo* expression of α-SMA, a spindle-shaped phenotype and the ability to produce excessive amounts of extracellular matrix (Yang & Liu, 2001; Liu, 2004). We exposed proximal tubule cells in primary culture to different concentrations of TGF-β1 for 24 or 48h. We used doses of TGF-β1 (from 1 up to 50ng/ml) as previously described by others (Fan et al., 1999; Rhyu et al., 2005; Forino et al., 2006; Phanish et al., 2006).

Electron microscopical analysis showed that PTC lost their typical cobblestone morphology and epithelial characteristics such as microvilli and apical-to-basolateral polarity and converted into a elongated, spindle-like shape with pronounced actin bundles (stress fibers) coalescing into focal densities and front-end to back-end morphology, which are all typical characteristics of myofibroblasts (Powell et al., 1999). These observations have been described previously by Fan et al. (Fan et al., 1999) in a rat kidney epithelial cell line (NRK52E) and in human primary cultures of PTC by Tian et al. (Tian et al., 2003). Morphological changes induced by TGF-β1 were more pronounced in cells grown on thermanox® coverslips as compared to cells grown on collagen-coated membranes.

Since morphological observations showed that our cells converted into a myofibroblast–like cell, we assessed our primary PTC for the expression of α-SMA, a typical myofibroblast marker which is expressed *de novo* in epithelial cells during EMT (Badid and others 2001). Cultured proximal tubule cells stained positive for α-SMA after exposure to TGF-β1. The expression of α-SMA was dose and time-dependent and seemed to be initiated in cells that surrounded gaps in the monolayer. As the dose of TGF-β1 increased, more gaps in the monolayer occurred and cellular staining for α-SMA increased. The disruption of the typical epithelial monolayer might indicate a rearrangement or loss of tight junctions. This was investigated by staining for ZO-1, a marker for the zonula occludens protein-1 which is present in the tight junction (Van Itallie & Anderson, 2004). In untreated cells, ZO-1 staining was clearly observed at the cell membrane, indicating its presence at the tight junction.

Exposure to TGF-β1 resulted in a gradually, dose-dependent decrease of ZO-1 staining at the membrane while more ZO-1 was detected in the cytoplasm. These observations indicate that ZO-1 is retrieved from the tight junction and internalized. However, in cells that already changed their morphology, no ZO-1 staining could be observed.

In a recent report by Sakairi et al. (Sakairi et al., 2007), the intermediate filament protein, nestin, has been implicated in renal tubulointerstitial fibrosis. Here, nestin re-expression has been observed in rat tubular cells and interstitial myofibroblasts after ureter obstruction. Also the degree of nestin expression was closely related with that of tubulointerstitial fibrosis. When primary mouse PTC were stained for nestin, in the present study, an increased expression was observed with increasing doses of TGF-β1. Furthermore, in cells with changed morphology, nestin positive filaments were detected throughout the cytoplasm and dense staining could be observed around the cell-cell or cell-matrix contacts. This re-expression of nestin shows that our cells are undergoing extensive remodelling with the conversion to an immature phenotype.

Another typical feature of myofibroblasts is the focal densities at the intercellular junctions, also called fibronexus (Eyden, 1993). The fibronexus is composed of intracellular actin filaments and the extracellular matrix protein, fibronectin (Dugina et al., 2001; Hinz, 2006). In PTC grown on thermanox®, exposure to TGF-β1 for 48h resulted in a positive staining for fibronectin, which was dense at the intercellular junctions. When cells were cultured on collagen-coated filters, the expression of fibronectin was less pronounced, since not all PTC expressed fibronectin after 48h. Fibronectin staining was found around gaps in the monolayer. This was also the case in α-SMA expression.

Changes in cell morphology are usually associated with an increased cellular granularity and nuclear hypertrophy, indicative of the high biosynthetic activity of the dedifferentiated cell. As indicated by TEM, the number of polyribosomes and dense vacuoles in the cytoplasm of PTC incubated with TGF-β1 increased. This indicates the synthesis of new proteins by polyribosomes and the break-down of "old" proteins by lysosomes and storage into dense vacuoles. Nuclear hypertrophy was also assessed.

Exposure to the highest dose of TGF-β1 for 48h increased nuclear diameter up to 50%. No difference in nuclear hypertrophy could be observed between cells cultured on collagen-coated membranes and those grown on thermanox®.

Overall, it seems that cells grown on collagen-coated membranes are somewhat protected against phenotypic alterations induced by TGF-β1, compared to cells grown on coverslips. The latter show a more pronounced conversion with the lowest concentration of TGF-β1 after 48h exposure while not all cells on membranes express α-SMA (only 67%) or develop a fibroblastic phenotype. Possible explanations for the difference in sensitivity to TGF-β1 might be the higher degree of differentiation of PTC grown on filter membranes as already suggested in chapter 3 or the role of the coating of the culture support. The more fibroblast-like nature and the slower growth of untreated cells grown on thermanox® might indicate that PTC grown on filter are better differentiated and in this way, they might be more resistant to stress factors like TGF-β1. The culture support and its coating have previously been indicated to play a role in the growth and differentiation of cells in culture (Cook et al., 1989; Wang et al., 1990). In a recent study by Forino and co-workers, the effect of coating of the culture substratum on the induction of EMT in proximal tubule cells was investigated (Forino et al., 2006). The authors observe an opposite effect: coating with collagen induced a more fibroblast-like phenotype. However, there are major differences between our study and the study of Forino et al.. First, although they showed a change in cell morphology, no expression of α-SMA was observed, indicating that a complete conversion to a α-SMA$^+$-myofibroblast was not attained. Secondly, not a permeable but a solid culture surface (plastic coverslips) was used to investigate the effect of coating with collagen. Finally, primary cells were studied in a subconfluent stage after one passage. Both conditions tend to favour a less differentiated status of the cells, since cell-cell contacts are essential for a proper differentiation of the cells and previous studies indicated that cells grown on permeable supports retain a higher degree of differentiation (Cereijido et al., 1978; Handler et al., 1984; Cook et al., 1989; Candia et al., 1993; Bergin et al., 2000). Given these differences, a good comparison between their findings and our results is not appropriate.

PTFE-membranes were shown to be osteopromotive (Zellin & Linde, 1996). However, no indications for an osteoinductive effect were found since primary

cultured proximal tubule cells under control conditions developed a normal epithelial phenotype and functional properties of the proximal tubule (as described in chapter 3). Furthermore, the effects induced by TGF-β1 were more pronounced in cells grown on plastic coverslips than in cells grown on PTFE-membranes.

In summary, the results indicate that our primary PTCs are capable of undergoing EMT after exposure to TGF-β1 since a clear transformation into α-SMA$^+$-myofibroblast can be observed, accompanied with the loss of epithelial morphology, an increased production of the extracellular matrix protein, fibronectin and an alteration of the intercellular junctions from a tight junction to a focal adhesion complex or fibronexus. The tight junction was disassembled as observed by the disappearance of ZO-1 staining at the membrane. Also, other intermediate filaments such as nestin are expressed during EMT, thereby underlying the role of different elements in the process of EMT.

Chapter 6

General discussion and Summary

Summary

This thesis describes the establishment of a primary cell culture of mouse proximal tubule cells and its use in both physiological and pathological assays. Not only did we attempt to define a fast and simple method, cells were also extensively characterized. Different specific proximal tubule properties were demonstrated on a morphological, functional and electrophysiological level. Besides the normal cell physiology, we showed that the primary cultures are useful in the investigation of the cellular events underlying tubulointerstitial fibrosis. To this end, primary cultures were exposed to TGF-β1 and different aspects of epithelial-to-mesenchymal transdifferentiation were investigated.

In chapter 3, the culture method and the characterization of the primary cultures were described. A simple method that avoids oxidative and mechanical stress during isolation was established to culture mouse proximal tubule cells. The use of permeable filter supports allowed the access of both apical and basolateral side and thus improved vectorial transport and cell polarity. Morphological assessment of the primary cultures revealed typical properties of proximal tubule cells, such as apical microvilli, tight junctions at the apical pole, basolateral infolds, numerous mitochondria and cytoplasmic vesicles, and a primary cilium at the apical membrane. Functional properties include the presence of receptor-mediated endocytosis of albumin, Na^+-dependent transport of α-MG, responsiveness to bradykinin and angiotensin II, and high activity of the brush-border enzymes, alkaline phosphatase and γ-glutamyl transferase. Immunoreactivity against proximal tubule markers, AQP1 and SGLT type 1 and 2 as well as the presence of endocytosis markers, ClC-5, megalin and V-ATPase strengthen the proximal tubule origin of the cells in primary culture.

In chapter 4, the electrophysiological properties of the primary cultures were defined. The primary cultures displayed typical characteristics of a leaky epithelium such as a low transepithelial resistance (R_T) and a high transepithelial current. Furthermore, primary cultures behaved as a Na^+-transporting epithelium since replacement of Na^+ for $NMDG^+$ resulted in a complete abolishment of the measured short-circuit current (I_{SC}). The presence of phosphate, glucose and amino acid transport was also demonstrated.

Impedance measurements revealed that the lateral intercellular space (LIS) behaved as a dynamic compartment that expanded when Na^+ was transported and closed upon omission of Na^+ from the perfusion solution. The primary cultures showed electrophysiological properties of a leaky proximal tubule epithelium.

In chapter 5, the primary cultures were used to investigate the effects of the profibrotic cytokine, TGF-β1, in the setting of tubulointerstitial fibrosis. Exposure to TGF-β1 induced changes in cell morphology from a cuboid epithelial cell to a spindle-shaped elongated fibroblast-like cell. The change in morphology coincided with the expression of myofibroblast markers, α-SMA, fibronectin and nestin; and with the disassembly of the tight junction as shown by the disappearance of ZO-1. Nuclear hypertrophy which is characteristic for tubulointerstitial fibrosis was also observed. The effects of TGF-β1 were time- as well as dose-dependent. Incubation with 1 to 5ng/ml TGF-β1 for 24h induced only minor changes while higher concentrations (10 to 50 ng/ml) and longer exposure times (up to 48h) caused profound changes. Epithelial-to-mesenchymal transdifferentiation can be induced in primary cultures of mouse proximal tubule cells exposed to TGF-β1.

General discussion

In vitro models are a good mean to study cellular phenotype or physiology in a controlled manner. Cell-lines are used frequently in this type of studies. The characteristics of the most frequently used cell lines with (presumed proximal tubule phenotype) are given in table 6.1. However, their capability to survive indefinitely causes down- or up-regulation of markers or ascribes functions to the cell which are different from the cellular phenotype of the parental cell. Furthermore, the originating cell type of some cell-lines is not clearly known, making the interpretation of the cellular phenotype rather difficult. Another *in vitro* model system to study renal function is the isolated perfused tubule. Although, this model is a step closer to the *in vivo* situation, a number of technical difficulties are connected to this type of study. From a technical point of view, the primary cell culture is a good *in vitro* model since it is fairly easy to obtain and the cells can be studied in a controlled and well-defined environment. In order to retain a high degree of differentiation, the isolation procedure and culture conditions should be optimized in function of the cell of interest. Different methods have been described to isolate and culture proximal tubules of the kidney. The most frequently used ones are summarized in table 6.2 and are compared to the method described in this thesis (chapter 3).

Overall, a good isolation method should have a high yield of purified and viable cell material. By microdissecting individual tubules, one can obtain 100% pure starting material, however, it is a time-consuming technique and the yield is very low. Lengthy isolation procedures should be avoided when culturing proximal tubule cells, since they are highly energetic cells that rely on an oxidative metabolism (Mandel, 1985) and thus they are very sensitive to decreases in oxygen tension. Other purification procedures, like Percoll or Ficoll gradient centrifugation, apply enormous mechanical stress to the cells (high-speed centrifugation >20000g) and also prolong the isolation procedure (Vinay et al., 1981; Lash & Tokarz, 1989).

We therefore choose a fast and simple culture method that yielded a suspension enriched in proximal tubules from which the cell culture was initiated. Unlike other methods, we cultured proximal tubule cells on a permeable filter support. On solid supports, active transepithelial transport is evident by the formation of

domes, which are protrusion of the cell monolayer due to accumulation of transported water underneath the monolayer (Bell et al., 1988).

As more water is transported, the hydrostatic pressure in the dome will build up. This could prevent transepithelial transport or cause backleak to the apical compartment. It could even cause a release of the cells from the monolayer (Tanner et al., 1984). On permeable supports, dome formation is not observed, since water can freely diffuse through the support towards the basolateral compartment (Cereijido et al., 1978). Culturing cells on permeable supports should thus improve the degree of differentiation as previously stated by Handler and co-workers (Handler et al., 1984). However, the rapid dedifferentiation of our cell cultures might be the results of a chronic local hypoxia that is known to induce dedifferentiation of cells in culture (Sahai et al., 1997; Sahai et al., 1999). Proximal tubule cells in culture experience low oxygen tensions as demonstrated by the change from an aerobic to an anaerobic metabolism (Nowak et al., 1996). Another possible factor might be the deficiency of epidermal growth factor (EGF), a growth factor that is essential for normal cell proliferation and differentiation (Singh & Harris, 2004).

Assessment of the phenotype revealed that our primary cultures possessed specific characteristics of the proximal tubule. Routinely, the activity of brush border enzymes, like alkaline phosphatase, γ-glutamyl transferase and/or leucine aminopeptidase, the Na^+-dependent uptake of glucose or phosphate and the responses to hormones are assessed in primary cultures of proximal tubule cells. We further analyzed receptor-mediated endocytosis by measuring the uptake of albumin and the presence of V-ATPase, ClC-5 and megalin by immunoblotting and -staining. Our cultures also expressed AQP1.

However, the major advantage of culturing our cells on permeable filter supports is that in this way, they can be characterized electrophysiologically in an Ussing-type chamber (chapter 4). Up to now, there is no clear characterization of the electrophysiological properties of primary cultures of mouse proximal tubules. There is one report in primary cultures of rabbit proximal tubule cells (Bello-Reuss & Weber, 1986). Although, this study reports transepithelial resistances (R_T) and potentials (V_T) that reflect those for a leaky epithelium, the authors did not define whether this primary culture was a Na^+-transporting epithelium, nor did they measure transport rates. Furthermore, the authors state that the

measured R_T was corrected for the series resistance (R_S). However, R_S was only measured at the end of the experiment in the absence of the epithelium and there was no continuous registration and correction. In our setup, we simultaneously measured short-circuit current (I_{SC}), conductance (G_T) and transepithelial capacitance (C_T). By applying impedance measurements, the transepithelial resistance (R_T) and series resistance (R_S) could be identified throughout the experiment and also the measured I_{SC} was continuously corrected according to these values.

Electrophysiological analysis revealed that our primary cultures possess typical properties of a leaky, Na^+-transporting epithelium. We were also able to show that our primary cultures were able to transport phosphate, amino acids and glucose. As stated in previous reports, we observed that the lateral intercellular space (LIS) is a dynamic compartment involved in the active transcellular transport of Na^+ and water (Sackin & Boulpaep, 1975; Spring & Hope, 1979; Spring, 1998; Van Driessche et al., 1999).

After assessing the normal physiological properties of our primary cultures, we used them as a model system to test the effects of the stress factor, TGF-β1 (chapter 5). From *in vivo* studies (Ng et al., 1998), TGF-β1 was appointed one of the prime mediators involved in the development of tubulointerstitial fibrosis. Also evidence was presented that myofibroblasts were derived from the tubule epithelial cells via a process called epithelial-to-mesenchymal transdifferentiation (EMT) (Iwano et al., 2002) and that TGF-β1 could induce EMT in proximal tubule cells (Tian et al., 2003; Lan, 2003). In this study, we describe the morphological transformation of proximal tubule cells to a myofibroblast-like cell after exposure to TGF-β1. Furthermore, *de novo* expression of α-SMA, fibronectin and nestin, all markers for tubulointersitial fibrosis, was observed. The disassembly of the tight junction, as monitored by the disappearance of ZO-1, was an early event in the process of EMT. ZO-1 staining at the tight junction decreased after exposure to 5ng/ml TGF-β1 for 24h while a complete morphological transformation was evident after 48h with a similar concentration. Furthermore, we identified nestin as an early marker in the process of EMT. The expression of nestin was already evident after 24h with low concentrations of TGF-β1 and it coincided with the disappearance of ZO-1 staining.

Table 6.1: Cellular characteristics of frequently used renal epithelial cell lines with (presumed) proximal tubule origin

	Cells	Origin	Morphology	BB-enzyme actvity	Hormone response	Transport activity	Electrophysiology	Frequently used in studies for:
Unknown parental cell type	LLC-PK_1 (Hull et al., 1976)	Cortical mince of Hampshire pig	Apical microvilli Tight junctions BLM infoldings	γ-GT LAP ALP ACP	↑ cAMP by ADH and CT(*)	Na^+-glucose Na^+-aa Na^+-PO_4 Na^+-K^+-$2Cl^-$	$R_T \geq 200\ \Omega.cm^2$ $I_{SC} = \pm 13\ \mu A/cm^2$ $P_D = \pm -2.7$ mV	Hormone action Glucose and phosphate transport
	OK (Koyama et al., 1978)	Kidney of American opossum	Apical microvilli Tight junctions	γ-GT LAP	↑ cAMP by PTH and CT	Na^+-glucose Na^+-aa Na^+-PO_4 Na^+-H^+	$R_T \leq 50\ \Omega.cm^2$ $I_{SC} \leq 1\mu A/cm^2$ $P_D = \pm 0.28$ mV	Na^+-PO_4-transport Na^+/H^+-exchanger Endocytosis
Defined parental cell type	HK-2 (Ryan et al., 1994)	HPV-transformed human PTC	Apical microvilli Tight junctions Glycogen deposits	γ-GT LAP ALP ACP	↑ cAMP by PTH	Na^+-glucose		Cytotoxicity Toxic agents Drugs
	MCT (Haverty et al., 1988)	SV40-transformed mouse PTC	Apical microvilli Tight junctions	ALP				Regulation of TGF-β1 synthesis ATII effects
This thesis	PTC	Primary cultures of mouse PTC	Apical microvilli Tight junctions BLM infoldings Primary cilium	γ-GT ALP	↑ $[Ca^{2+}]_i$ by ATII and BK	Na^+-glucose Na^+-aa Na^+-PO_4	$R_T = \pm 54\ \Omega.cm^2$ $I_{SC} = \pm 14\ \mu A/cm^2$	

BB: brush-border; PTC: proximal tubule cell; BLM: basolateral membrane; γ-GT: γ-glutamyltransferase; LAP: leucine aminopeptidase; ALP: alkaline phosphatase; ACP: acid phosphatase; SV40: simian virus 40; HPV: human papilloma virus; PTH: parathyroid hormone; CT: calcitonin; aa: amino acids; R_T: transepithelial resistance; I_{SC}: short-circuit current; P_D: potential difference; ATII: angiotensin II; BK: bradykinin. (*) distal nephron hormone profile

Table 6.2: Overview of major isolation techniques, culture conditions and investigated characteristics

Authors	Isolation method	Medium			Culture support		Duration until confluence	Species	Characteristics tested
		ITS	FCS	HC	Solid	Permeable			
This thesis	Macrodissection → Collagenase digestion → Sieving	+	1%	+		Collagen-coated PTFE-filters	7 days	Mouse	• Markers: AQP1, ClC-5, V-ATPase, Megalin, SGLT1, SGLT2 • Brush-border enzymes: AP and γ-GT • Na^+-dependent uptake of α-MG • Receptor-mediated endocytosis • Electrophysiological properties: Na^+-dependent I_{SC} and Na^+-dependent uptake of glucose, phosphate and amino acids • Bradykinin and angiotensin II-stimulated $[Ca^{2+}]_i$ increase
Bell et al., 1988	Collagenase digestion → Sedimentation by density	+	24h/ 10%	+	35-mm dishes	Collagen gels(**)	6 days	Mouse	• PTH-stimulated cAMP-production • Production of dihydroxyvitamin D_3 • Alkaline phosphatase activity • Na^+-dependent uptake of PO_4^{2-} and α-MG

Chung et al., 1982	Iron oxide perfusion → Collagenase digestion	+	24h/ 10%	+	35-mm dishes	2 weeks	Rabbit	• PTH-stimulated cAMP-production • Na^+-dependent uptake of α-MG • Brush-border enzymes: LAP, AP and γ-GT
Rosenberg & Michalopoulos, 1987	Collagenase perfusion → Ficoll centrifugation	+	10% (*)	+	Collagen-coated plates	5 - 7 days	Rat	• Brush-border enzyme: γ-GT • Glucose-6-phosphatase activity • Brush-border staining with PAS
Vinay et al., 1981	Collagenase digestion → Percoll centrifugation	Pure suspension			Pure suspension	N/A	Rat	• Accumulation of p-aminohippurate • PTH-stimulated cAMP-production • Metabolism of glutamine, lactate and glucose • Brush-border enzymes: AP and γ-GT

ITS: Insuline-Transferrin-Selenium; FCS: fetal Calf serum; HC: hydrocortisone;(*): Collagen-coated plates were inoculated with 10% FCS before culture; (**) Collagen gels do not have a clearly defined basolateral compartment, since the gels are layered on a cultured dishes, and thus should in fact be defined as a solid culture surface. + means the substance is present in the culture medium. AP: alkaline phosphatase; γ-GT: γ-glutamyl transferase; LAP: leucine aminopeptidase; I_{sc}: short-circuit current.

Future directions

Our main goal in this thesis was to establish a method for culturing mouse renal proximal tubule cells that retain a high degree of morphological and functional differentiation. Since still a lot of (patho-) physiological properties remain unexplored, this primary culture offers a good model system to investigate a broad range of both (electro-) physiological and pathological responses (like exposure to cadmium, oxidative stress) under well-defined conditions.

With the use of the Ussing chamber setup, it is possible to assess the responses of different hormones or substances on the electrophysiological properties of the proximal tubule cells.

In this thesis, it was established that EMT could occur in proximal tubule cells after exposure to TGF-β1. Also a timeline of the different changes with respect to morphology or expression of different markers was investigated and it was established that after 24h exposure to TGF-β1 cells already dedifferentiated to a certain extent. Hence the following question arises: Is there a point of no return? Or can the effects of TGF-β1 be reversed? Therefore, an interesting aspect to study in this primary culture would be the effect of BMP-7, the natural antidote of TGF-β1, in the setting of EMT. Preliminary results show that simultaneous administration of 100ng/ml BMP-7 and TGF-β1 (up to 10ng/ml) for 24h protects the cells against EMT. However, further studies are required to elucidate the precise nature of the protective effects of BMP-7.

Algemene discussie en samenvatting

Samenvatting

Deze thesis beschrijft het op punt stellen van een primaire cultuur van proximale tubuluscellen van de muis en het gebruik ervan voor zowel fysiologische als pathologische onderzoeksdoeleinden. Een snelle en eenvoudige methode werd uitgewerkt en de cellen werden uitgebreid gekarakteriseerd: morfologische, functionele en elektrofysiologische kenmerken van de proximale tubuluscel werden teruggevonden. Naast de normale celfysiologie, waren we ook geïnteresseerd in het gebruik van deze primaire culturen in het onderzoek naar de cellulaire mechanismen die optreden tijdens tubulointerstitiële fibrose. Hiervoor werden primaire celculturen blootgesteld aan TGF-β1, waarna verschillende aspecten van epitheliale-naar-mesenchymale transdifferentiatie werden onderzocht.

Hoofdstuk 3 beschrijft de cultuurmethode en de karakterisering van de primaire celculturen. Om proximale tubuluscellen van de muis in cultuur te brengen, werd een eenvoudige methode die oxidatieve en mechanische stress tijdens de isolatie vermijdt, op punt gesteld. Het gebruik van een permeabele filter maakte toegang tot de apicale en basolaterale zijde mogelijk en dit verbeterde het vectoriaal transport en de celpolariteit. Morfologische analyse van de celculturen toonde typische proximale tubulus eigenschappen aan zoals microvilli, een zonula occludens en een primair cilium aan het apicale membraan alsook invouwingen van het basolaterale membraan, talrijke mitochondria en cytoplasmatische vesikels. De functionele eigenschappen betroffen de aanwezigheid van receptor-gemedieerde endocytose van albumine, Na^+-afhankelijk transport van α-MG, hormoon-gevoeligheid aan bradykinine en angiotensine II en een hoge activiteit van borstelzoom-geassocieerde enzymen, zijnde alkalisch fosfatase en γ-glutamyl-transferase. Verder werd er een immunoreactiviteit waargenomen tegen proximale tubulaire merkers, AQP1 en SGLT type 1 en 2 alsook tegen merkers van de receptor-gemedieerde endocytose, ClC-5, megaline en V-type ATPase, wat de proximale tubulaire oorsprong van de cellen versterkt.

In hoofdstuk 4 werden de elektrofysiologische eigenschappen van de primaire culturen bestudeerd. De primaire culturen vertoonden typische kenmerken van een lek epitheel zoals een lage transepitheliale weerstand (R_T) en een hoge transepitheliale stroom. Het vervangen van Na^+ door $NMDG^+$ zorgde voor het verdwijnen van de kortsluitstroom (I_{SC}), waaruit afgeleid kon worden dat de primaire culturen zich gedroegen als een Na^+-transporterend epitheel. De aanwezigheid van een transportsysteem voor fosfaat, glucose en aminozuren werd ook aangetoond. Impedantiemeting toonde dat de laterale intercellulaire ruimte (LIS) een dynamisch compartiment is dat uitzet tengevolge van Na^+-transport en inkrimpt na verwijdering van Na^+ uit de perfusie-oplossing. Deze resultaten toonden dat de primaire culturen elektrofysiologische eigenschappen van een lek proximaal tubulair epitheel bezitten.

In hoofdstuk 5, werden de primaire culturen gebruik om de effecten van het profibrotisch cytokine, TGF-β1, in de context van tubulointersitiële fibrose te onderzoeken. Blootstelling aan TGF-β1 resulteerde in een veranderde celmorfologie van een epitheliale kubusvormige cel naar een spoelvormige langgerekte fibroblastachtige cel. De morfologische verandering ging gepaard met de expressie van merkers eigen aan de myofibroblast, zoals α-SMA, fibronectine en nestine alsook met het ontmantelen van de zonula occludens, wat bleek uit het verdwijnen van ZO-1. Nucleaire hypertrofie, een ander kenmerk van tubulointerstitiële fibrose, werd tevens waargenomen. De effecten van TGF-β1 waren dosis- en tijdsafhankelijk. Blootstelling aan 1 tot 5 ng/ml TGF-β1 gedurende 24u induceerde slechts milde veranderingen terwijl hoge concentraties (van 10 tot 50 ng/ml) en lange blootstellingtijden (tot 48u) drastische veranderingen veroorzaakten. Deze resultaten toonden aan dat epitheliale-naar-mesenchymale transdifferentiatie kan optreden in primaire culturen van muis proximale tubulaire cellen na blootstelling aan TGF-β1.

Algemene discussie

In vitro systemen zijn een goed middel voor het onderzoek van het cellulaire fenotype of de celfysiologie. Cellijnen worden vaak voor deze doeleinden gebruikt. De karakteristieken van de meest frequent gebruikte cellijnen met (vermoedelijk) proximaal fenotype zijn beschreven in tabel 6.3. Weliswaar bezitten cellijnen een oneindige delingscapaciteit, die een veranderde expressie van merkers kan veroorzaken of zelfs functies aan de cellen kan verlenen die niet overeenkomen met het cellulaire fenotype van de ouderlijke cel. Verder is het zo dat van sommige cellijnen het celtype waarvan ze afstammen niet goed gekend is, waardoor de interpretatie van het cellulaire fenotype bemoeilijkt wordt. Een ander *in vitro* systeem om de nierfunctie te bestuderen is de geïsoleerde geperfundeerde tubulus. Ondanks het feit dat dit model een stap dichter bij de *in vivo* situatie staat, wordt dit soort studie bemoeilijkt door de technische moeilijkheden die ermee verbonden zijn. Dus vanuit een technisch standpunt is de primaire celcultuur een goed *in vitro* model daar cellen op een relatief eenvoudige manier kunnen bekomen worden omdat ze kunnen bestuderen worden onder controleerbare omstandigheden. Om een zo hoog mogelijke graad van differentiatie te behouden, is het noodzakelijk dat de isolatieprocedure en de cultuurcondities aangepast zijn aan het beoogde celtype. Verschillende methoden zijn al beschreven om niercellen te isoleren en in cultuur te brengen. De meest voorkomende technieken staan beschreven in tabel 6.4 en deze worden vergeleken met de methode gebruikt in deze thesis (hoofdstuk 3).
Algemeen bekeken moet een goede isolatiemethode een zo hoog mogelijke opbrengst van levende cellen van één welbepaald celtype hebben. Met behulp van microdissectie is het mogelijk om een 100% pure suspensie te verkrijgen, maar de techniek is tijdsrovend en de opbrengst is heel laag. Bovendien zouden langdurige isolatiemethoden voor het in cultuur brengen van proximale tubulaire cellen vermeden moeten worden. Proximale tubuluscellen hebben een hoog metabolisme dat afhankelijk is van de verbranding van zuurstof (Mandel, 1985), wat hen zeer gevoelig maakt aan veranderingen in de zuurstofspanning. Andere zuiveringsprocedures zoals Ficoll of Percoll gradiëntcentrifugatie, veroorzaken enorme mechanische stress aan de cellen (centrifugatie aan hoge snelheden >20000g) en bovendien verlengen ze de isolatieprocedure (Vinay et al., 1981; Lash & Tokarz, 1989). Omwille van bovengenoemde redenen opteerden we voor

een snelle en eenvoudige cultuurmethode met als opbrengst een suspensie verrijkt aan proximale tubuli waarmee de cultuur opgestart werd. In tegenstelling tot andere methoden, werden de proximale tubuli in cultuur gebracht op permeabele filters. Op vaste cultuurbodems is actief transepitheliaal transport zichtbaar door de vorming van uitstulpingen van de celmonolaag ("domes") tengevolge van de opeenhoping van het getransporteerde water onder de cellaag (Bell et al., 1988). Het aanhoudende transport van water zorgt voor een verhoging van de hydrostatische druk in de welving. Dit kan het transepitheliaal transport belemmeren of een terugvloeien naar het apicale compartiment veroorzaken. Tevens kan het leiden tot het loslaten van cellen en een ruptuur in de monolaag veroorzaken (Tanner et al., 1984). Bij culturen op permeabele filters wordt de vorming van "domes" niet waargenomen aangezien water vrij kan diffunderen doorheen de filter naar het basolaterale compartiment (Cereijido et al., 1978). Zoals eerder werd waargenomen door Handler en medewerkers (Handler et al., 1984), verhoogt de differentiatiegraad van de cellen die op een permeabele filter in cultuur werden gebracht. De snelle dedifferentiatie van onze cellen kan toe te schrijven zijn aan de chronische lokale hypoxie, die bekend staat als dedifferentiatie factor van cellen in cultuur (Sahai et al., 1997; Sahai et al., 1999). Proximale tubuluscellen in cultuur ondervinden een lage zuurstofspanning, aantoonbaar door de overschakeling van een aëroob naar anaëroob metabolisme (Nowak et al., 1996). Een andere mogelijke factor is het ontbreken van epidermale groeifactor (EGF), die essentieel is voor normale celproliferatie en -differentiatie (Singh & Harris, 2004),

De karakterisering van het fenotype toonde ons dat de primaire culturen specifieke kenmerken van de proximale tubulus hadden. In de meeste studies worden de activiteit van borstelzoom-geassocieerde enzymen zoals het alkalische fosfatase, γ-glutamyl transferase alsook leucine aminopeptidase, het Na^+-afhankelijke transport van glucose of fosfaat en de hormoongevoeligheid van de primaire culturen getest. Naast deze kenmerken, hebben we tevens de receptor-gemedieerde endocytose van albumine en de aanwezigheid van het AQP1, V-ATPase, ClC-5 en megaline aangetoond.

Het grootste voordeel van de celcultuur op een permeabele filter is dat ze op deze manier elektrofysiologisch getest kunnen worden in een Ussing kamer

(chapter 4). Tot heden is er nog geen duidelijke karakterisering van de elektrofysiologische eigenschappen van een primaire cultuur van muis proximale tubuli, tenzij in slechts één studie waarin gebruik werd gemaakt van primaire culturen van de proximale tubulus van het konijn (Bello-Reuss & Weber, 1986). Niettegenstaande er in deze studie transepitheliale weerstanden (R_T) en potentialen (V_T) werden waargenomen vergelijkbaar met deze van een lek epitheel, werd het niet duidelijk gedefinieerd of de primaire cultuur een Na^+-transporterend epitheel was, noch werden transportsnelheden gemeten. Bovendien beweerden de auteurs dat de gemeten R_T gecorrigeerd werd voor de serie weerstand (R_S), die slechts eenmalig aan het eind van ieder experiment bepaald werd. In onze setup, was er een continue registratie en correctie voor R_S, bovendien was het mogelijk om simultaan de kortsluitstroom (I_{SC}), de conductantie (G_T) en de transepitheliale capaciteit (C_T) te meten. Door impedantie analyse toe te passen, werden de transepitheliale (R_T) en de seriële weerstand (R_S) gedurende het experiment geanalyseerd en de gemeten I_{SC} werd naargelang deze waarden gecorrigeerd. Elektrofysiologische karakterisering van de primaire culturen toonden ons de typische eigenschappen van een lek, Na^+-transporterend epitheel. Bovendien konden we het transport van fosfaat, glucose en aminozuren in de primaire culturen aantonen. Zoals ook eerder werd waargenomen, is de laterale intercellulaire ruimte (LIS) een dynamisch compartiment dat een rol speelt in het actieve transcellulaire transport van Na^+ en water (Sackin & Boulpaep, 1975; Spring & Hope, 1979; Spring, 1998; Van Driessche et al., 1999).

Eens we de normale fysiologie van onze celculturen hadden vastgesteld, werden ze gebruikt als modelsysteem om de effecten van de stress factor, TGF-β1, te onderzoeken (hoofdstuk 5). Uitgaande van *in vivo* studies (Ng et al., 1998), werd TGF-β1 aangeduid als de belangrijkste mediator in de ontwikkeling van tubulointerstitiële fibrose. Bovendien was er bewijs dat myofibroblasten afkomstig waren van het tubulair epitheel door het proces genaamd epitheliale-naar-mesenchymale transdifferentiatie (EMT) (Iwano et al., 2002) en dat TGF-β1 in staat was om EMT te induceren in proximale tubuluscellen (Tian et al., 2003; Lan, 2003). In deze studie beschrijven wij de morfologische transformatie van de proximale tubuluscellen naar een myofibroblast-achtige cel na blootstelling aan TGF-β1. Bovendien werden merkers van tubulointerstitiële fibrose zoals de

"*de novo*" expressie van α-SMA, fibronectine en nestine waargenomen. De ontmanteling van de zonula occludens, waargenomen door het verdwijnen van ZO-1, was een vroeg optredende gebeurtenis tijdens EMT.

Kleuring van ZO-1 aan de zonula occludens verminderde na blootstelling aan 5ng/ml TGF-β1 gedurende 24u. Terwijl bij eenzelfde concentratie, een volledige morfologische transformatie van de cellen pas duidelijk was na 48u blootstelling. Bovendien konden we nestine aantonen als een vroege merker van EMT. De expressie van nestine was duidelijk na 24h blootstelling aan lage concentraties TGF-β1 en ging gepaard met het verdwijnen van ZO-1 kleuring.

Toekomstperspectieven

Het hoofddoel van deze thesis was de oppuntstelling van een methode voor het in cultuur brengen van muis proximale tubuluscellen met behoud van een hoge graad van morfologische en functionele differentiatie. Hoewel heel wat (patho-)fysiologische kenmerken nog niet ontrafeld zijn, biedt deze primaire cultuur een goed modelsysteem om een brede waaier van zowel (elektro-)fysiologische als pathologische situaties (zoals blootstelling aan cadmium of oxidatieve stress) in controleerbare omstandigheden te bestuderen.

Het gebruik van de Ussing kamer laat toe om de effecten van verschillende hormonen of stoffen op de elektrofysiologische eigenschappen van de proximale tubuluscellen in kaart te brengen.

In deze thesis werd vastgesteld dat EMT kan optreden in proximale tubuluscellen na blootstelling aan TGF-β1. Bovendien kon er een tijdlijn van de verschillende veranderingen m.b.t. de morfologie of expressie van verschillende merkers worden opgesteld, waaruit duidelijk werd dat na 24h blootstelling aan TGF-β1 de proximale cellen al tot een zekere graad gedifferentieerd waren. Daaruit volgt de vraag: Is het proces omkeerbaar? Of kunnen de effecten van TGF-β1 tegengewerkt worden? Uit preliminaire resultaten blijkt dat gelijktijdige toediening van 100ng/ml BMP-7 en TGF-β1 (tot 10ng/ml) gedurende 24h de cellen beschermt tegen EMT. Verdere studies zijn echter nodig om de werkelijke aard van de bescherming van BMP-7 te ontrafelen.

Tabel 6.3: Cellulaire karakteristieken van frequent gebruikte renale epitheliale celijnen met (veronderstelde)proximale tubulaire herkomst

	Cellen	Herkomst	Morfologie	BB-enzyme activiteit	Hormonale response	Transport activiteit	Elektrofysiologie	Frequent gebruikt in studies naar:
Onbekend ouderlijk celtype	LLC-PK$_1$ (Hull et al., 1976)	Corticale snede van Hampshire varken	Apicale microvilli Zonula occludens BLM invouwingen	γ-GT LAP ALP ACP	↑ cAMP door ADH en CT(*)	Na^+-glucose Na^+-aa Na^+-PO_4 Na^+-K^+-$2Cl^-$	$R_T \geq 200\ \Omega.cm^2$ $I_{SC} = \pm 13\ \mu A/cm^2$ $P_D = \pm -2.7$ mV	Hormonale respons Glucose en fosfaat transport
	OK (Koyama et al., 1978)	Nier van de Amerikaanse opossum	Apicale microvilli Zonula occludens	γ-GT LAP	↑ cAMP door PTH en CT	Na^+-glucose Na^+-aa Na^+-PO_4 Na^+-H^+	$R_T \leq 50\ \Omega.cm^2$ $I_{SC} \leq 1\mu A/cm^2$ $P_D = \pm 0.28$ mV	Na^+-PO_4-transport Na^+/H^+-uitwisselaar Endocytose
Bekend ouderlijk celtype	HK-2 (Ryan et al., 1994)	HPV-ge-transformeerde humane PTC	Apicale microvilli Zonula occludens Glycogeen positieve vesikels	γ-GT LAP ALP ACP	↑ cAMP door PTH	Na^+-glucose		Cytotoxiciteit Toxische agentia Farmaca
	MCT (Haverty et al., 1988)	SV40-ge-transformeerde muis PTC	Apicale microvilli Zonula occludens	ALP				Regulatie van de TGF-β1 synthese ATII effecten
Deze thesis	PTC	Primaire cultuur van muis PTC	Apicale microvilli Zonula occludens BLM invouwingen Primair cilium	γ-GT ALP	↑ $[Ca^{2+}]_i$ door ATII en BK	Na^+-glucose Na^+-aa Na^+-PO_4	$R_T = \pm 54\ \Omega.cm^2$ $I_{SC} = \pm 14\ \mu A/cm^2$	

BB: borstelzoom; PTC: proximale tubulus cel; BLM: basolaterale membraan; γ-GT: γ-glutamyltransferase; LAP: leucine aminopeptidase; ALP: alkalisch fosfatase; ACP: zuur fosfatase; SV40: simian virus 40; HPV: humaan papilloma virus; PTH: parathyroid hormoon; CT: calcitonine; aa: amino zuren; R_T: transepitheliale weerstand; I_{SC}: kortsluitstroom; P_D: potentiaal verschil; ATII: angiotensine II; BK: bradykinine. (*) distaal nefron hormonaal profiel

Tabel 6.4: Overzicht van de belangrijkste isolatie technieken, cultuurcondities en onderzochte karakteristieken

Auteurs	Isolatie methode	Medium			Cultuur oppervlak		Duur tot confluentie	Species	Onderzochte karakteristieken
		ITS	FCS	HC	Solid	Permeable			
Deze thesis	Macrodissectie → Collagenase digestie → Zeven	+	1%	+		Collageen-gecoate PTFE-filters	7 dagen	Muis	• Merkers: AQP1, ClC-5, V-ATPase, Megaline, SGLT1, SGLT2 • Borstelzoom enzymes: AP en γ-GT • Na^+-afhankelijke opname van α-MG • Receptor-gemedieerde endocytose • Elektrofysiologische eigenschappen: Na^+-afhankelijke I_{SC}, en opname van glucose, fosfaat en aminozuren • Bradykinine en angiotensine II gestimuleerde $[Ca^{2+}]_i$ stijging
Bell et al., 1988	Collagenase digestie → Sedimentatie door densiteit	+	24h/ 10%	+	35-mm petrischaal	Collageen gels(**)	6 dagen	Muis	• PTH-gestimuleerde cAMP-productie • Productie van dihydroxyvitamine D_3 • Alkalisch fosfatase activiteit • Na^+-afhankelijke opname van PO_4^{2-} en α-MG

Chung et al., 1982	Ijzeroxide perfusie → Collagenase digestie	+	24h/ 10%	+	35-mm petrischaal	2 weken	Konijn	• PTH-gestimuleerde cAMP-productie • Na^+-afhankelijke opname van α-MG • Borstelzoom enzymes: LAP, AP en γ-GT
Rosenberg & Michalopoulos, 1987	Collagenase perfusie → Ficoll centrifugatie	+	10% (*)	+	Collageen-gecoate platen	5 - 7 dagen	Rat	• Borstelzoom enzyme: γ-GT • Glucose-6-fosfatase activiteit • Borstelzoom kleuring met PAS
Vinay et al., 1981	Collagenase digestie → Percoll centrifugatie	Pure suspensie			Pure suspensie	N/A	Rat	• Accumulatie van p-aminohippurate • PTH-gestimuleerde cAMP-productie • Metabolisme van glutamine, lactaat en glucose • Borstelzoom enzymes: AP en γ-GT

ITS: Insuline-Transferrin-Selenium; FCS: foetal Calf serum; HC: hydrocortisone;(*): Collageen-gecoate platen werden vooraf geïncubeerd met 10% FCS; (**) Collageen gels hebben geen duidelijk gedefinieerd basolateraal compartiment aangezien de gels op cultuurplaten gelegd worden en zouden daarom gedefinieerd moeten worden als een vaste cultuurondergrond; + betekent dat het aanwezig is in de cultuur; AP: alkalisch fosfatase; γ-GT: γ-glutamyl transferase; LAP: leucine aminopeptidase; I_{sc}: kortsluitstroom.

Addendum

1. Complex Impedance

1.1 Definition

Electrical impedance, or simply impedance, is a measure of opposition of a circuit to a sinusoidal alternating electric current.

The impedance of a circuit element is defined as the ratio of the voltage across the element to the current through the element: Z = V/I.

1.2 Impedance of different devices

For a **resistor**:

$$Z_{\text{resistor}} = \frac{V_{\text{R}}}{I_{\text{R}}} = R \qquad \text{(Eq. 1)}$$

For a **capacitor**:

$$Z_{\text{capacitor}} = \frac{V_{\text{C}}}{I_{\text{C}}} = \frac{1}{j\omega C} = \frac{-j}{\omega C} \qquad \text{(Eq. 2)}$$

For an **inductor**:

$$Z_{\text{inductor}} = \frac{V_{\text{L}}}{I_{\text{L}}} = j\omega L \qquad \text{(Eq. 3)}$$

When resistors, capacitors, and inductors are combined in an AC circuit, the impedances of the individual components can be combined in the same way that the resistances are combined in a DC circuit. The resulting equivalent impedance is in general, a complex quantity. That is, the equivalent impedance has a Real part (Re) and an Imaginary part (Im). Thus:

$$Z_{eq} = \mathrm{Re}\,Z + j \cdot \mathrm{Im}\,Z \qquad \text{(Eq. 4)}$$

where *ReZ* is termed the resistive part of the impedance
ImZ is termed the *reactive* part of the impedance.

1.3 Combining impedances

Combining impedances in series or in parallel configurations is the same as for resistors. The difference is that combining impedances involves manipulation of complex numbers.

In series:

$$Z_s = Z_1 + Z_2 = (\mathrm{Re}_1 + \mathrm{Re}_2) + j \cdot (\mathrm{Im}_1 + \mathrm{Im}_2) \qquad \text{(Eq. 5)}$$

In parallel:

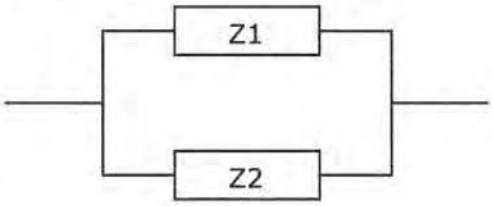

$$\frac{1}{Z_p} = \frac{1}{Z_1} + \frac{1}{Z_2} \quad \Rightarrow \quad Z_p = \frac{Z_1 \cdot Z_2}{Z_1 + Z_2} = \frac{(\mathrm{Re}_1 + j \cdot \mathrm{Im}_1) \cdot (\mathrm{Re}_2 + j \cdot \mathrm{Im}_2)}{(\mathrm{Re}_1 + \mathrm{Re}_2) + j \cdot (\mathrm{Im}_1 + \mathrm{Im}_2)}$$

(Eq. 6)

Now suppose we have the following circuit:

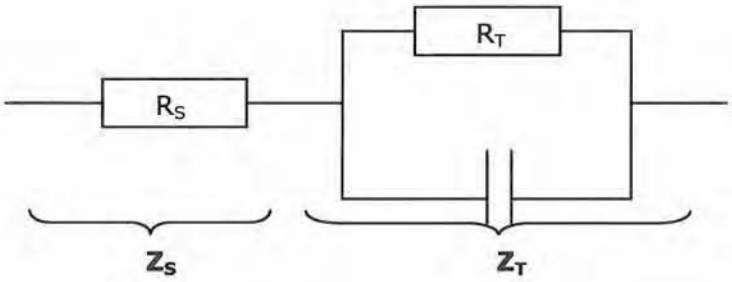

This circuit is a series combination between two impedances: Z_S (for the series resistance R_S) and Z_T (for the circuit R_TC_T parallel).
According to Eq. 5, the equivalent impedance for this series circuit is:

$$Z_{eq} = Z_s + Z_T = R_s + Z_T \qquad \text{(Eq. 7)}$$

According to Eq. 6, for the parallel Z_T we have:

$$Z_T = \frac{Z_1 \cdot Z_2}{Z_1 + Z_2} \quad ,with \quad Z_1 = R_T \quad and \quad Z_2 = \frac{1}{j \cdot \omega \cdot C_T}$$

$$Z_T = \frac{R_T \cdot \left(\frac{1}{j \cdot \omega \cdot C_T}\right)}{R_T + \frac{1}{j \cdot \omega \cdot C_T}} = \frac{R_T \cdot \left(\frac{1}{j \cdot \omega \cdot C_T}\right)}{\frac{j \cdot \omega \cdot R_T \cdot C_T + 1}{j \cdot \omega \cdot C_T}} = \frac{R_T}{j \cdot \omega \cdot R_T \cdot C_T + 1}$$

Here, like shown in the ratio of two complex numbers, we will multiply both the numerator and denominator with the **complex conjugate** of the denominator.
By doing this, we do not change the formula, but this will help to have at denominator only real numbers, and move **j** at numerator.

This is done in order to be able to separate in the end the real and imaginary components of the equivalent impedance of the circuit.

Thus:

$$Z_T = \frac{R_T}{1 + j \cdot \omega \cdot R_T \cdot C_T} = \frac{R_T \cdot (1 - j \cdot \omega \cdot R_T \cdot C_T)}{(1 + j \cdot \omega \cdot R_T \cdot C_T) \cdot (1 - j \cdot \omega \cdot R_T \cdot C_T)} \Rightarrow$$

$$Z_T = \frac{R_T - j \cdot \omega \cdot R_T^2 \cdot C_T}{1 + (\omega \cdot R_T \cdot C_T)^2}$$

To separate Z_T in real and imaginary part, we will distribute the denominator to each term in the numerator:

$$Z_T = \frac{R_T}{1 + (\omega \cdot R_T \cdot C_T)^2} - j \cdot \frac{\omega \cdot R_T^2 \cdot C_T}{1 + (\omega \cdot R_T \cdot C_T)^2} \qquad \text{(Eq. 8)}$$

Introducing Eq. 8 in Eq. 7, we obtain for the equivalent impedance of the circuit:

$$Z_{eq} = R_s + Z_T = R_s + \frac{R_T}{1 + (\omega \cdot R_T \cdot C_T)^2} - j \cdot \frac{\omega \cdot R_T^2 \cdot C_T}{1 + (\omega \cdot R_T \cdot C_T)^2}$$

And knowing that **Zeq =Re Z+j Im Z**, we obtain for the real and imaginary parts:

$$\text{Re } Z_{eq} = R_s + \frac{R_T}{1 + (\omega \cdot R_T \cdot C_T)^2} \qquad \text{(Eq. 9)}$$

$$\text{Im } Z_{eq} = -\frac{\omega \cdot R_T^2 \cdot C_T}{1 + (\omega \cdot R_T \cdot C_T)^2} \qquad \text{(Eq. 10)}$$

Extracting from the Real and Imaginary part of the impedance the values for C_T and R_T implies an estimation of R_S.

1.4 Estimation of R_S

Consider that we measure the Real and Imaginary part of the equivalent Impedance Zeq at 2 different frequencies.

Then we have:

Z_1 =Re Z_1+j Im Z_1 , for the frequency ν_1 ($\omega=2\pi\nu_1$)

Z_2 =Re Z_2+j Im Z_2 , for the frequency ν_2 ($\omega=2\pi\nu_2$)

(for simplicity, I denoted the equivalent total impedances $Z_{eq\ 1}$ and $Z_{eq\ 2}$ simply, as Z_1 and Z_2)

With the Eq. 9 and Eq. 10, we can rewrite the real and imaginary parts of Z_1 and Z_2 as:

$$\begin{cases} \mathrm{Re}\,Z_1 = R_s + \dfrac{R_T}{1+(\omega_1 \cdot R_T \cdot C_T)^2} \\ \mathrm{Im}\,Z_1 = -\dfrac{\omega_1 \cdot R_T^2 \cdot C_T}{1+(\omega_1 \cdot R_T \cdot C_T)^2} \end{cases} \qquad \begin{cases} \mathrm{Re}\,Z_2 = R_s + \dfrac{R_T}{1+(\omega_2 \cdot R_T \cdot C_T)^2} \\ \mathrm{Im}\,Z_2 = -\dfrac{\omega_2 \cdot R_T^2 \cdot C_T}{1+(\omega_2 \cdot R_T \cdot C_T)^2} \end{cases}$$

Now we will try to simplify these equations, by rearranging the terms.

We move R_S to the left side of the equation in the Real terms and divide ImZ by ω:

$$\begin{cases} \mathrm{Re}\,Z_1 - R_s = \dfrac{R_T}{1+(\omega_1 \cdot R_T \cdot C_T)^2} & \text{(Eq. 11)} \\ \dfrac{\mathrm{Im}\,Z_1}{\omega_1} = -\dfrac{R_T^2 \cdot C_T}{1+(\omega_1 \cdot R_T \cdot C_T)^2} & \text{(Eq. 12)} \end{cases} \qquad \begin{cases} \mathrm{Re}\,Z_2 - R_s = \dfrac{R_T}{1+(\omega_2 \cdot R_T \cdot C_T)^2} & \text{(Eq. 13)} \\ \dfrac{\mathrm{Im}\,Z_2}{\omega_2} = -\dfrac{R_T^2 \cdot C_T}{1+(\omega_2 \cdot R_T \cdot C_T)^2} & \text{(Eq. 14)} \end{cases}$$

Now we see that in both Eq. 11 and Eq. 12 we have a common term:

$$\frac{R_T}{1+(\omega_1 \cdot R_T \cdot C_T)^2}$$

Similar for Eq. 13 and Eq. 14: $\dfrac{R_T}{1+(\omega_2 \cdot R_T \cdot C_T)^2}$

If we divide term by term Eq. 12 to Eq. 11, we can then get rid of this big term. Similar for Eq. 13 and Eq. 14:

$$\begin{cases} \dfrac{\dfrac{\mathrm{Im}\,Z_1}{\omega_1}}{\mathrm{Re}\,Z_1 - R_s} = -\dfrac{\dfrac{R_T^2 \cdot C_T}{1+(\omega_1 \cdot R_T \cdot C_T)^2}}{\dfrac{R_T}{1+(\omega_1 \cdot R_T \cdot C_T)^2}} \end{cases} \qquad \begin{cases} \dfrac{\dfrac{\mathrm{Im}\,Z_2}{\omega_2}}{\mathrm{Re}\,Z_2 - R_s} = -\dfrac{\dfrac{R_T^2 \cdot C_T}{1+(\omega_2 \cdot R_T \cdot C_T)^2}}{\dfrac{R_T}{1+(\omega_2 \cdot R_T \cdot C_T)^2}} \end{cases}$$

And we get:

$$\begin{cases} \dfrac{\dfrac{\mathrm{Im}\,Z_1}{\omega_1}}{\mathrm{Re}\,Z_1 - R_s} = -R_T \cdot C_T \end{cases} \quad \text{(Eq.15)} \qquad \begin{cases} \dfrac{\dfrac{\mathrm{Im}\,Z_2}{\omega_2}}{\mathrm{Re}\,Z_2 - R_s} = -R_T \cdot C_T \end{cases} \quad \text{(Eq.16)}$$

If we take the term $-R_TC_T$ from Eq. 16 and substitute it in Eq. 15, we obtain:

$$\frac{\dfrac{\mathrm{Im}\,Z_1}{\omega_1}}{\mathrm{Re}\,Z_1 - R_s} = \frac{\dfrac{\mathrm{Im}\,Z_2}{\omega_2}}{\mathrm{Re}\,Z_2 - R_s} \Rightarrow \frac{\mathrm{Im}\,Z_1}{\omega_1} \cdot (\mathrm{Re}\,Z_2 - R_s) = \frac{\mathrm{Im}\,Z_2}{\omega_2} \cdot (\mathrm{Re}\,Z_1 - R_s) \Rightarrow$$

$$\frac{\mathrm{Im}\,Z_1}{\omega_1} \cdot \mathrm{Re}\,Z_2 - \frac{\mathrm{Im}\,Z_1}{\omega_1} \cdot R_s = \frac{\mathrm{Im}\,Z_2}{\omega_2} \cdot \mathrm{Re}\,Z_1 - \frac{\mathrm{Im}\,Z_2}{\omega_2} \cdot R_s$$

Now we separate on left side the terms containing R_S, and on the right side the rest of the terms:

$$\frac{\mathrm{Im}\,Z_2}{\omega_2}\cdot R_s - \frac{\mathrm{Im}\,Z_1}{\omega_1}\cdot R_s = \frac{\mathrm{Im}\,Z_2}{\omega_2}\cdot \mathrm{Re}\,Z_1 - \frac{\mathrm{Im}\,Z_1}{\omega_1}\cdot \mathrm{Re}\,Z_2 \quad \Rightarrow$$

$$\left(\frac{\mathrm{Im}\,Z_2}{\omega_2} - \frac{\mathrm{Im}\,Z_1}{\omega_1}\right)\cdot R_s = \frac{\mathrm{Im}\,Z_2}{\omega_2}\cdot \mathrm{Re}\,Z_1 - \frac{\mathrm{Im}\,Z_1}{\omega_1}\cdot \mathrm{Re}\,Z_2 \quad \Rightarrow$$

$$R_s = \frac{\dfrac{\mathrm{Im}\,Z_2}{\omega_2}\cdot \mathrm{Re}\,Z_1 - \dfrac{\mathrm{Im}\,Z_1}{\omega_1}\cdot \mathrm{Re}\,Z_2}{\left(\dfrac{\mathrm{Im}\,Z_2}{\omega_2} - \dfrac{\mathrm{Im}\,Z_1}{\omega_1}\right)}$$

This is how R_S can be calculated, measuring the impedance at 2 different frequencies.

1.5 Estimation of C_T and R_T

Now, having the value for R_S, we go back to the Eq. 9 and Eq. 10, to calculate C_T and R_T.

We have at one measured frequency:

$$\begin{cases} \mathrm{Re}\,Z = R_s + \dfrac{R_T}{1+\left(\omega\cdot R_T\cdot C_T\right)^2} \\ \mathrm{Im}\,Z = -\dfrac{\omega\cdot R_T^2\cdot C_T}{1+\left(\omega\cdot R_T\cdot C_T\right)^2} \end{cases}$$

Like in the previous calculations, we will move R_S to the left side of the equation in the Real term and divide ImZ by ω:

$$\begin{cases} \mathrm{Re}\,Z - R_s = \dfrac{R_T}{1+(\omega \cdot R_T \cdot C_T)^2} & \text{(Eq. 15)} \\ \dfrac{\mathrm{Im}\,Z}{\omega} = -\dfrac{R_T^2 \cdot C_T}{1+(\omega \cdot R_T \cdot C_T)^2} & \text{(Eq. 16)} \end{cases}$$

Then we divide Eq. 16 by Eq. 15:

$$\frac{\dfrac{\mathrm{Im}\,Z}{\omega}}{\mathrm{Re}\,Z - R_s} = -R_T \cdot C_T \quad \Rightarrow \quad R_T \cdot C_T = -\frac{\dfrac{\mathrm{Im}\,Z}{\omega}}{\mathrm{Re}\,Z - R_s} \qquad \text{(Eq. 17)}$$

We will substitute now the expression of R_TC_T into Eq. 15, in order to obtain R_T:

$$\mathrm{Re}\,Z - R_s = \frac{R_T}{1+(\omega \cdot R_T \cdot C_T)^2} \quad \Rightarrow \quad \mathrm{Re}\,Z - R_s = \frac{R_T}{1+\left(\omega \cdot \left(-\dfrac{\dfrac{\mathrm{Im}\,Z}{\omega}}{\mathrm{Re}\,Z - R_s}\right)\right)^2} \quad \Rightarrow$$

after simplifying with ω:

$$\mathrm{Re}\,Z - R_s = \frac{R_T}{1+\dfrac{(\mathrm{Im}\,Z)^2}{(\mathrm{Re}\,Z - R_s)^2}} \quad \Rightarrow \quad \mathrm{Re}\,Z - R_s = \frac{R_T}{\dfrac{(\mathrm{Re}\,Z - R_s)^2 + (\mathrm{Im}\,Z)^2}{(\mathrm{Re}\,Z - R_s)^2}} \quad \Rightarrow$$

$$\mathrm{Re}\,Z - R_s = \frac{R_T \cdot (\mathrm{Re}\,Z - R_s)^2}{(\mathrm{Re}\,Z - R_s)^2 + (\mathrm{Im}\,Z)^2} \qquad \text{(Eq. 18)}$$

Now we can simplify both terms in Eq. 18 with ($\mathrm{Re}\,Z - R_s$) and get:

$$1 = \frac{R_T \cdot (\mathrm{Re}\,Z - R_s)}{(\mathrm{Re}\,Z - R_s)^2 + (\mathrm{Im}\,Z)^2} \quad \Rightarrow \quad (\mathrm{Re}\,Z - R_s)^2 + (\mathrm{Im}\,Z)^2 = R_T \cdot (\mathrm{Re}\,Z - R_s) \quad \Rightarrow$$

$$\boxed{R_T = \frac{(\mathrm{Re}\,Z - R_s)^2 + (\mathrm{Im}\,Z)^2}{\mathrm{Re}\,Z - R_s}} \qquad \text{(Eq. 19)}$$

Now, having the expresion for R_T, we go back to Eq. 17 to determine C_T.
We have:

$$R_T \cdot C_T = -\frac{\mathrm{Im}\,Z}{\omega} \quad \Rightarrow \quad C_T = -\frac{1}{R_T} \cdot \frac{\mathrm{Im}\,Z}{\omega} \quad \Rightarrow$$

$$C_T = -\frac{1}{\frac{(\mathrm{Re}\,Z - R_s)^2 + (\mathrm{Im}\,Z)^2}{(\mathrm{Re}\,Z - R_s)}} \cdot \frac{\frac{\mathrm{Im}\,Z}{\omega}}{(\mathrm{Re}\,Z - R_s)} \quad \Rightarrow$$

We simplify with the term: Re Z-R_S and get:

$$C_T = -\frac{1}{(\mathrm{Re}\,Z - R_s)^2 + (\mathrm{Im}\,Z)^2} \cdot \frac{\mathrm{Im}\,Z}{\omega} \quad \Rightarrow$$

$$\boxed{C_T = -\frac{\mathrm{Im}\,Z}{\omega \cdot \left((\mathrm{Re}\,Z - R_s)^2 + (\mathrm{Im}\,Z)^2\right)}}$$

References

Abbate M, Zoja C, Remuzzi G. (2006). How does proteinuria cause progressive renal damage? J Am Soc Nephrol 17(11):2974-84.

Aboolian A, Nord EP. (1988). Bradykinin increases cytosolic free [Ca2+] in proximal tubule cells. Am J Physiol 255(3 Pt 2):F486-93.

Agre P, King LS, Yasui M, Guggino WB, Ottersen OP, Fujiyoshi Y, Engel A, Nielsen S. (2002). Aquaporin water channels--from atomic structure to clinical medicine. J Physiol 542(Pt 1):3-16.

Alberts B, Johnson A, Lewis J, Raff M, Roberts K, Walter P. (2002). Cell junctions, cell adhesion and the extracellular matrix. In: Molecular biology of the cell, ed. Alberts B et al. New York: Garland Science, p.1065-1126.

Aronson PS. (2006). Essential roles of CFEX-mediated Cl(-)-oxalate exchange in proximal tubule NaCl transport and prevention of urolithiasis. Kidney Int 70(7):1207-13.

Badid C, Vincent M, Fouque D, Laville M, Desmouliere A. (2001). Myofibroblast: a prognostic marker and target cell in progressive renal disease. Ren Fail 23(3-4):543-9.

Baines AD, Shaikh N, Ho P. (1990). Mechanisms of perfused kidney cytoprotection by alanine and glycine. Am J Physiol 259(1 Pt 2):F80-7.

Barratt LJ, Rector FC Jr, Kokko JP, Seldin DW. (1974). Factors governing the transepithelial potential difference across the proximal tubule of the rat kidney. J Clin Invest 53(2):454-64.

Bell CL, Tenenhouse HS, Scriver CR. 1988. Initiation and characterization of primary mouse kidney epithelial cultures. In Vitro Cell Dev Biol 24(7):683-95.

Bello-Reuss E, Weber MR. (1986). Electrophysiological studies on primary cultures of proximal tubule cells. Am J Physiol 251(3 Pt 2):F490-8.

Bergin E, Levine JS, Koh JS, Lieberthal W. (2000). Mouse proximal tubular cell-cell adhesion inhibits apoptosis by a cadherin-dependent mechanism. Am J Physiol 278(5):F758-68.

Birn H. (2006). The kidney in vitamin B12 and folate homeostasis: characterization of receptors for tubular uptake of vitamins and carrier proteins. Am J Physiol 291(1):F22-36.

Birn H, Christensen EI. (2006). Renal albumin absorption in physiology and pathology. Kidney Int 69(3):440-49.

Bonventre JV, Cheung JY. (1986). Cytosolic free calcium concentration in cultured renal epithelial cells. Am J Physiol 250(2 Pt 2):F329-38.

Border WA, Noble NA. (1994). Transforming growth factor beta in tissue fibrosis. N Engl J Med 331(19):1286-92.

Boron WF. (2006). Acid-base transport by the renal proximal tubule. J Am Soc Nephrol 17(9):2368-82.

Bottinger EP, Bitzer M. (2002). TGF-beta signaling in renal disease. J Am Soc Nephrol 13(10):2600-10.

Boulpaep EL, Seely JF. (1971). Electrophysiology of proximal and distal tubules in the autoperfused dog kidney. Am J Physiol 221(4):1084-96.

Bradford MM. (1976). A rapid and sensitive method for the quantitation of microgram quantities of protein utilizing the principle of protein-dye binding. Anal Biochem 72:248-54.

Broer S. (2006). The SLC6 orphans are forming a family of amino acid transporters. Neurochem Int 48(6-7):559-67.

Brown D, Hirsch S, Gluck S. (1988). Localization of a proton-pumping ATPase in rat kidney. J Clin Invest 82(6):2114-26.

Burckhardt BC, Lorenz J, Kobbe C, Burckhardt G. (2005). Substrate specificity of the human renal sodium dicarboxylate cotransporter, hNaDC-3, under voltage-clamp conditions. Am J Physiol 288(4):F792-9.

Camargo SM, Makrides V, Virkki LV, Forster IC, Verrey F. (2005). Steady-state kinetic characterization of the mouse B(0)AT1 sodium-dependent neutral amino acid transporter. Pflügers Arch 451(2):338-48.

Campean V, Kricke J, Ellison D, Luft FC, Bachmann S. (2001). Localization of thiazide-sensitive Na(+)-Cl(-) cotransport and associated gene products in mouse DCT. Am J Physiol 281(6):F1028-35.

Caruso-Neves C, Provenzano K, Luz FF, Santos FM, Fernandes MS, Leao-Ferreira LR, Lopes AG. (2003). Bradykinin counteracts the stimulatory effect of angiotensin-(1-7) on the proximal tubule Na+ -ATPase activity through B2 receptor. Regul Pept 110(3):207-12.

Caruso-Neves C, Siqueira AS, Iso-Cohen G, Lopes AG. (1999). Bradykinin modulates the ouabain-insensitive Na+-ATPase activity from basolateral membrane of the proximal tubule. Biochim Biophys Acta 1431(2):483-91.

Chan YL, Biagi B, Giebisch G. (1982). Control mechanisms of bicarbonate transport across the rat proximal convoluted tubule. Am J Physiol 242(5):F532-43.

Chan YL, Giebisch G. (1981). Relationship between sodium and bicarbonate transport in the rat proximal convoluted tubule. Am J Physiol 240(3):F222-30.

Choi JS, Kim KR, Ahn DW, Park YS. (1999). Cadmium inhibits albumin endocytosis in opossum kidney epithelial cells. Toxicol Appl Pharmacol 161(2):146-52.

Cereijido M, Robbins ES, Dolan WJ, Rotunno CA, Sabatini DD. 1978. Polarized monolayers formed by epithelial cells on a permeable and translucent support. J Cell Biol 77(3):853-80.

Cereijido M, Valdes J, Shoshani L, Contreras RG. (1998). Role of tight junctions in establishing and maintaining cell polarity. Annu Rev Physiol 60:161-77.

Christensen EI, Birn H. (2001). Megalin and cubilin: synergistic endocytic receptors in renal proximal tubule. Am J Physiol 280(4):F562-73.

Christensen EI, Devuyst O, Dom G, Nielsen R, Van der Smissen P, Verroust P, Leruth M, Guggino WB, Courtoy PJ. (2003). Loss of chloride channel ClC-5 impairs endocytosis by defective trafficking of megalin and cubilin in kidney proximal tubules. Proc Natl Acad Sci U S A 100(14):8472-7.

Chung SD, Alavi N, Livingston D, Taub M. (1982). Characterization of primary rabbit kidney cultures that express proximal tubule functions in a hormonally defined medium.J Cell Biol 95:118-26.

Cook JR, Crute BE, Patrone LM, Gabriels J, Lane ME, Van Buskirk RG. (1989). Microporosity of the substratum regulates differentiation of MDCK cells in vitro. In vitro Cell Dev Biol 25(10):914-22.

Cummings BS, Lasker JM, Lash LH. (2000). Expression of glutathione-dependent enzymes and cytochrome P450s in freshly isolated and primary cultures of proximal tubular cells from human kidney. J Pharmacol Exp Ther 293(2):677-85.

Dallas SL, Sivakumar P, Jones CJP, Chen Q, Peters DM, Mosher DF, Humphries MJ, Kielty CM. (2005). Fibronectin regulates latent transforming growth factor-β (TGF-β) controlling matrix assembly of latent TGFβ-binding protein-1. J Biol Chem 280(19):18871-18880.

D'Amico G , Bazzi C. (2003). Pathophysiology of proteinuria. Kidney Int 63(3):809-25.

Del Valle PL, Trifillis A, Ruegg CE, Kane AS. (2002). Characterization of glucose transport by cultured rabbit kidney proximal convoluted and proximal straight tubule cells. In Vitro Cell Dev Biol Anim 38(4):218-27.

Devuyst O, Christie PT, Courtoy PJ, Beauwens R, Thakker RV. (1999). Intra-renal and subcellular distribution of the human chloride channel, CLC-5, reveals a pathophysiological basis for Dent's disease. Hum Mol Genet 8(2):247-57.

Devuyst O, Jouret F, Auzanneau C, Courtoy PJ. (2005). Chloride channels and endocytosis: new insights from Dent's disease and ClC-5 knockout mice. Nephron Physiol 99(3):p69-73.

Douglas JG. (1987). Angiotensin receptor subtypes of the kidney cortex. Am J Physiol 253(1 Pt 2):F1-7.

D'Souza-Schorey C, Chavrier P. (2006). Arf proteins: roles in membrane traffic and beyond. Nat Rev Mol Cell Biol 7(5):347-58.

Du Z, Duan Y, Yan Q, Weinstein AM, Weinbaum S, Wang T. (2004). Mechanosensory function of microvilli of the kidney proximal tubule. Proc Natl Acad Sci U S A 101(35):13068-73.

Du Z, Yan Q, Duan Y, Weinbaum S, Weinstein AM, Wang T. (2006). Axial flow modulates proximal tubule NHE3 and H-ATPase activities by changing microvillus bending moments. Am J Physiol 290(2):F289-96.

Dugina V, Fontao L, Chaponnier C, Vasiliev J, Gabbiani G. (2001). Focal adhesion features during myofibroblastic differentiation are controlled by intracellular and extracellular factors. J Cell Sci 114(Pt 18):3285-96.

Eckardt KU, Bernhardt WM, Weidemann A, Warnecke C, Rosenberger C, Wiesener MS, William C. (2005). Role of hypoxia in the pathogenesis of renal disease. Kidney Int 68(Suppl 99): S46-S51.

Eddy AA. (1996). Molecular insights into renal interstitial fibrosis. J Am Soc Nephrol 7(12):2495-508.

El Annan J, Brown D, Breton S, Bourgoin S, Ausiello DA, Marshansky V. (2004). Differential expression and targeting of endogenous Arf1 and Arf6 small GTPases in kidney epithelial cells in situ. Am J Physiol 286(4):C768-78.

Elliget KA, Trump BF. (1991). Primary cultures of normal rat kidney proximal tubule epithelial cells for studies of renal cell injury. In Vitro Cell Dev Biol 27A(9):739-48.

Eyden BP. (1993). Brief review of the fibronexus and its significance for myofibroblastic differentiation and tumor diagnosis. Ultrastruct Pathol 17(6):611-22.

Fan JM, Ng YY, Hill PA, Nikolic-Paterson DJ, Mu W, Atkins RC, Lan HY. (1999). Transforming growth factor-beta regulates tubular epithelial-myofibroblast transdifferentiation in vitro. Kidney Int 56(4):1455-67.

Figueroa CD, Gonzalez CB, Grigoriev S, Abd Alla SA, Haasemann M, Jarnagin K, Muller-Esterl W. (1995). Probing for the bradykinin B2 receptor in rat kidney by anti-peptide and anti-ligand antibodies. J Histochem Cytochem 43(2):137-48.

Fine LG, Bandyopadhay D, Norman JT. (2000). Is there a common mechanism for the progression of different types of renal diseases other than proteinuria? Towards the unifying theme of chronic hypoxia. Kidney Int 57(Suppl 75):S22-6.

Forino M, Torregrossa R, Ceol M, Murer L, Vella MD, Prete DD, D'Angelo A, Anglani F. (2006). TGFbeta1 induces epithelial-mesenchymal transition, but not myofibroblast transdifferentiation of human kidney tubular epithelial cells in primary culture. Int J Exp Pathol 87(3):197-208.

Forster IC, Hernando N, Biber J, Murer H. (2006). Proximal tubular handling of phosphate: A molecular perspective. Kidney Int 70(9):1548-59.

Frömter E. (1972). Electrophysiology and isotonic fluid absorption of proximal tubules of mammalian kidney. In: MTP International review of science, Kidney and urinary tract physiology, Physiology series one, ed. Guyton AC and Thurau K. Baltimore: Butterworths University Park Press, p.1-38.

Frömter E, Gessner K. (1974). Free-flow potential profile along rat kidney proximal tubule. 1974. Pflügers Arch 351(1):69-83.

Garza-Quintero R, Weinberg JM, Ortega-Lopez J, Davis JA, Venkatachalam A. (1993). Conservation of structure in ATP-depleted proximal tubules: role of calcium, phosphoinositides and glycine. Am J Physiol 265(34):F605-23.

Gekle M. (2001). Crosstalk between endocytosis and Na+/H+-Exchange. Kidney Blood Press Res 24: 425-7.

Gekle M, Drumm K, Mildenberger S, Freudinger R, Gassner B, Silbernagl S. (1999). Inhibition of Na+-H+ exchange impairs receptor-mediated albumin endocytosis in renal proximal tubule-derived epithelial cells from opossum. J Physiol 520 Pt 3:709-21.

Gekle M, Mildenberger S, Freudinger R, Silbernagl S. (1996). Functional characterization of albumin binding to the apical membrane of OK cells. Am J Physiol 271(2 Pt 2):F286-91.

Gekle M, Volker K, Mildenberger S, Freudinger R, Shull GE, Wiemann M. (2004). NHE3 Na+/H+ exchanger supports proximal tubular protein reabsorption in vivo. Am J Physiol 287(3):F469-73.

Goligorsky MS, Loftus DJ, Hruska KA. (1986). Cytoplasmic calcium in individual proximal tubular cells in culture. Am J Physiol 251(5 Pt 2):F938-44.

Gonzalez-Mariscal L, Namorado MC, Martin D, Luna J, Alarcon L, Islas S, Valencia L, Muriel P, Ponce L, Reyes JL. (2000). Tight junction proteins ZO-1, ZO-2, and occludin along isolated renal tubules. Kidney Int 57(6):2386-402.

Gordon LG, Kottra G, Frömter E. (1989). Electrical impedance analysis for leaky epithelia: theory, techniques and leak artifact problems. Methods Enzymol 171:642-63.

Gould SE, Day M, Jones SS, Dorai H. (2002). BMP-7 regulates chemokine, cytokine, and hemodynamic gene expression in proximal tubule cells. Kidney Int 61(1):51-60.

Grynkiewicz G, Poenie M, Tsien RY. (1985). A new generation of Ca2+ indicators with greatly improved fluorescence properties. J Biol Chem 260(6):3440-50.

Gu F, Gruenberg J. (2000). Arf1 regulates pH-dependent COP functions in the early endocytic pathway. J Biol Chem 275(11):8154-60.

Guggino SE. (2007). Mechanisms of disease: what can mouse models tell us about the molecular processes underlying Dent disease? Nat Clin Pract Nephrol 3(8):449-55.

Guo P, Weinstein AM, Weinbaum S. (2003). A dual-pathway ultrastructural model for the tight junction of rat proximal tubule epithelium. Am J Physiol 285(2):F241-57.

Halestrap AP, Price NT. (1999). The proton-linked monocarboxylate transporter (MCT) family: structure, function and regulation. Biochem J 343 Pt 2:281-99.

Handler JS, Preston AS, Steele RE. (1984). Factors affecting the differentiation of epithelial transport and responsiveness to hormones. Fed Proc 43(8):2221-4.

Hanigan MH, Gallagher BC, Townsend DM, Gabarra V. (1999). Gamma-glutamyl transpeptidase accelerates tumor growth and increases the resistance of tumors to cisplatin in vivo. Carcinogenesis 20(4):553-9.

Haverty TP, Kelly CJ, Hines WH, Amenta PS, Watanabe M, Harper RA, Kefalides NA, Neilson EG. (1988). Characterization of a renal tubular epithelial cell line which secretes the autologous target antigen of autoimmune experimental interstitial nephritis. J Cell Biol 107(4):1359-68.

He Q, Madsen M, Kilkenney A, Gregory B, Christensen EI, Vorum H, Hojrup P, Schäffer AA, Kirkness EF, Tanner SM, de la Chapelle A, Giger U, Moestrup SK, Fyfe JC. (2005). Amnionless function is required for cubilin brush-border expression and intrinsic factor-cobalamin (vitamin B12) absorption in vivo. Blood 106(4):1447-53.

Helman SI, Liu X. (1997). Substrate-dependent expression of Na+ transport and shunt conductance in A6 epithelia. Am J Physiol 273(2 Pt 1):C434-41.

Hinz B. (2006). Masters and servants of the force: the role of matrix adhesions in myofibroblast force perception and transmission. Eur J Cell Biol 85(3-4):175-81.

Hocking DC, Sottile J, Langenbach KJ. (2000). Stimulation of integrin-mediated cell contractility by fibronectin polymerization. J Biol Chem 275(14):10673-10682.

Horster MF, Braun GS, Huber SM. (1999). Embryonic renal epithelia: induction, nephrogenesis, and cell differentiation. Physiol Rev 79(4):1157-91.

Hoyer J, Gogelein H. (1991). Sodium-alanine cotransport in renal proximal tubule cells investigated by whole-cell current recording. J Gen Physiol 97(5):1073-94.

Hryciw DH, Ekberg J, Pollock CA, Poronnik P. (2006). ClC-5: a chloride channel with multiple roles in renal tubular albumin uptake. Int J Biochem Cell Biol 38(7):1036-42.

Hull RH, Cherry WR, Weaver GW. (1976). Origin and characteristics of a pig kidney cell strain LLC-PK1. In vitro 12(10):670-7.

Iwano M, Plieth D, Danoff TM, Xue C, Okada H, Neilson EG. (2002). Evidence that fibroblasts derive from epithelium during tissue fibrosis. J Clin Invest 110(3):341-50.

Jans F, Vandenabeele F, Helbert M, Lambrichts I, Ameloot M, Steels P. (2000). A simple method for obtaining functionally and morphologically intact primary cultures of the medullary thick ascending limb of Henle's loop (MTAL) from rabbit kidneys. Pflügers Arch 440(4):643-51.

Jentsch TJ. (2002). Chloride channels are different. Nature 415(6869):276-7.

Jentsch TJ. (2005). Chloride transport in the kidney: lessons from human disease and knockout mice. J Am Soc Nephrol 16(6):1549-61.

Jentsch TJ, Maritzen T, Zdebik AA. (2005). Chloride channel diseases resulting from impaired transepithelial transport or vesicular function. J Clin Invest 115(8):2039-46.

Jentsch TJ. (2007). Chloride and the endosomal-lysosomal pathway: emerging roles of CLC chloride transporters. J Physiol 578(Pt 3):633-40.

Jouret F, Igarashi T, Gofflot F, Wilson PD, Karet FE, Thakker RV, Devuyst O. (2004). Comparative ontogeny, processing, and segmental distribution of the renal chloride channel, ClC-5. Kidney Int 65(1):198-208.

Jouret F, Bernard A, Hermans C, Dom G, Terryn S, Leal T, Lebecque P, Cassiman JJ, Scholte BJ, de Jonge HR, Courtoy PJ, Devuyst O. (2007). Cystic fibrosis is associated with a defect in apical receptor-mediated endocytosis in mouse and human kidney. J Am Soc Nephrol 18(3):707-18.

Kalluri R, Neilson EG. (2003). Epithelial-mesenchymal transition and its implications for fibrosis. J Clin Invest 112(12):1776-84.

Kang DH, Kanellis J, Hugo C, Truong L, Anderson S, Kerjaschki D, Schreiner GF, Johnson RJ. (2002). Role of the microvascular endothelium in progressive renal disease. J Am Soc Nephrol 13(3):806-816.

Kim J, Kim YH, Cha JH, Tisher CC, Madsen KM. (1999). Intercalated cell subtypes in connecting tubule and cortical collecting duct of rat and mouse. J Am Soc Nephrol 10(1):1-12.

Klahr S, Morrissey J. (2000). The role of vasoactive compounds, growth factors and cytokines in the progression of renal disease. Kidney Int 57(Suppl 75):S7-14.

Klahr S, Morrissey J. (2002). Obstructive nephropathy and renal fibrosis. Am J Physiol 283(5):F861-75.

Koda M, Takemura G, Okada H, Kanoh M, Maruyama R, Esaki M, Li Y, Miyata S, Kanamori H, Li L, Ogino A, Kondo T, Minatoguchi S, Fujiwara T, Fujiwara H. (2006). Nuclear hypertrophy reflects increased biosynthetic activities in myocytes of human hypertrophic hearts. Circ J 70:710-8.

Kopp JB. (2002). BMP-7 and the proximal tubule. Kidney Int 61(1):351-2.

Koenig K. (2001). Cellular response to laser radiation in fluorescence microscopes. In: Methods in Cellular Imaging, ed. Periasamy A. Oxford, UK: Oxford University Press, p. 236-251.

Kottra G, Frömter E. (1983). Functional properties of the paracellular pathway in some leaky epithelia. J Exp Biol 106:217-29.

Kottra G, Frömter E. (1993). Tight-junction tightness of Necturus gall bladder epithelium is not regulated by cAMP or intracellular Ca2+. II. Impedance measurements. Pflügers Arch 425(5-6):535-45.

Koyama H, Goodpasture C, Miller MM, Teplitz RL, Riggs AD. (1978). Establishment and characterization of a cell line from the American opossum (Didelphys virginiana). In vitro 14(3): 239-46.

Kriz W, Bankir L. (1988). A standard nomenclature for structures of the kidney. The Renal Commission of the International Union of Physiological Sciences (IUPS). Kidney Int 33(1):1-7.

Lakowicz JR. (2006). Principles of fluorescence spectroscopy. Plenum Press, New York.

Lan HY. (2003). Tubular epithelial-myofibroblast transdifferentiation mechanisms in proximal tubule cells. Curr Opin Nephrol Hypertens 12(1):25-9.

Lapointe JY, Laprade R, Cardinal J. (1984). Transepithelial and cell membrane electrical resistances of the rabbit proximal convoluted tubule. Am J Physiol 247(4 Pt 2):F637-49.

Lash LH, Tokarz JJ. 1989. Isolation of two distinct populations of cells from rat kidney cortex and their use in the study of chemical-induced toxicity. Anal Biochem 182(2):271-9.

Lazzara MJ, Deen WM. (2007). Model of albumin reabsorption in the proximal tubule. Am J Physiol 292 (1):F430-9.

Lebeau C, Arlt VM, Schmeiser HH, Boom A, Verroust PJ, Devuyst O, Beauwens R. (2001). Aristolochic acid impedes endocytosis and induces DNA adducts in proximal tubule cells. Kidney Int 60(4):1332-42.

Lee JM, Dedhar S, Kalluri R, Thompson EW. (2006). The epithelial-mesenchymal transition: new insights in signalling, development, and disease. J Cell Biol 172(7):973-81.

Lewis SA, Clausen C, Wills NA. (1996). Impedance analysis of epithelia. In: Epithelial transport, ed. Wills NK, Reuss L & Lewis SA. London: Chapman & Hall, p. 118-145.

Lindemann B. (2001). Hans Ussing, experiments and models. J Membr Biol 184(3):203-10.

Liu Y. (2004). Epithelial to mesenchymal transition in renal fibrogenesis: pathologic significance, molecular mechanism, and therapeutic intervention. J Am Soc Nephrol 15(1):1-12.

Lo CM, Keese CR, Giaever I. (1999). Cell-substrate contact: another factor may influence transepithelial electrical resistance of cell layers cultured on permeable filters. Exp Cell Res 250(2):576-80.

Loffing J, Loffing-Cueni D, Valderrabano V, Klausli L, Hebert SC, Rossier BC, Hoenderop JG, Bindels RJ, Kaissling B. (2001). Distribution of transcellular calcium and sodium transport pathways along mouse distal nephron. Am J Physiol 281(6):F1021-7.

Loffing J, Vallon V, Loffing-Cueni D, Aregger F, Richter K, Pietri L, Bloch-Faure M, Hoenderop JG, Shull GE, Meneton P et al. (2004). Altered renal distal tubule structure and renal Na(+) and Ca(2+) handling in a mouse model for Gitelman's syndrome. J Am Soc Nephrol 15(9):2276-88.

Lodish H, Baltimore D, Berk A, Zipursky SL, Matsudaira P, Darnell J. (1995). Microtubules and intermediate filaments. In: Molecular cell biology, ed. Lodish et al. New York: Scientific American Books Inc., p.1051-1122.

Loo DDF, Hirayama BA, Meinild AK, Chandy G, Zeuthen A, Wright EM. (1999). Passive water and ion transport by cotransporters. J Physiol 518(1):195-202.

Loo DDF, Zeuthen T, Chandy G, Wright EM. (1996). Cotransport of water by the Na+/glucose cotransporter. Proc Natl Acad Sci USA 93(23): 13367-13370.

Lotscher M, Scarpetta Y, Levi M, Halaihel N, Wang H, Zajicek HK, Biber J, Murer H, Kaissling B. (1999). Rapid downregulation of rat renal Na/P(i) cotransporter in response to parathyroid hormone involves microtubule rearrangement. J Clin Invest 104(4):483-94.

Madara JL. (1998). Regulation of the movement of solutes across tight junctions. Annu Rev Physiol 60:143-59.

Mandel LJ. (1985). Metabolic substrates, cellular energy production, and the regulation of proximal tubular transport. Annu Rev Physiol 47:85-101.

Markovich D, Aronson PS. (2007). Specificity and regulation of renal sulfate transporters. Annu Rev Physiol 69:361-75.

Marshansky V, Bourgoin S, Londono I, Bendayan M, Maranda B, Vinay P. (1997). Receptor-mediated endocytosis in kidney proximal tubules: recent advances and hypothesis. Electrophoresis 18(14):2661-76.

Maude DL. (1972). Mechanisms of tubular transport of salt and water. In: MTP International review of science, Kidney and urinary tract physiology, Physiology series one, ed. Guyton AC and Thurau K. Baltimore: Butterworths University Park Press, p.39-78.

Maunsbach AB, Boulpaep EL. (1984). Quantitative ultrastructure and functional correlates in proximal tubule of Ambystoma and Necturus. Am J Physiol 246(5 Pt 2):F710-24.

Maunsbach AB, Giebisch GH, Stanton BA. (1987a). Effects of flow rate on proximal tubule ultrastructure. Am J Physiol 253(3 Pt 2):F582-7.

Maunsbach AB, Tripathi S, Boulpaep EL. (1987b). Ultrastructural changes in isolated perfused proximal tubules during osmotic water flow. Am J Physiol 253(6 Pt 2):F1091-104.

Maunsbach A, Christensen E. (1992). Functional ultrastructure of the proximal tubule. In: Handbook of Physiology, Renal Physiology, ed. Windhager EE. New York: Oxford University Press, p. 41-107.

Meneton P, Ichikawa I, Inagami T, Schnermann J. (2000). Renal physiology of the mouse. Am J Physiol 278(3):F339-51.

Mitic LL, Anderson JM. (1998). Molecular architecture of tight junctions. Annu Rev Physiol 60:121-42.

Miyata N, Park F, Li XF, Cowley AW Jr. (1999). Distribution of angiotensin AT1 and AT2 receptor subtypes in the rat kidney. Am J Physiol 277(3 Pt 2):F437-46.

Moret C, Dave MH, Schulz N, Jiang JX, Verrey F, Wagner CA. (2007). Regulation of renal amino acid transporters during metabolic acidosis. Am J Physiol 292(2):F555-66.

Moschen I, Setiawan I, Broer S, Murer H, Lang F. (2001). Effect of NaPi-mediated phosphate transport on intracellular pH. Pflügers Arch 441(6):802-6.

Moscher DF. (2001). A role for fibronectin in self-repair after ischemic injury. Nat Med 7(3):324-330.

Moser M, Dahmen S, Kluge R, Gröne H, Dahmen J, Kunz D, Schorle H, Buettner R. (2003). Terminal renal failure in mice lacking transcription factor AP-2β. Lab Invest 83(4):571-8.

Murer H, Hernando N, Forster I, Biber J. (2003). Regulation of Na/Pi transporter in the proximal tubule. Annu Rev Physiol 65:531-42.

Murer H, Kohler K, Lambert G, Stange G, Biber J, Forster I. (2002). The renal type IIa Na/Pi cotransporter: structure-function relationships. Cell Biochem Biophys 36(2-3):215-20.

Murer H, Sigrist-Nelson K, Hopfer U. (1975). On the mechanism of sugar and amino acid interaction in intestinal transport. J Biol Chem 250(18):7392-6.

Nakajima H, Takenaka M, Kaimori JY, Hamano T, Iwatani H, Sugaya T, Ito T, Hori M, Imai E. (2004). Activation of the signal transducer and activator of transcription signalling pathway in renal proximal tubular cells by albumin. J Am Soc Nephrol 15(2):276-85.

Nakhoul NL, Hamm LL. (2002). Vacuolar H(+)-ATPase in the kidney. J Nephrol 15 (S5):S22-31.

Nangaku M. (2007). The heat is on: an expanding role for hypoxia-inducible factors in kidney transplantation. J Am Soc Nephrol 18(1):13-5.

Neilson EG. (2005). Setting a trap for tissue fibrosis. Nat Med 11(4):373-4.

Neilson EG. (2006). Mechanisms of disease: fibroblasts – a new look at an old problem. Nat Clin Pract Nephrol 2(2):101-8.

Ng YY, Huang TP, Yang WC, Chen ZP, Yang AH, Mu W, Nikolic-Paterson DJ, Atkins RC, Lan HY. (1998). Tubular epithelial-myofibroblast transdifferentiation in progressive tubulointerstitial fibrosis in 5/6 nephrectomized rats. Kidney Int 54(3):864-76.

Norden AG, Lapsley M, Igarashi T, Kelleher CL, Lee PJ, Matsuyama T, Scheinman SJ, Shiraga H, Sundin DP, Thakker RV et al. (2002). Urinary megalin deficiency implicates abnormal tubular endocytic function in Fanconi syndrome. J Am Soc Nephrol 13(1):125-33.

Nouwen EJ, De Broe ME. (1994). Human intestinal versus tissue-nonspecific alkaline phosphatase as complementary urinary markers for the proximal tubule. Kidney Int Suppl 47:S43-51.

Nowak G, Griffin JM, Schnellmann RG. (1996). Hypoxia and proliferation are primarily responsible for induction of lactate dehydrogenase activity in cultured cells. J Toxicol Environ Health 49(4):439-52.

O'Donnell MP. (2000). Renal tubulointerstitial fibrosis: New thoughts on its development and progression. Postgrad Med 108(1):159-72.

Pan C, Bai X, Fan L, Ji Y, Li X, Chen Q. (2005). Cytoprotection by glycine against ATP-depletion-induced injury is mediated by glycine receptor in renal cells. Biochem J 390(2):447-53.

Pan J, Wang Q, Snell WJ. (2005). Cilium-generated signaling and cilia-related disorders. Lab Invest 85(4):452-63.

Paolicchi A, Sotiropuolou M, Perego P, Daubeuf S, Visvikis A, Lorenzini E, Franzini M, Romiti N, Chieli E, Leone R et al. (2003). gamma-Glutamyl transpeptidase catalyses the extracellular detoxification of cisplatin in a human cell line derived from the proximal convoluted tubule of the kidney. Eur J Cancer 39(7):996-1003.

Park CH, Maack T. (1984). Albumin absorption and catabolism by isolated perfused proximal convoluted tubules of the rabbit. J Clin Invest 73(3):767-77.

Patschan D, Michurina T, Shi HK, Dolff S, Brodsky SV, Vasilieva T, Cohen-Gould L, Winaver J, Chander PN, Enikolopov G et al. (2007). Normal distribution and medullary-to-cortical shift of Nestin-expressing cells in acute renal ischemia. Kidney Int 71(8):744-54.

Phanish MK, Wahab NA, Colville-Nash P, Hendry BM, Dockrell ME. (2006). The differential role of Smad2 and Smad3 in the regulation of pro-fibrotic TGFbeta1 responses in human proximal-tubule epithelial cells. Biochem J 393(Pt 2):601-7.

Pollock CA, Poronnik P. (2007). Albumin transport and processing by the proximal tubule: physiology and pathophysiology. Curr Opin Nephrol Hypertens 16(4):359-64.

Pontoglio M. (2000). Hepatocyte nuclear factor 1, a transcription factor at the crossroads of glucose homeostasis. J Am Soc Nephrol 11(S16):S140-3.

Powell DW, Mifflin RC, Valentich JD, Crowe SE, Saada JI, West AB. (1999). Myofibroblasts. I. Paracrine cells important in health and disease. Am J Physiol 277(1 Pt 1):C1-9.

Praetorius HA, Spring KR. (2005). A physiological view of the primary cilium. Annu Rev Physiol 67:515-29.

Preisig PA, Ives HE, Cragoe EJ Jr, Alpern RJ, Rector FC Jr. (1987). Role of the Na+/H+ antiporter in rat proximal tubule bicarbonate absorption. J Clin Invest 80(4):970-8.

Preisig PA, Rector FC Jr. (1988). Role of Na+-H+ antiport in rat proximal tubule NaCl absorption. Am J Physiol 255(3 Pt 2):F461-5.

QI W, Chen X, Holian J, Mreich E, Twigg S, Gilbert RE, Pollock CA. (2006). Transforming growth factor-beta1 differentially mediates fibronectin and inflammatory cytokine expression in kidney tubular cells. Am J Physiol 291(5): F1070-7.

Remuzzi G, Bertani T. (1998). Pathophysiology of progressive nephropathies. N Engl J Med 339(20):1448-56.

Reuss L. (2001). Ussing's two-membrane hypothesis: the model and half a century of progress. J Membr Biol 184(3):211-7.

Rhyu DY, Yang Y, Ha H, Lee GT, Song JS, Uh ST, Lee HB. (2005). Role of reactive oxygen species in TGF-beta1-induced mitogen-activated protein kinase activation and epithelial-mesenchymal transition in renal tubular epithelial cells. J Am Soc Nephrol 16(3):667-75.

Rodeheaver DP, Aleo MD, Schnellmann RG. (1990). Differences in enzymatic and mechanical isolated rabbit renal proximal tubules: comparison in long-term incubation. In Vitro Cell Dev Biol 26(9):898-904.

Romero MF, Hopfer U, Madhun ZT, Zhou W, Douglas JG. (1991). Angiotensin II actions in the rabbit proximal tubule. Angiotensin II mediated signaling mechanisms and electrolyte transport in the rabbit proximal tubule. Ren Physiol Biochem 14(4-5):199-207.

Rosenberg MR, Michalopoulos G. (1987). Kidney proximal tubular cells isolated by collagenase perfusion grow in defined media in the absence of growth factors. J Cell Physiol 131(1):107-13.

Ryan MJ, Johnson G, Kirk J, Fuestenberg SM, Zager RA, Torok-Storb B. (1994). HK-2: An immortalized proximal tubule epithelial cell line from normal adult human kidney. Kidney Int 45(1):48-57.

Sackin H, Boulpaep EL. (1975). Models for coupling of salt and water transport; Proximal tubular reabsorption in Necturus kidney. J Gen Physiol 66(6):671-733.

Sahai A, Mei C, Zavosh A, Tannen RL. (1997). Chronic hypoxia induces LLC-PK1 cell proliferation and dedifferentiation by activation of protein kinase C. Am J Physiol 272(6pt2):F809-15.

Sahai A, Mei C, Schrier RW, Tannen RL. (1999). Mechanisms of chronic hypoxia-induced renal cell growth. Kidney Int 56(4):1277-81.

Sakairi T, Hiromura K, Yamashita S, Takeuchi S, Tomioka M, Ideura H, Maeshima A, Kaneko Y, Kuroiwa T, Nangaku M et al. (2007). Nestin expression in the kidney with an obstructed ureter. Kidney Int 11: epub ahead of print.

Sakamoto H, Sado Y, Naito I, Kwon TH, Inoue S, Endo K, Kawasaki M, Uchida S, Nielsen S, Sasaki S et al. (1999). Cellular and subcellular immunolocalization of ClC-5 channel in mouse kidney: colocalization with H+-ATPase. Am J Physiol 277(6 Pt 2):F957-65.

Sakhrani LM, Badie-Dezfooly B, Trizna W, Mikhail N, Lowe AG, Taub M, Fine LG. (1984). Transport and metabolism of glucose by renal proximal tubular cells in primary culture. Am J Physiol 246(6 Pt 2):F757-64.

Schaaf GJ, de Groene EM, Maas RF, Commandeur JN, Fink-Gremmels J. (2001). Characterization of biotransformation enzyme activities in primary rat proximal tubular cells. Chem Biol Interact 134(2):167-90.

Scheel O, Zdebik AA, Lourdel S, Jentsch TJ. (2005). Voltage-dependent electrogenic chloride/proton exchange by endosomal CLC proteins. Nature 436(7049):424-7.

Schmidt-Ott KM, Lan D, Hirsh BJ, Barasch J. (2006). Dissecting stages of mesenchymal-to-epithelial conversion during kidney development. Nephron Physiol 104(1):p56-60.

Schmitz PG. (2000). Progressive renal insufficiency: Office strategies to prevent or slow progression of kidney disease. Postgrad Med 108(1):145-54.

Schnaper HW, Hayashida T, Hubchak SC, Poncelet AC. (2003). TGF-beta signal transduction and mesangial cell fibrogenesis. Am J Physiol 284(2):F243-52.

Schneeberger EE, Lynch RD. (2004). The tight junction: a multifunctional complex. Am J Physiol 286(6):C1213-28.

Schwegler JS, Heppelmann B, Mildenberger S, Silbernagl S. (1991). Receptor-mediated endocytosis of albumin in cultured opossum kidney cells: a model for proximal tubular protein reabsorption. Pflügers Arch 418(4):383-92.

Shayakul C, Kanai Y, Lee WS, Brown D, Rothstein JD, Hediger MA. (1997). Localization of the high-affinity glutamate transporter EAAC1 in rat kidney. Am J Physiol 273(6 Pt 2):F1023-9.

Sheridan AM, Schwartz JH, Kroshian VM, Tercyak AM, Laraia J, Masino S, Lieberthal W. (1993). Renal mouse proximal tubular cells are more susceptible than MDCK cells to chemical anoxia. Am J Physiol 265(3 Pt 2):F342-50.

Shivakumar BR, Wang Z, Hammond TG, Harris RC. (2005). EP24.15 interacts with the angiotensin II type I receptor and bradykinin B2 receptor. Cell Biochem Funct 23(3):195-204.

Silbernagl S. (1988). The renal handling of amino acids and oligopeptides. Physiol Rev 68(3):911-1007.

Simmons NL. (1992). Acetylcholine and kinin augmentation of Cl- secretion stimulated by prostaglandin in a canine renal epithelial cell line. J Physiol 447:1-15.

Singh AB, Harris RC. (2004). Epidermal growth factor receptor activation differentially regulates claudin expression and enhances transepithelial resistance in Madin-Darby canine kidney cells. J Biol Chem 279(5):3543-52.

Spring KR. (1998). Routes and mechanism of fluid transport by epithelia. Annu Rev Physiol 60:105-19.

Spring KR, Hope A. (1979). Fluid transport and the dimensions of cells and interspaces of living Necturus gallbladder. J Gen Physiol 73(3):287-305.

Srinivas SR, Gopal E, Zhuang L, Itagaki S, Martin PM, Fei YJ, Ganapathy V, Prasad PD. (2005). Cloning and functional identification of slc5a12 as a sodium-coupled low-affinity transporter for monocarboxylates (SMCT2). Biochem J 392(Pt 3):655-64.

Steinmeyer K, Schwappach B, Bens M, Vandewalle A, Jentsch TJ. (1995). Cloning and functional expression of rat CLC-5, a chloride channel related to kidney disease. J Biol Chem 270(52):31172-7.

Suzuki M, Kawaguchi Y, Kurihara S, Miyahara T. (1989). Heterogeneous response of cytoplasmic free Ca2+ in proximal convoluted and straight tubule cells in primary culture. Am J Physiol 257(5 Pt 2):F724-31.

Szasz G. (1969). A kinetic photometric method for serum gamma-glutamyl transpeptidase. Clin Chem 15(2):124-36.

Tanako M, Nakanishi N, Kitahara Y, Sasaki Y, Murakami T, Nagai J. (2002). Cisplatin-induced inhibition of receptor-mediated endocytosis of protein in the kidney. Kidney Int 62(5):1707-17.

Tanner C, Frambach DA, Misfeldt DS. (1984). Biophysics of domes formed by the renal cell line Madin-Darby canine kidney. Fed Proc 43(8):2217-20.

Taub ML, Yang IS, Wang Y. (1989). Primary rabbit kidney proximal tubule cell cultures maintain differentiated functions when cultured in a hormonally defined serum- free medium. In Vitro Cell Dev Biol 25(9):770-5.

Teng Y, Zeisberg M, Kalluri R. (2007). Transcriptional regulation of epithelial-mesenchymal transition. J Clin Invest 117(2):304-6.

Tian YC, Fraser D, Attisano L, Phillips AO. (2003). TGF-beta1-mediated alterations of renal proximal tubular epithelial cell phenotype. Am J Physiol 285(1):F130-42.

Tian YC, Phillips AO. (2002). Interaction between the transforming growth factor-beta type II receptor/Smad pathway and beta-catenin during transforming growth factor-beta1-mediated adherens junction disassembly. Am J Pathol 160(5):1619-28.

Tiwari MM, Prather PL, Mayeux PR. (2005). Mechanism of bradykinin-induced Ca2+ mobilization in murine proximal tubule epithelial cells. J Pharmacol Exp Ther 313(2):798-805.

Tiwari MM, Stimers JR, Mayeux PR. (2007). Bradykinin-induced chloride conductance in murine proximal tubule epithelial cells. Mol Cell Biochem 297(1-2):1-8.

Ullrich KJ. (1979). Sugar, amino acid, and Na+ cotransport in the proximal tubule. Annu Rev Physiol 41:181-95.

Vallon V, Grahammer F, Richter K, Bleich M, Lang F, Barhanin J, Volkl H, Warth R. (2001). Role of KCNE1-dependent K+ fluxes in mouse proximal tubule. J Am Soc Nephrol 12(10):2003-11.

Van den Bergh V, Boens N, De Schryver FC, Ameloot M, Steels P, Gallay J, Vincent M, Kowalczyk A. (1995). Photophysics of the fluorescent Ca2+ indicator Fura-2. Biophys J 68(3):1110-9.

Van der Biest I , Nouwen EJ, Van Dromme SA, De Broe ME. (1994). Characterization of pure proximal and heterogeneous distal human tubular cells in culture. Kidney Int 45(1):85-94.

Van Driessche W, De Vos R, Jans D, Simaels J, De Smet P, Raskin G. (1999). Transepithelial capacitance decrease reveals closure of lateral intercellular space in A6 epithelia. Pflügers Arch 437(5):680-90.

Van Itallie CM, Anderson JM. (2004). The molecular physiology of tight junction pores. Physiology (Bethesda) 19:331-8.

Van Itallie CM, Anderson JM. (2006). Claudins and epithelial paracellular transport. Annu Rev Physiol 68:403-29.

Venkov CD, Link AJ, Jennings JL, Plieth D, Inoue T, Nagai K, Xu C, Dimitrova YN, Rauscher FJ, Neilson EG. (2007). A proximal activator of transcription in epithelial-mesenchymal transition. J Clin Invest 117(2):482-91.

Verrey F, Ristic Z, Romeo E, Ramadan T, Makrides V, Dave MH, Wagner CA, Camargo SM. (2005). Novel renal amino acid transporters. Annu Rev Physiol 67:557-72.

Vinay P, Gougoux A, Lemieux G. (1981). Isolation of a pure suspension of rat proximal tubules. Am J Physiol 241(4):F403-11.

Vukicevic S, Kopp JB, Luyten FP, Sampath TK. (1996). Induction of nephrogenic mesenchyme by osteogenic protein 1 (bone morphogenetic protein 7). Proc Natl Acad Sci USA 93: 9021-6.

Wagner CA, Finberg KE, Breton S, Marshansky V, Brown D, Geibel JP. (2004). Renal vacuolar H+-ATPase. Physiol Rev 84(4):1263-314.

Wagner CA, Lukewille U, Valles P, Breton S, Brown D, Giebisch GH, Geibel JP. (2003). A rapid enzymatic method for the isolation of defined kidney tubule fragments from mouse. Pflügers Arch 446(5):623-32.

Walter K, Schütt C. (1974). Acid and alkaline phosphatase in serum (two point method). In: Methods of enzymatic analysis, ed. Bergmeyer HU. New York: Academic, p. 856-64.

Wang AZ, Ojakian GK, Nelson WJ. (1990). Steps in the morphogenesis of a polarized epithelium. I. Uncoupling the roles of cell-cell and cell-substratum contact in establishing plasma membrane polarity in multicellular epithelial (MDCK) cysts. J Cell Sci 95(1):137-51.

Wang R, Clark RAF, Mosher DF, Ren XD. (2005). Fibronectin's central cell-binding domain supports focal adhesion formation and Rho signal transduction. J Biol Chem 280(31):28803-28810.

Wang SS, Devuyst O, Courtoy PJ, Wang XT, Wang H, Wang Y, Thakker RV, Guggino S, Guggino WB. (2000). Mice lacking renal chloride channel, CLC-5, are a model for Dent's disease, a nephrolithiasis disorder associated with defective receptor-mediated endocytosis. Hum Mol Genet 9(20):2937-45.

Wang Y, Cai H, Cebotaru L, Hryciw DH, Weinman EJ, Donowitz M, Guggino SE, Guggino WB. (2005). ClC-5: role in endocytosis in the proximal tubule. Am J Physiol 289(4):F850-62.

Weinberg JM, Venkatachalam MA, Garzo-Quintero R, Roeser NF, Davis JA. (1990). Structural requirements for protection by small amino acids against hypoxic injury in kidney proximal tubules. FASEB J 4(15):3347-54.

Weinstein AM, Weinbaum S, Duan Y, Du Z, Yan Q, Wang T. (2007). Flow-dependent transport in a mathematical model of rat proximal tubule. Am J Physiol 292(4):F1164-81.

Weinstein AM. (2000). Chapter 49: Sodium and Chloride transport: Proximal nephron. In: The kidney: Physiology and Pathophysiology, ed. Seldin DW & Giebisch G. Philadelphia: Lippincott Williams & Wilkins, p. 1287-1331.

Welbourne TC, Matthews JC. (1999). Glutamate transport and renal function. Am J Physiol 277(4 Pt 2):F501-5.

Welling LW, Welling DJ. (1975). Surface areas of brush border and lateral cell walls in the rabbit proximal nephron. Kidney Int 8(6):343-8.

Welling LW, Welling DJ. (1988). Relationship between structure and function in renal proximal tubule. J Electron Microsc Tech 9(2):171-85.

Welling LW, Welling DJ, Holsapple JW, Evan AP. (1987). Morphometric analysis of distinct microanatomy near the base of proximal tubule cells. Am J Physiol 253(1 Pt 2):F126-40.

Welsh C, Dubyak G, Douglas JG. (1988). Relationship between phospholipase C activation and prostaglandin E2 and cyclic adenosine monophosphate production in rabbit tubular epithelial cells. Effects of angiotensin, bradykinin, and arginine vasopressin. J Clin Invest 81(3):710-9.

Witzgall R. (1999). The proximal tubule phenotype and its disruption in acute renal failure and polycystic kidney disease. Exp Nephrol 7(1):15-9.

Wolf G, Wenzel U, Burns KD, Harris RC, Stahl RAK, Thaiss F. (2002). Angiotensin II activates nuclear transcription factor-κB through AT1 and AT2 receptors. Kidney Int 61(6):1986-95.

Wood IS, Trayhurn P. (2003). Glucose transporters (GLUT and SGLT): expanded families of sugar transport proteins. Br J Nutr 89(1):3-9.

Wright EM. (2001). Renal Na(+)-glucose cotransporters. Am J Physiol 280(1):F10-8.

Yang J, Liu Y. (2001). Dissection of key events in tubular epithelial to myofibroblast transition and its implications in renal interstitial fibrosis. Am J Pathol 159(4):1465-75.

Zeisberg M, Bottiglio C, Kumar N, Maeshima Y, Strutz F, Muller GA, Kalluri R. (2003) Bone morphogenic protein-7 inhibits progression of chronic renal fibrosis associated with two genetic mouse models. Am J Physiol 285(6):F1060-7.

Zeisberg M, Hanai JI, Sugimoto H, Mammoto T, Charytan D, Strutz F, Kalluri R. (2003). BMP-7 counteracts TGF-β1-induced epithelial-to-mesenchymal transition and reverses chronic renal injury. Nat Med 9(7):964-8.

Zeisberg M, Shah AA, Kalluri R. (2005). Bone morphogenic protein-7 induces mesenchymal to epithelial transition in adult renal fibroblasts and facilitates regeneration of injured kidney. J Biol Chem 280(9):8094-8100.

Zellin G, Linde A. (1996). Effects of different osteopromotive membrane porosities on experimental bone neogenesis in rats. Biomaterials 17(7):695-702.

Zhai XY, Birn H, Jensen KB, Thomsen JS, Andreasen A, Christensen EI. (2003). Digital three-dimensional reconstruction and ultrastructure of the mouse proximal tubule. J Am Soc Nephrol 14(3):611-9.

Zhai XY, Nielsen R, Birn H, Drumm K, Mildenberger S, Freudinger R, Moestrup SK, Verroust PJ, Christensen EI, Gekle M. (2000). Cubilin- and megalin-mediated uptake of albumin in cultured proximal tubule cells of opossum kidney. Kidney Int 58(4):1523-33.

Zhang XL, Selbi W, de la Motte C, Hascall V, Phillips AO. (2005). Bone morphogenic protein-7 inhibits monocyte-stimulated TGF-β1 generation in renal proximal tubular epithelial cells. J Am Soc Nephrol 16(1):79-89.

Curriculum vitae

Curriculum vitae

Sara Terryn was born on the 7th of December, 1978 in Hasselt (Belgium). From 1990 to 1993, she attended the secondary grade school (Latin-Mathematics) in the Sinter-Pieters college in Beringen and from 1993 to 1996, in Mariaburcht in Stevoort (Sport-Sciences). Between 1996 and 2000 she studied at the Faculty of Medicine at the Vrije Universiteit Brussel (Belgium). In June 2000, she graduated as Master ("Licentiaat") in the Biomedical Sciences. In September 2000, she joined the group of Cell Physiology at the Universiteit Hasselt where she taught Physiology at the Faculty of Medecine and performed the research described in this thesis.

Publications in International Journals

Darville MI, **Terryn S**, Eizirik DL. (2004). An octamer motif is required for activation of the inducible nitric oxide synthase promoter in pancreatic beta-cells. Endocrinology 145(3):1130-6.

Jouret F, Bernard A, Hermans C, Dom G, **Terryn S**, Leal T, Lebecque P, Cassiman JJ, Scholte BJ, de Jonge HR, Courtoy PJ, Devuyst O. (2007). Cystic fibrosis is associated with a defect in apical receptor-mediated endocytosis in mouse and human kidney. J Am Soc Nephrol 18(3):707-18.

Ahrabi AK, **Terryn S**, Valenti G, Caron N, Serradeil-Le Gal C, Raufaste D, Nielsen S, Horie S, Verbavatz JM, Devuyst O. (2007). PKD1 Haploinsufficiency Causes a Syndrome of Inappropriate Antidiuresis in Mice. J Am Soc Nephrol 18(6):1740-53.

Terryn S, Jouret F, Vandenabeele F, Smolders I, Moreels M, Devuyst O, Steels P, Van Kerkhove E. (2007). A Primary culture of mouse proximal tubular cells, established on collagen-coated membranes. Am J Physiol 293(2):F476-85.

Terryn S, Vandenabeele F, Steels P, Van Kerkhove E. Mouse proximal tubule cells in primary culture transdifferentiate in α-SMA$^+$ myofibroblasts after exposure to TGF-β1. *In preparation*

Terryn S, Van Driessche W, Steels P, Van Kerkhove E. Electrophysiological properties of mouse proximal tubule cells in primary culture. *In preparation*

Poster presentations

Terryn S, Vandenabeele F, Steels P, Van Kerkhove E. (2002).
A simple method to obtain a primary culture of highly differentiated mouse proximal tubular cells grown on collagen-coated membranes.
Belgisch genootschap voor de fundamentele en Klinische Fysiologie en Farmacologie, 16.11.2002 UZ Gent (Belgium).
Eur J Physiol – Pflügers Archiv 2003;445:R1-R8.

Vandenabeele F, **Terryn S**, Moreels M, Steels P, Van Kerkhove E (presented by Terryn S). (2002).
Transforming growth factor beta induces myofibroblast transdifferentiation in (cultured) mouse proximal tubules epithelial cells.
Belgisch genootschap voor de fundamentele en Klinische Fysiologie en Farmacologie, 16.11.2002 UZ Gent (Belgium).
Eur J Phys – Pflügers Archiv 2003;445:R1-R8.

Terryn S, Vandenabeele F, Moreels M, Steels P, Van Kerkhove E. (2003)
Proximal tubule cells in primary culture, a model to study chronic cadmium exposure and interstitial fibrosis. Transdifferentiation to myofibroblasts occurs in the presence of TGF-β_1.
World Congress of Nephrology, 8 – 12.06.03, Berlin (Germany).
Nephol Dial Transplant 2003;18(S4):A16-W201.

Van Kerkhove E, **Terryn S**, Vandenabeele F, Smolders I, Moreels M, Steels P (presented by Terryn S). (2004).
Mouse proximal tubular cells in primary culture transdifferentiate into α-SMA$^+$ myofibroblasts after exposure to TGF-β_1.
Experimental biology meeting 2004 of the FASEB, 17 - 21.04.04, Washington DC (USA).
FASEB J 2004;18(4):A1322.

Terryn S, Jouret F, Vandenabeele F, Smolders I, Moreels M, Devuyst O, Steels P, Van Kerkhove E. (2005).
A primary culture of mouse proximal tubule cells, established on collagen-coated membranes.
4th International Conference on Aquaporins, 10 - 13.09.05, Genval (Belgium).

Terryn S, Jouret F, Vandenabeele F, Smolders I, Moreels M, Devuyst O, Steels P, Van Kerkhove E. (2006).
A primary culture of mouse proximal tubule cells, established on collagen-coated membranes.
The 43rd congress of the European renal association (ERA-EDTA), 15 - 18.07.06, Glasgow (UK).
Nephrol Dial Transplant 21(7);S4:iv 59-SP132.

Oral Presentation

Van Kerkhove E, **Terryn S**, Vandenabeele F, Smolders I, Moreels M, Steels P. (2004).
Mouse proximal tubular cells in primary culture transdifferentiate into α-SMA$^+$ myofibroblasts after exposure to TGF-β_1.
Experimental biology meeting 2004 of the FASEB, 17 - 21.04.04, Washington DC (USA).

Terryn S, Vandenabeele F, Smolders I, Moreels M, Steels P, Van Kerkhove E. (2004).
Mouse proximal tubular cells in primary culture transdifferentiate into α-SMA$^+$ myofibroblasts after exposure to TGF-β_1.
Belgisch genootschap voor de fundamentele en Klinische Fysiologie en Farmacologie, 08.05.04, UZ Gent (Belgium).

Terryn S, Jouret F, Vandenabeele F, Smolders I, Moreels M, Devuyst O, Steels P, Van Kerkhove E. (2007).
A primary culture of mouse proximal tubule cells, established on collagen-coated membranes.
Leiden International Medical Student Conference, 15 - 17.03.07, LUMC Leiden (Nederland).

Awards

Terryn S, Jouret F, Vandenabeele F, Smolders I, Moreels M, Devuyst O, Steels P, Van Kerkhove E. (2005).
A primary culture of mouse proximal tubule cells, established on collagen-coated membranes. 4th International Conference on Aquaporins, 10 - 13.09.05, Genval (Belgium).

Young investigator award

Terryn S, Jouret F, Vandenabeele F, Smolders I, Moreels M, Devuyst O, Steels P, Van Kerkhove E. (2006).
A primary culture of mouse proximal tubule cells, established on collagen-coated membranes. The 43rd congress of the European renal association (ERA-EDTA), 15 - 18.07.06, Glasgow (UK).

Award for best poster presentation

Dankwoord

Het lijkt alsof het gisteren was...7 jaren geleden werd ik 's middags op sollicitatiegesprek in Diepenbeek verwacht en 's avonds kreeg ik al telefoon van Prof. Steels dat ik mocht beginnen. Nu ik erover nadenk, de afgelopen 7 jaren zijn bijna even snel gegaan. Van de vele dingen die ik geleerd, ervaren en beleefd heb, is er eentje dat er uitspringt: een thesis maken doe je niet zonder de hulp van vele anderen. Daarom dat ik nu op het eind van de rit, eventjes wil stil staan en de tijd nemen om een woordje van dank te zeggen.

Emmy, als promoter van het project, wil ik je vooreerst bedanken voor de kansen die je me gaf om te groeien als onderzoeker en om mij de mogelijkheden te bieden om mijn doctoraatsthesis te maken tot wat het nu geworden is. Ik heb niet alleen mogen proeven van het onderzoek in het labo celfysiologie, maar je gaf me ook de unieke kans om een stage te doen in het labo van Prof. Catherine Jumarie in Montreal. Ik liep net niet meer verloren op de UHasselt en ik mocht al naar het buitenland. Ik moet je eerlijk bekennen, ik stond wel een beetje perplex.

Als onderwijsassistent werd ik ook ingewijd in het lesgeven. Prof. Steels, bedankt voor de vele uurtjes die je spendeerde om mij de kneepjes van het doceren bij te brengen. Ik bewonder je kennis van de wondere wereld van de (nier)fysiologie en ik ben je zeer dankbaar dat je deze wilde delen met mij. Als copromoter van deze thesis, dank ik je ook voor het grondige naleeswerk en leerzame inbreng tijdens mijn gehele doctoraat.

Marcel, hoewel je niet rechtstreeks betrokken was met mijn thesis, wil ik je bedanken voor alle hulp bij de fluorescentie metingen op de Nikon en de confocale. Het gedacht dat ik op jou en Martin kon rekenen als er (weer) iets dreigde mis te gaan tijdens de metingen, was goud waard. Martin, ook jij bedankt voor alle technische hulp bij de fluorescentie metingen.

Tijdens mijn zoektocht naar de karakteristieken van de proximale tubulus kwam ik tot de vaststelling, dat er slechts heel weinig gepubliceerd was over de elektrofysiologische kenmerken van dit epitheel. Ondertussen heb ik achterhaald waarom: Elektrische metingen doen op een lek epitheel loopt helemaal niet van

een leien dakje. Gelukkig kon ik op de deskundige hulp van Prof. Van Driessche en Danny rekenen. Prof. Van Driessche, jouw vaardige ontwerpen van de Ussing kamer en de meetopstellingen hebben mij in staat gesteld de stromen, weerstanden en capaciteiten in deze cellen te bestuderen. Het verbaast me nog steeds hoe je tussen Kerst en Nieuwjaar, zomaar eventjes, een volledig nieuwe kamer ontwierp, helemaal aangepast aan de noden van deze culturen. Hartelijk dank om steeds weer klaar te staan met raad en daad en mij de microbe van de elektrofysiologie door te geven. Zonder jou en Danny zouden er heel wat meer "kortsluitingen (in mijn hoofd dan vooral)" zijn ontstaan!

Je voudrai remercier Prof. Devuyst pour son aimable et efficace collaboration. En effet, j'ai beaucoup apprécié votre aide et la latitude que vous m'avez laissée pour pratiquer mes expérimentations. En outre il suffisait d'un simple e-mail ou d'un bref coup de téléphone pour obtenir de votre part une entière disponibilité. J'espère que nous pourrons prolonger cette fructueuse association.

Op een wetenschappelijke bijeenkomst vroeg een spreker aan de zaal wat de drie peilers zijn van goed onderzoek. Hoewel het niet meteen geraden werd, was iedereen er van overtuigd dat communicatie gaande van wetenschappelijke publicaties tot collegiale aan-de-koffietafel-besprekingen, een belangrijke bijdrage leverde tot goed onderzoek. En inderdaad moet ik bekennen dat de gezellige sfeer en fijne werkomgeving zeker hebben bijgedragen tot deze thesis. Voor allerhande technische snufjes kon ik steeds rekenen op Patrick en Roland, bedankt hiervoor. Jo, zonder jou waren er zeker niet genoeg muisjes (gesneuveld) geweest om dit doctoraat te voltooien. Bedankt voor de hulp en raad bij de celculturen en de muizen. Rosette, ik ben je zeer dankbaar voor de extra culturen die je voor mij maakte alsook voor de vele oplossingen. Ze hebben een groot verschil gemaakt en het onderzoekswerk aanzienlijk doen opschieten. Jeanine en de mensen op histologie, als er een cultuurtje te kleuren was kon ik steeds aankloppen en het resultaat mocht altijd gezien worden. Wilfried, bedankt voor het helpen opstarten van de muizenkweek en de hulp hierbij. Kathleen, Josette en Paula, bedankt voor alle hulp betreffende

secretariaatsaangelegenheden en papierwerk. Marc en Magda, jullie slaagden er steeds weer in om mijn figuren en posters er mooi te laten uitzien.
Jimmy, Roeland, Daniel, Katherine, Sheen, Koen en Ann, bedankt voor de vele leuke en grappige momenten aan de koffietafel. Het is altijd leuk om 's middags even stoom te kunnen afblazen. Allemaal heel veel succes gewenst met het maken van jullie thesis. Prof. Rigo, ook al stond je ver van mijn thesis, het was fijn te weten dat je deur openstond.
Ilse, toen ik hier pas begon stond je op punt je thesis te verdedigen. Nu ik daar zelf aan toe ben, sta jij ook op een kruispunt in je carrière. Ik wil je heel veel succes wensen in je verdere loopbaan en je bedanken voor alle leuke gesprekken en de raad over het onderzoek, lesgeven en niet-werk gerelateerde onderwerpen zoals zwangerschap en opvoeden. Ellen, ik bewonder je moed en je werklust om steeds weer verder te doen als het eventjes moeilijk gaat. En ik geloof erin dat je volgend jaar een pracht van een thesis zal verdedigen. Inge, het is alweer een tijdje geleden dat je kwam aankloppen op mijn deur met de vraag of je bij mij een masterthesis zou mogen maken. Natuurlijk kon ik zo'n vraag niet weigeren. Van thesisstudent tot collega assistent, samen met Ellen, waren het superleuke tijden op onze werkplek beneden, ik zal ze zeker missen.

Ook de ex-collega's Bert en Frank, bedankt voor de vele uurtjes carpoolen en de fijne vriendschap. Sandy, bedankt voor het organiseren van de kerstfeestjes alsook de fijne babbels.

I would also like to thank the members of the jury for critically reviewing my thesis. All the helpful and interesting comments have certainly added to this work.

Er zijn natuurlijk nog heel wat mensen die ik weliswaar niet opgesomd heb, maar weet dat ik jullie allemaal dankbaar ben.

Ik was hier natuurlijk nooit geraakt zonder de oneindige steun van mijn hele familie en schoonfamilie. Een simpel vraagje van: 'Hoe gaat het met de thesis?' doet soms wonderen.

Mama en papa, voor jullie een apart woordje van dank. Jullie hebben er altijd gestaan voor mij, langs de kantlijn te supporteren en met het volle geloof dat ik erin zou slagen. Bedankt voor alle kansen en het onbezorgd kunnen opgroeien in een liefdevolle, warme thuis zodat ik kon worden tot wie ik nu ben.

En dan mijn Pieter-Jan, het boekje dat hier ligt, is voor een groot deel aan jou te danken. De energie en je vastberadenheid om van ons huisje een mooie en liefdevolle thuis te maken voor mij en Femke, geven me elke dag weer de kracht om de lange afstanden tussen Mechelen en Diepenbeek te overbruggen en om kleine beslommeringen van het werk, "als het weer eens niet wilde lukken", in een ander perspectief te plaatsen. De laatste maanden slorpte veel van onze tijd op, bedankt voor het begrip dat je hiervoor opbracht. Nu sta ik weer helemaal klaar voor jou en voor Femke en kunnen we weer samen verder werken aan ons huis, onze thuis. Bedankt om met mij te trouwen, voor Femke en om elke dag te geloven in mij.